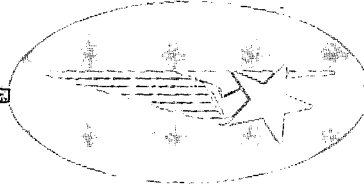


2
CMI 8X



(NASA-CR-124051) CONTROL SYSTEM
OPTIMIZATION STUDIES. VOLUME 2: HIGH
FREQUENCY CUTOFF FILTER ANALYSIS Final
Report, 1 Jul. 1971 - (Lockheed Missiles
and Space Co.) 100 p HC \$7.00 CSCL 22B N73-18861
G3/31 17123 Unclas

Lockheed

HUNTSVILLE RESEARCH & ENGINEERING CENTER

LOCKHEED MISSILES & SPACE COMPANY, INC.
A SUBSIDIARY OF LOCKHEED AIRCRAFT CORPORATION

HUNTSVILLE, ALABAMA

LOCKHEED MISSILES & SPACE COMPANY
HUNTSVILLE RESEARCH & ENGINEERING CENTER
HUNTSVILLE RESEARCH PARK
4800 BRADFORD DRIVE, HUNTSVILLE, ALABAMA

CONTROL SYSTEM OPTIMIZATION
STUDIES

FINAL REPORT

VOLUME II

HIGH FREQUENCY CUTOFF
FILTER ANALYSIS

March 1972

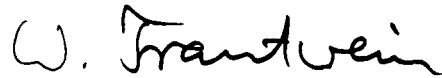
Contract NAS8-30515
(Appendix F)

Prepared for National Aeronautics and Space Administration
Marshall Space Flight Center, Alabama 35812

by

M.H. Fong

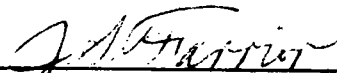
APPROVED:



W. Trautwein, Supervisor
Flight Dynamics & Control Section



T. R. Beal, Manager
Dynamics & Guidance Dept.



J. S. Farrior
Resident Director

FOREWORD

This report documents the results of a study on high frequency cutoff filter analysis and was performed by Lockheed's Huntsville Research & Engineering Center for NASA-Marshall Space Flight Center under Contract NAS8-30515.

The present study was performed during the period 1 July 1971 to 6 March 1972 in accordance with Modification 9 of Appendix F. A second independent study -- "Payload Deployment Study," was completed under this same contract and is documented in Volume I.

The NASA-MSFC technical coordinators for the study were Mr. S. N. Carroll and Mr. H. H. Hosenthien of S&E-ASTR-A.

SUMMARY

The problem of digital implementation of a cutoff filter developed by Lockheed Missiles and Space Company's Huntsville Research and Engineering Center is approached with consideration to word length, sampling rate, accuracy requirements, computing time and hardware restrictions.

Computing time and hardware requirements for four possible programming forms for the linear portions of the filter are determined. Upper bounds for the steady state system output error due to quantization for digital control systems containing a digital network programmed both in the direct form and in the canonical form are derived. This is accomplished by defining a set of error equations in the z domain and then applying the final value theorem to the solution. Quantization error was found to depend upon the digital word length, sampling rate, and system time constants. The error bound developed may be used to estimate the digital word length and sampling rate required to achieve a given system specification. From the quantization error accumulation, computing time and hardware point of view, and the fact that complex poles and zeros must be realized, the canonical form of programming seems preferable.

Finally, the basic input-output characteristics of the digitized high frequency cutoff filter is investigated. The filter has demonstrated its ability to pass signals with minimum distortion in a given frequency band while minimizing signals whose frequencies lie outside the band.

For dc or dc plus a single high frequency signal, the dc signal is transmitted and the high frequency signal is blocked by the digital filter. When a low frequency signal, or a low frequency plus a dc signal appears at the input, the passage is characterized by hysteresis. This is not critical and is shown to be insignificant at frequencies less than 0.4 of the cutoff frequency.

The phase lag due to hysteresis for a low frequency signal decreases with decreasing input frequency, f , below cutoff, f_c (from 11.5° for $f = 0.9 f_c$ to 0.7° for $f = 0.2 f_c$), while the output-input amplitude ratio increases with decreasing input frequency below cutoff (from 0.26 for $f = 0.9 f_c$ to 0.986 for $f = 0.2 f_c$).

If the input contains multiple high frequency components in addition to a low frequency component, the latter is passed in a "quasi-sampled" manner. When a high frequency signal alone appears at the input, sharp cutoff occurs and the input signal is subdued. If the input consists of two out-of-phase high frequency signals, a periodic step waveform appears and the magnitude of the output signal is very small compared to the magnitude of the input waveform. The period of the output waveform is equal to the least common multiple of the periods of the high frequency signals and the sampling period. For efficient filter operation, studies show that the cutoff frequency should be in the neighborhood of one half the lowest expected frequency above cutoff.

CONTENTS

Section	Page
FOREWORD	ii
SUMMARY	iii
1 INTRODUCTION	1
2 DIGITAL IMPLEMENTATION OF THE HIGH FREQUENCY CUTOFF FILTER	2
2.1 Basic Description of the High Frequency Cutoff Filter	2
2.2 Digital Configuration	2
2.3 Synthesis of Linear Digital Filter	5
2.4 Frequency Response of Linear Filter	9
2.5 Programming Method	15
2.6 Quantization Error	24
2.7 Analytical Description of Diode Bridge Circuit	40
3 HIGH FREQUENCY CUTOFF FILTER PERFORMANCE	45
3.1 Analog Filter Performance	45
3.2 Digital Filter Performance	50
4 CONCLUSIONS AND RECOMMENDATIONS	86
5 REFERENCES	88
APPENDIX A: Hysteresis of Digital High Frequency Cutoff Filter	A-1

ILLUSTRATIONS

Figure		Page
2-1	Block Diagram of Continuous High Frequency Cutoff Filter	3
2-2	Digital Implementation of High Frequency Cutoff Filter	4
2-3	Magnitude Comparison for Filter Leg 1	11
2-4	Magnitude Comparison for Filter Leg 2	12
2-5	Phase Comparison for Filter Leg 1	13
2-6	Phase Comparison for Filter Leg 2	14
2-7	General Block Diagram of the Direct Programming Form for a Digital System	17
2-8	General Block Diagram of the Canonical Programming Form for a Digital System	19
2-9	General Block Diagram of the Cascade Programming Form	20
2-10	General Block Diagram of the Normal Programming Form for a Digital System	22
2-11	Input-Output Characteristics of a Truncation Quantizer	25
2-12	Input-Output Characteristics of a Roundoff Quantizer	25
2-13	Block Diagram of Digital Control System	27
2-14	Canonical Programming Form with Quantizers	30
2-15	Direct Programming Form with Quantizers	38
2-16	Nonlinear Part of Cutoff Filter	41
3-1	Analog Simulation Diagram for Nonlinear Filter	46
3-2	Input-Output Characteristics of the Cutoff Filter	47
3-3	Step Function Response of the Cutoff Filter for Filter Parameters Shown in Table 3-1	47
3-4	Modified Cutoff Filter Representation	49
3-5	DC Input-Output Characteristic of Modified Cutoff Filter with $e_i = e_{in(dc)} + 10\sin\omega t$ volts, dc bias = 25 volts	49

ILLUSTRATIONS (Continued)

Figure		Page
3-6	Responses to Step Input Plus Sinusoid for $\omega = 5\pi$ and $\omega_c = \pi$, with $e_{bias} = 25$ volts	51
3-7	Flow Chart of Digital Program to Calculate HFCF Coefficients, Frequency Characteristics and Time Responses	52
3-8 thru 3-17	Time Response of Digital Filter	53 thru 62
3-18	Time Response of High Frequency Cutoff Filter for Three Different Values of ζ_1	64
3-19	Log Magnitude Diagram for the HFCF for Several Combinations of ζ_1 and ζ_2	65
3-20	Phase Diagram for the HFCF for Several Combinations of ζ_1 and ζ_2	66
3-21 thru 3-24	Time Response of High Frequency Cutoff Filter	67 thru 70
3-25	DC Input-Output Characteristics of the Digital Cutoff Filter with $e_i = e_{in(dc)} + \sin 5\omega_c t$	71
3-26 thru 3-31	Time Response of High Frequency Cutoff Filter	74 thru 79
3-32 thru 3-34	Filter Response to High Frequency Signal	81 thru 83
3-35 and 3-36	Filter Response to Out-of-Phase High Frequency Signals	84 and 85

TABLES

Table		Page
2-1	Linear Filter Coefficients	10
2-2	Equipment and Operation Requirements for D(z) Realization	23
2-3	Bridge Output as a Function of Respective Input and Output Voltages	43
3-1	Parameter Values used in the Simulation of Fig. 3-1	45
A-1	Values for Describing Function	A-2

Section 1 INTRODUCTION

In most aerospace control problems, it is desirable to have a filter which passes signals with minimum distortion in a given frequency band while minimizing signals whose frequencies lie outside the given band. One simple filter which has performed this task quite well in a number of simulations is the high frequency cutoff filter containing a diode bridge developed by Lockheed-Huntsville. In previous studies (Refs. 1, 2 and 3), Lockheed had simulated the filter in both analog and digital forms. The resulting simulation methods were primarily intended to be used in evaluating control loop performance on Saturn vehicles in the presence of winds. These studies have shown the cutoff filter to be as good or better than linear filters which were designed around specific frequencies, while the cutoff filter is virtually independent of the frequency of disturbance (so long as it lies sufficiently above the cutoff frequency). The primary purpose of this report is to develop a basic analysis technique for evaluating equipment requirements in order to obtain satisfactory performance, and to investigate the basic characteristics of the digitized high frequency cutoff filter.

The main body of this study is divided into four sections. The layout of subsequent material is as follows: Section 2 describes an analog version of the high frequency cutoff filter (HFCF), develops its digital implementation, and presents a technique for evaluating equipment requirements. Section 3 presents the basic input-output characteristics of the HFCF. Finally, Section 4 embodies the conclusions and recommendations.

|

Section 2

DIGITAL IMPLEMENTATION OF THE HIGH
FREQUENCY CUTOFF FILTER

2.1 BASIC DESCRIPTION OF THE HIGH FREQUENCY CUTOFF FILTER

A block diagram of the continuous high frequency cutoff filter (HFCF) is shown in Fig. 2-1. The purpose of the HFCF is to minimize all frequency components in the incoming signal which are above a certain value, ω_c . Signal components below the cutoff frequency, ω_c , are to be passed with a minimum of distortion. To accomplish this, the filter utilizes a diode bridge in conjunction with the linear networks, as illustrated in the figure. The incoming signal, e_{in} , is first passed through a second-order lag network, then split into two paths. The purpose of this splitting is to develop two signals, e_1 and e_2 , which are in phase at low frequencies (below ω_c) and 180 degrees out of phase at high frequencies (above ω_c). When the high frequencies are passed to the diode bridge, e_2 appears at x_1 when e_1 is positive and at x_2 when e_1 is negative. This minimizes passage of the high frequency signals. When low frequency signals occur at the bridge, the signals pass with a minimum of distortion.

2.2 DIGITAL CONFIGURATION

A block diagram of the digital configuration of the continuous HFCF is shown in Fig. 2-2. The incoming continuous signal, $e_{in}(t)$, is converted by the analog to digital converter to a sequence of numerical values denoted by $e_{in}(n)$, where

$$e_{in}(n) = e_{in}(nT), n = 0, 1, 2, \dots \quad (1)$$

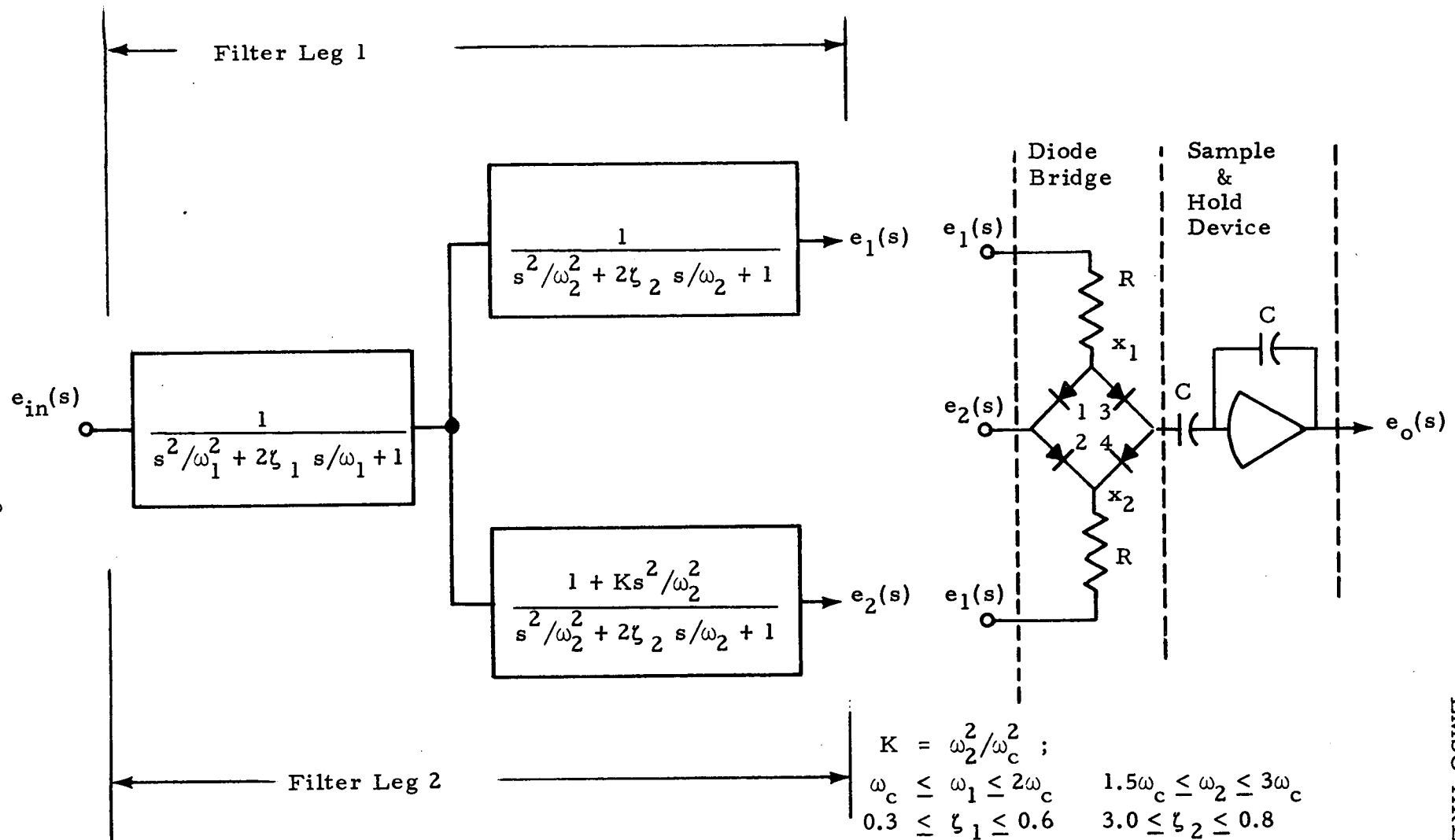


Fig. 2-1 - Block Diagram of Continuous High Frequency Cutoff Filter

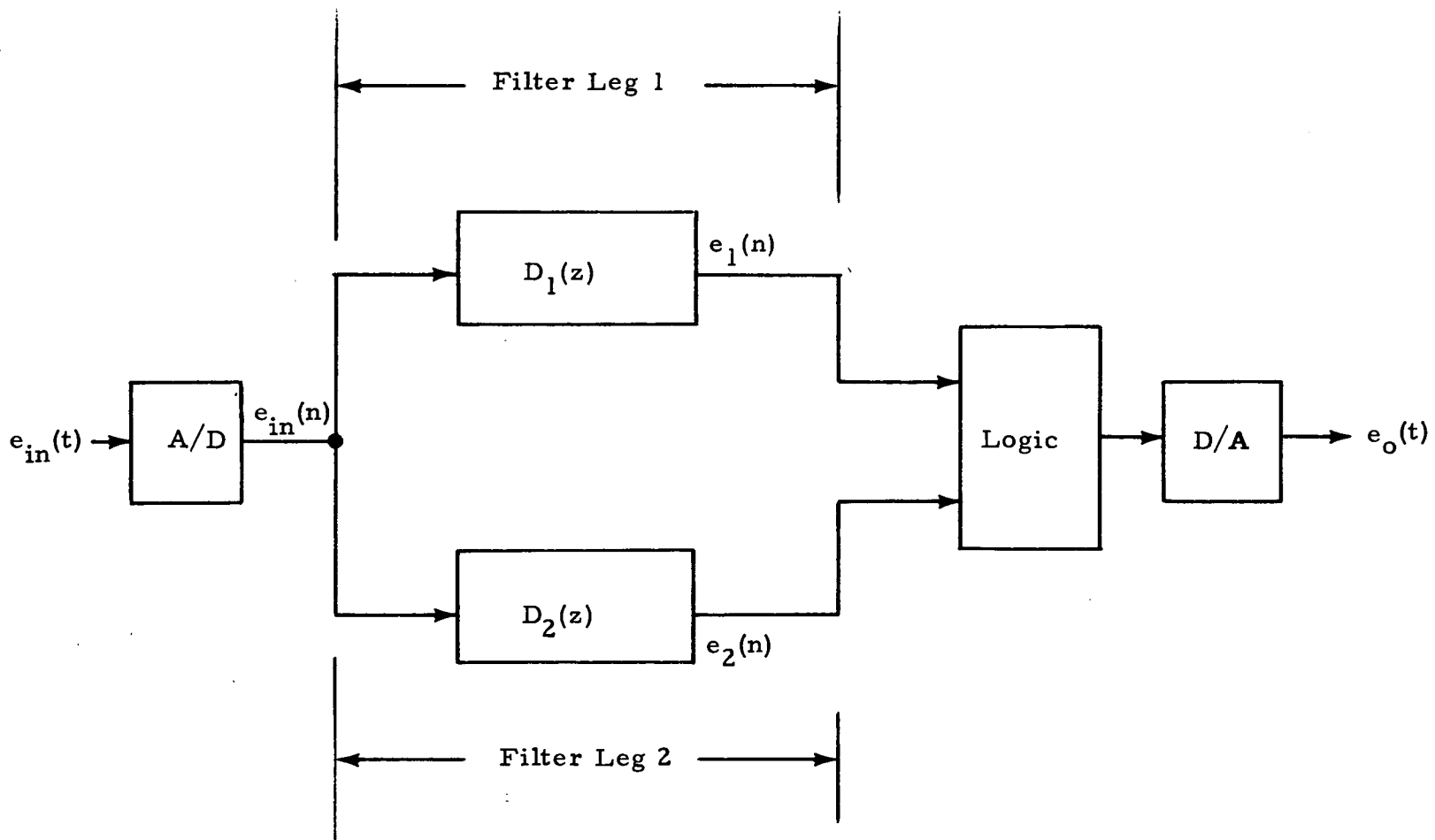


Fig.- 2-2 - Digital Implementation of High Frequency Cutoff Filter

The operators $D_1(z)$ and $D_2(z)$ symbolically represent linear recursion formulas or difference equations that can be programmed in a computer. These formulas perform the same signal-splitting and phase-shifting functions as the linear networks in the analog configuration. The block marked digital logic represents a set of logic statements that will perform the same function as the diode bridge and output amplifier for the analog filter.

The method used to obtain the difference equations and the development of the logic are discussed below under individual headings.

2.3 SYNTHESIS OF LINEAR DIGITAL FILTER

One useful approach in designing a linear digital filter involves finding a set of difference equations having a system impulse transfer function that closely resembles a known analog filter transfer function. The method used for determining the impulse transfer functions represented by $D_1(z)$ and $D_2(z)$ in Fig. 2-2 is based on a substitution rule developed by Shaw (Ref. 4). The substitution rule was derived by comparing the classical results of linear differential and difference equations. Thus, the transient responses of filters related by the substitution rule agree exactly at the sampling points. Consequently, the digital filter corresponding to a stable analog filter is stable.

The transition from differential equation to difference equation (Ref. 4) is made in the following manner.

Substitution Rule

Consider the differential equation

$$f(D) y(t) = K g(D) x(t) \quad (2)$$

where D is the differential operator, $Dy(t) = dy/dt$, f and g are polynomials of degree p and p' , respectively, each with leading coefficient unity. The functions $x(t)$ and $y(t)$ are filter input and output, and K is a gain constant.

Next, consider the difference equation

$$\bar{f}(E) y(n) = \bar{K} \bar{g}(E) x(n) \quad (3)$$

where E is the shifting operator, $Ey(nT) = y(nT + 1)$, and T is the sampling interval. The functions \bar{f} and \bar{g} are polynomials in the operator E . The steps in the transition from Eq. (2) to Eq. (3) are as follows:

- (1) Express $f(D)$ and $g(D)$ as products of linear factors, i.e.,

$$f(D) = \prod_{i=1}^p (D - \rho_i), \quad g(D) = \prod_{j=1}^{p'} (D - \rho_j)$$

- (2) Replace D by E

- (3) Replace each root ρ by $e^{T\rho}$

- (4) Replace K by $K(TE^{1/2})^{p-p'}$

- (5) Expand the result, i.e.,

$$\bar{f}(E) = \prod_i^p (E - e^{T\rho_i})$$

$$\bar{g}(E) = \prod_j^{p'} (E - e^{T\rho_j})$$

$$\bar{K} = K(TE^{1/2})^{p-p'}$$

The multiplier of K , $E^{(p-p')/2}$, is the proper phase adjustment which adds $(p-p')/2$ to all input subscripts and amounts to central approximation.

Impulse Transfer Function

Based upon the substitution rule, the impulse transfer function, $D(z)$, of the digital filter is obtained from the transfer function, $F(s)$, of a known analog filter via the correspondence

$$F(s) = K \frac{\prod_{i=1}^{p'} (s - \rho_i')}{\prod_{i=1}^p (s - \rho_i)} \Rightarrow K (T z^{1/2})^{p-p'} \frac{\prod_{i=1}^{p'} (z - e^{T \rho_i'})}{\prod_{i=1}^p (z - e^{T \rho_i})} = D(z) \quad (4)$$

Example:

The transfer function of the analog filter Leg 2 is

$$\begin{aligned} F(s) &= \frac{1 + s^2/\omega_c^2}{(s^2/\omega_1^2 + 2\zeta_1 s/\omega_1 + 1)(s^2/\omega_2^2 + 2\zeta_2 s/\omega_2 + 1)} \\ &= \frac{(\omega_1^2 \omega_2^2 / \omega_c^2) (s + j\omega_c)(s - j\omega_c)}{(s - \rho_1)(s - \rho_2)(s - \rho_3)(s - \rho_4)} \end{aligned} \quad (5)$$

with

$$\rho_1 = -\zeta_1 \omega_1 + j(\omega_1^2 - \omega_1^2 \zeta_1^2)^{1/2}$$

$$\rho_2 = -\zeta_1 \omega_1 - j(\omega_1^2 - \omega_1^2 \zeta_1^2)^{1/2}$$

$$\rho_3 = -\zeta_2 \omega_2 + j(\omega_2^2 - \omega_2^2 \zeta_2^2)^{1/2}$$

$$\rho_4 = -\zeta_2 \omega_2 - j(\omega_2^2 - \omega_2^2 \zeta_2^2)^{1/2}$$

where ω_c is the cutoff frequency. The correspondence Eq. (4) leads to the impulse transfer function

$$D(z) = \frac{(\omega_1^2 \omega_2^2 / \omega_c^2) (T z^{1/2})^2 (z - e^{-j\omega_c T}) (z - e^{j\omega_c T})}{(z - e^{T\rho_1}) (z - e^{T\rho_2}) (z - e^{T\rho_3}) (z - e^{T\rho_4})} \quad (6)$$

Expanding Eq. (6) yields

$$D(z) = \frac{(\omega_1^2 \omega_2^2 / \omega_c^2) (T^2) (c_1 z^3 + c_2 z^2 + c_3 z)}{z^4 + d_1 z^3 + d_2 z^2 + d_3 z + d_4}$$

or

$$D(z) = \frac{(\omega_1^2 \omega_2^2 / \omega_c^2) (T^2) (c_1 z^{-1} + c_2 z^{-2} + c_3 z^{-3})}{1 + d_1 z^{-1} + d_2 z^{-2} + d_3 z^{-3} + d_4 z^{-4}} \quad (7)$$

where

$$c_1 = 1$$

$$c_2 = -2 \cos \omega_c T$$

$$c_3 = 1$$

$$d_1 = -2 (\epsilon^{-\zeta_2 \omega_2 T} \cos \omega_2 (1 - \zeta_2)^{1/2} T + \epsilon^{-\zeta_1 \omega_1 T} \cos \omega_1 (1 - \zeta_1)^{1/2} T)$$

$$d_2 = \epsilon^{-2\zeta_1 \omega_1 T} + \epsilon^{-2\zeta_2 \omega_2 T} + 4\epsilon^{-(\zeta_1 \omega_1 + \zeta_2 \omega_2) T} (\cos \omega_1 (1 - \zeta_1)^{1/2} T) (\cos \omega_2 (1 - \zeta_2)^{1/2} T)$$

$$d_3 = -2(\epsilon^{-(2\zeta_1\omega_1 + \zeta_2\omega_2)T} \cos \omega_2(1-\zeta_2)^{1/2}T + \epsilon^{-(2\zeta_2\omega_2 + \zeta_1\omega_1)T} \cos \omega_1(1-\zeta_1)^{1/2}T)$$

$$d_4 = \epsilon^{-2(\zeta_1\omega_1 + \zeta_2\omega_2)T}$$

In this study, the digital filter coefficients were normalized to have a gain of one at zero frequency. The coefficients of the linear portion of the HFCE are tabulated in Table 2-1 for the following parameters.

$$\omega_c = 3.0 \text{ rad/sec}$$

$$\omega_1 = 4.5 \text{ rad/sec}, \zeta_1 = 0.5$$

$$\omega_2 = 6.0 \text{ rad/sec}, \zeta_2 = 0.6.$$

2.4 FREQUENCY RESPONSE OF LINEAR FILTER

Replacing s by $j\omega$ in Eq. (4) gives the frequency-characteristic function of the analog filter as $F(j\omega)$. Hence, the log magnitude and phase functions are $20 \log |F(j\omega)|$ and $\tan^{-1} [\text{Im } F(j\omega)/\text{Re } F(j\omega)]$, respectively.

Similarly, replacing z by $\epsilon^{j\omega T}$ in Eq. (4) gives the frequency characteristic function of the digital filter as $D(\epsilon^{j\omega T})$. The corresponding log magnitude and phase functions are $20 \log |D(\epsilon^{j\omega T})|$ and $\tan^{-1} [\text{Im } D(\epsilon^{j\omega T})/\text{Re } D(\epsilon^{j\omega T})]$, respectively.

The frequency characteristics of the linear networks of the high frequency cutoff filter are plotted in Figs. 2-3 through 2-6. The log amplitude curves for the linear digital networks are very close to that of the analog networks except near the Nyquist frequency (i.e., half of the sampling frequency). Such departure

Table 2-1
LINEAR FILTER COEFFICIENTS

Sampling Interval T = .04 sec			T = .0872664 sec		T = .2617993 sec	
	Filter Leg 1	Filter Leg 2	Filter Leg 1	Filter Leg 2	Filter Leg 1	Filter Leg 2
a_0	0.0	0.0	0.0	0.0	0.0	0.0
a_1	0.0	0.1024040	0.0	0.3676234	0.0	1.131135
a_2	0.0014728	-0.2033352	0.0250528	-0.7101939	0.6626039	-1.599667
a_3	0.0	0.1024040	0.0	0.3676234	0.0	1.131135
b_1	-3.505654		-2.883835		-0.8213607	
b_2	4.654637		3.276310		0.5995070	
b_3	-2.773765		1.727651		0.1622874	
b_4	0.6262534		0.3602284		0.0467448	

Form of Impulse Transfer Function:

$$D(z) = \frac{a_0 + a_1 z^{-1} + a_2 z^{-2} + a_3 z^{-3}}{1 + b_1 z^{-1} + b_2 z^{-2} + b_3 z^{-3} + b_4 z^{-4}}$$

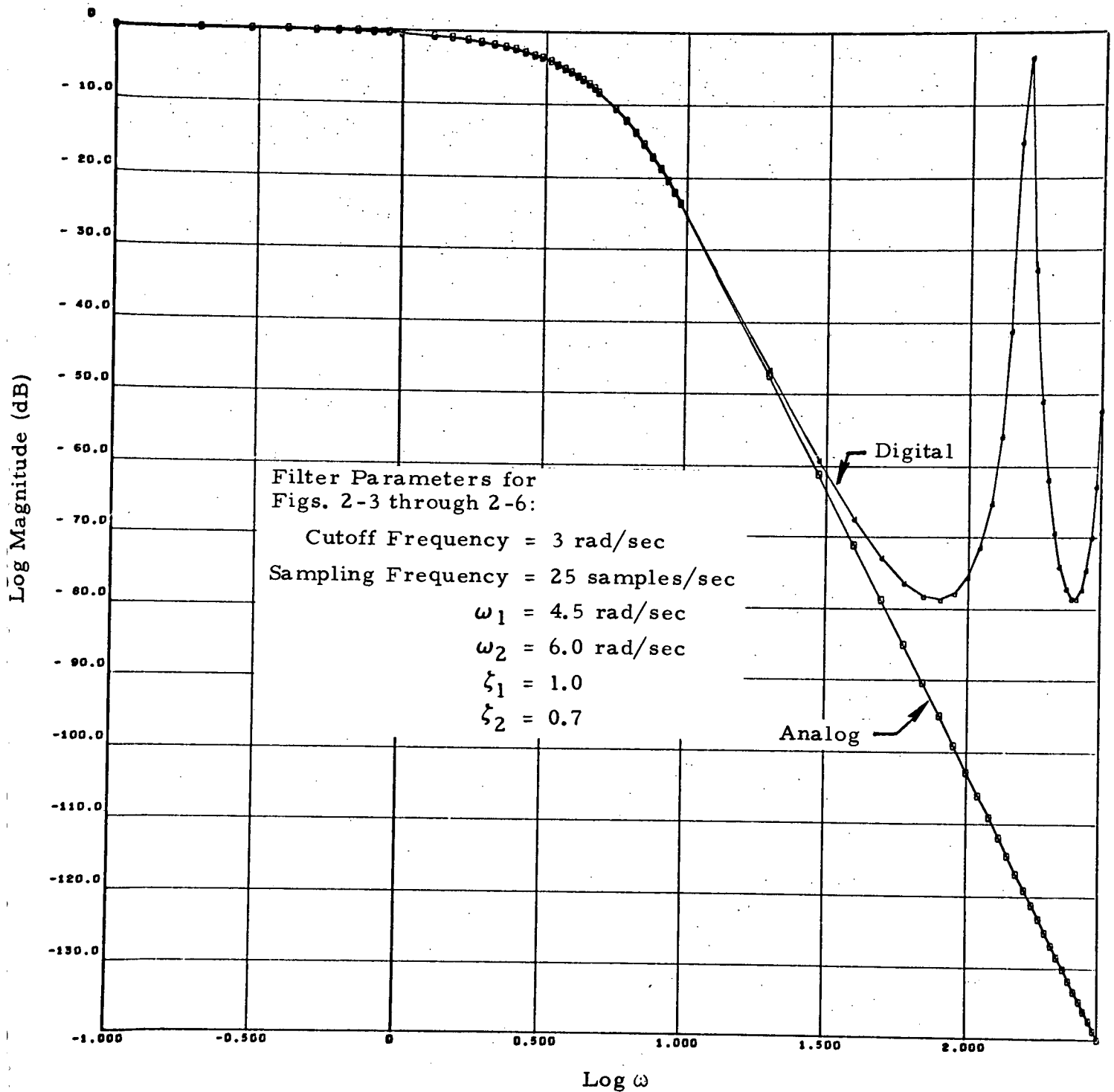


Fig. 2-3 - Magnitude Comparison for Filter Leg 1

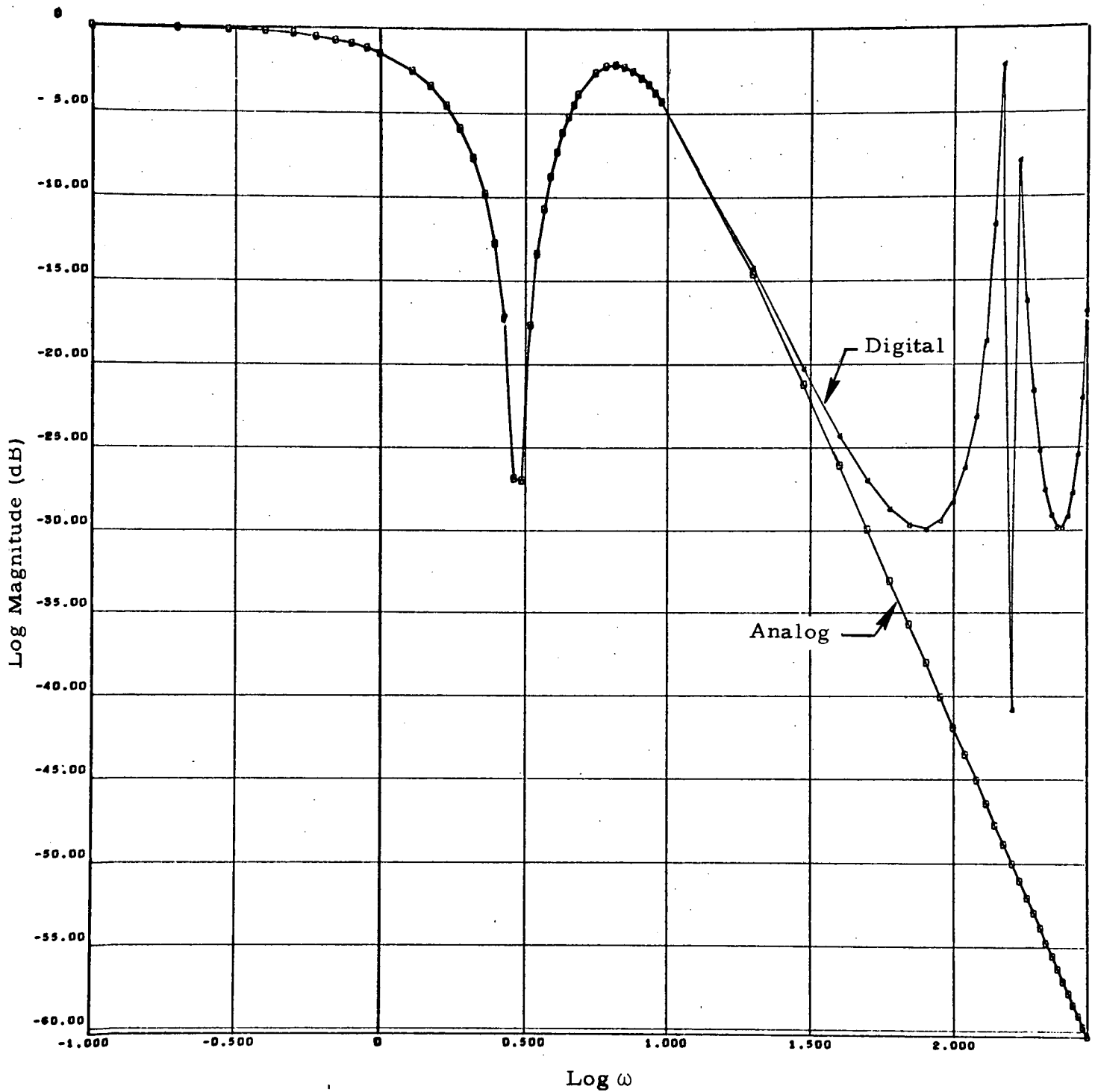


Fig. 2-4 - Magnitude Comparison for Filter Leg 2

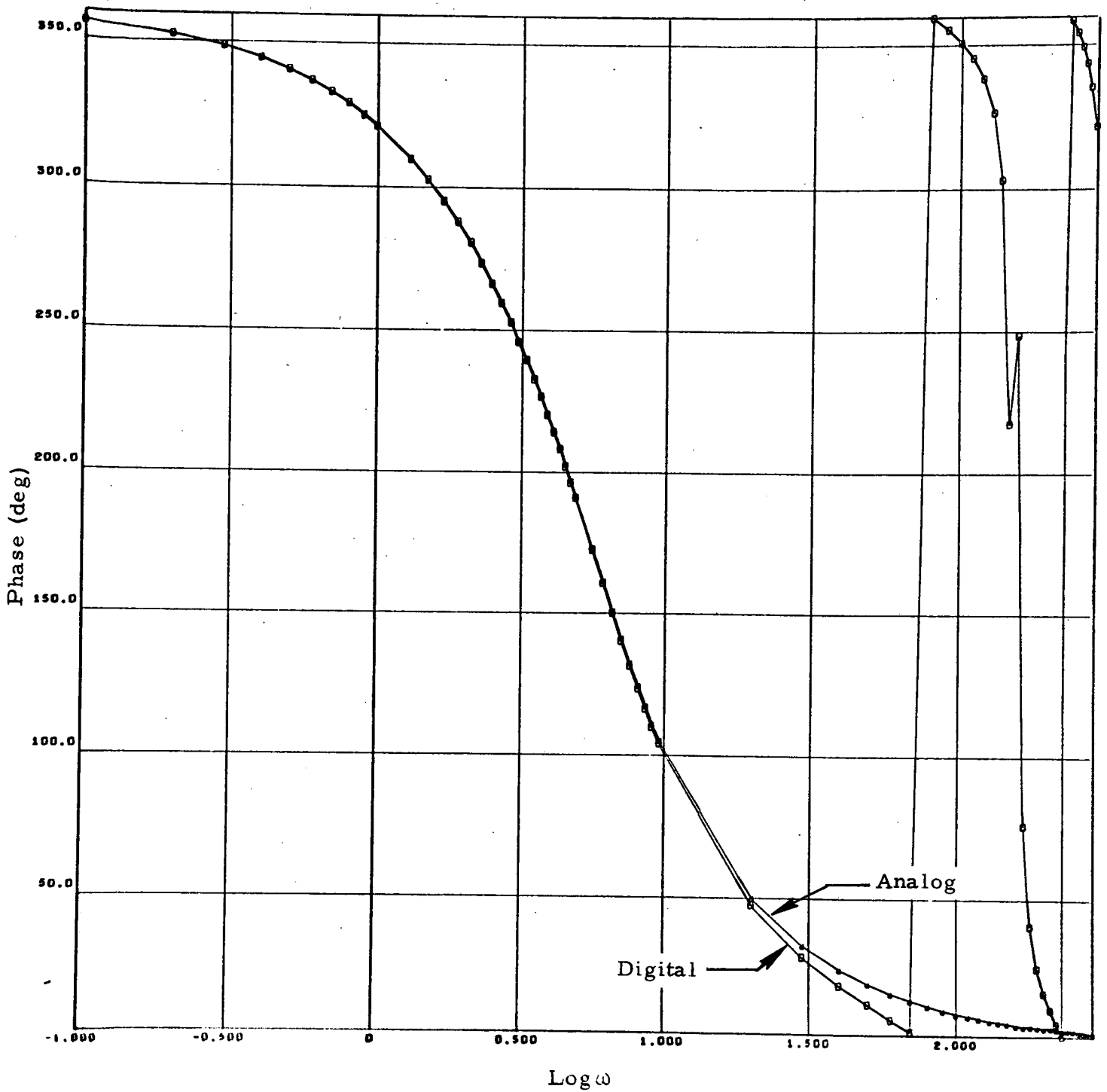


Fig. 2-5 - Phase Comparison for Filter Leg 1

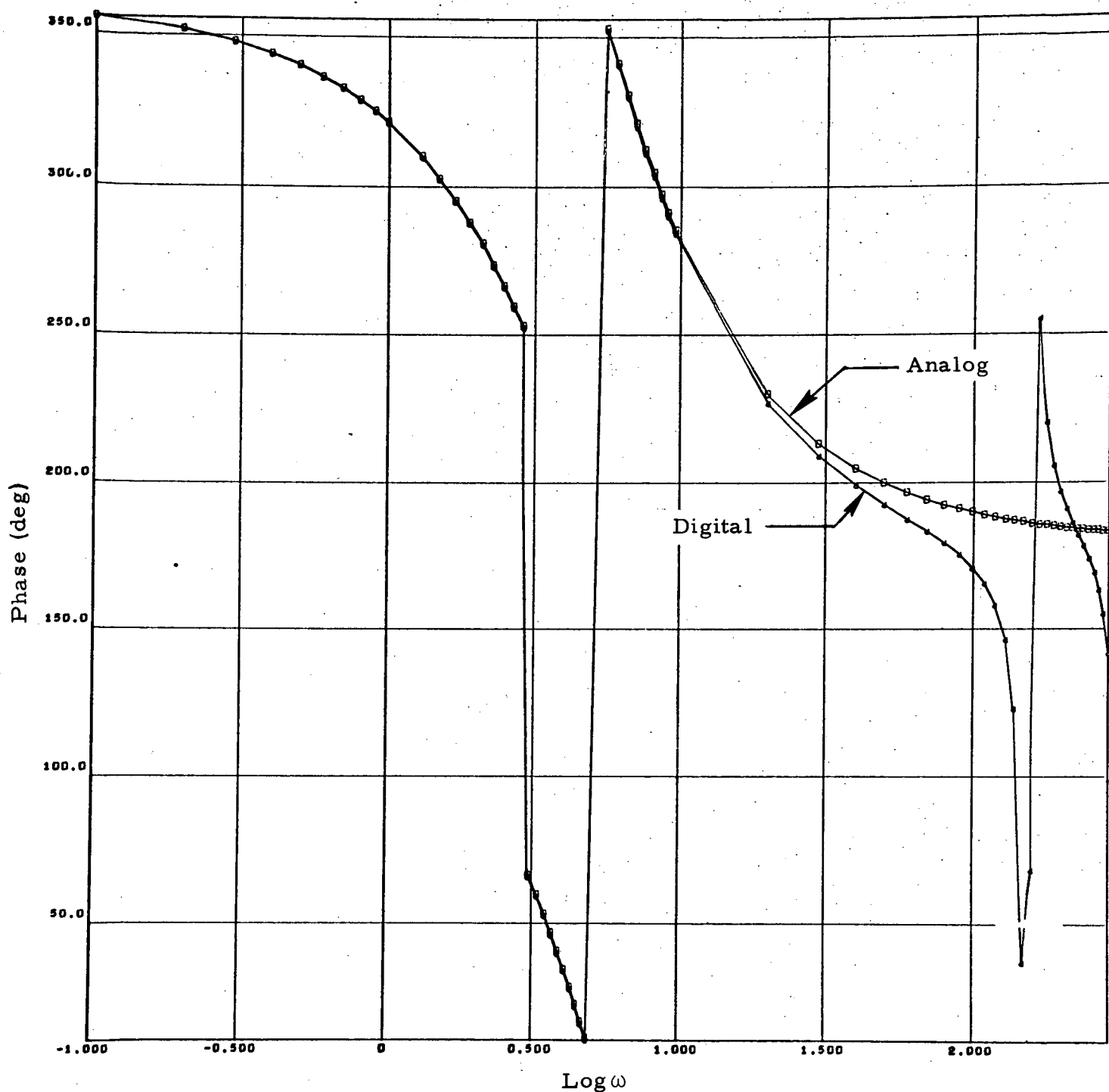


Fig. 2-6 - Phase Comparison for Filter Leg 2

of the log magnitude curves is inherent in the sampling system since the slope of the log magnitude function must be zero at the Nyquist frequency.

2.5 PROGRAMMING METHOD (References 5, 6 and 7)

Four possible programming forms were considered for implementing a pulse transfer function $D(z)$:

1. Direct Programming
2. Canonical Programming
3. Cascade Programming
4. Normal (or Parallel) Programming.

To determine a choice between these forms, some basis of comparison must be used. The scheme used for comparison in this study is based on the number of registers (memory size) required for data and coefficient storage, the computing time involved in additions, multiplications and data transfers, and error accumulated due to input, output and arithmetic quantization.

2.5.1 Direct Programming

An impulse transfer function $D(z)$ containing n poles and m zeros can be expressed in the following general form

$$D(z) = \frac{E_o(z)}{E_i(z)} = \frac{a_0 + a_1 z^{-1} + a_2 z^{-2} + \dots + a_m z^{-m}}{1 + b_1 z^{-1} + b_2 z^{-2} + \dots + b_n z^{-n}}, \quad m \leq n \quad (8)$$

The difference equation which describes the direct programming form can be obtained by cross multiplying Eq. (8) and taking the inverse transform. Thus

$$e_o(k) = \sum_{j=0}^m a_j e_i(k-j) - \sum_{j=1}^n b_j e_o(k-j) \quad (9)$$

where $e_i(k)$ denotes the input evaluated at time kT , and T is the sampling interval. A general block diagram of this form is shown in Fig. 2-7. If all the a_i and b_j are not zero and one, the number of storage registers for direct programming is

Data	$m+n$
Coefficients	$m+n+1$
Multiplications	$m+n+1$
Additions	$m+n$
Transfers	$m+n$

2.5.2 Canonical Programming

To derive the difference equations which describe this form, one may introduce an intermediate variable $F(z)$ into Eq. (8). Let

$$\frac{E_o(z)}{F(z)} = \sum_{j=0}^m a_j z^{-j} \quad (10)$$

$$\frac{F(z)}{E_i(z)} = \left(1 + \sum_{j=1}^n b_j z^{-j} \right)^{-1} \quad (11)$$

The inverse z -transform of Eqs. (10) and (11) are then

$$e_o(k) = \sum_{j=0}^m a_j f(k-j) \quad (12)$$

$$f(k) = e_i(k) - \sum_{j=1}^n b_j f(k-j) \quad (13)$$

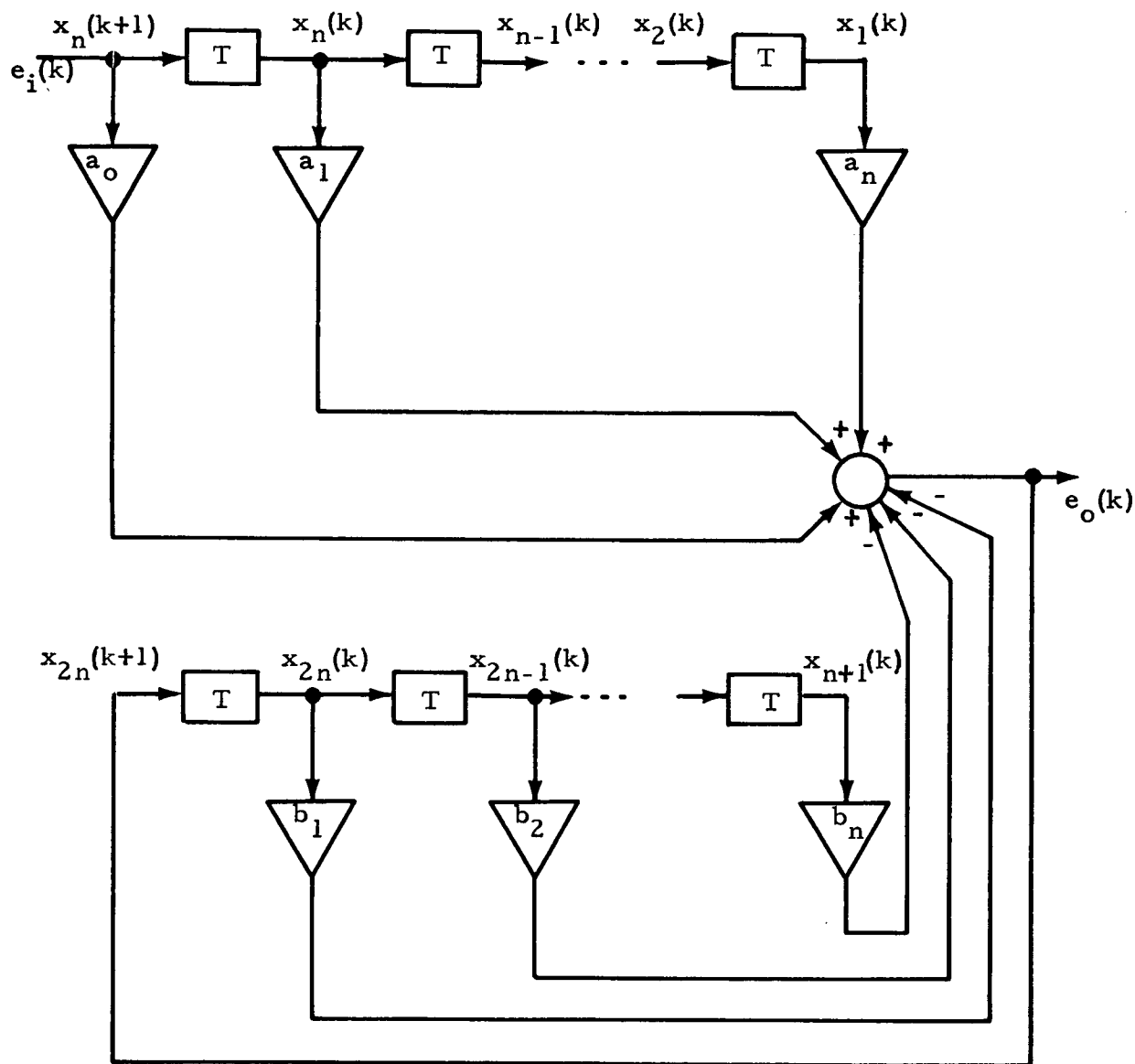


Fig. 2-7 - General Block Diagram of the Direct Programming Form for a Digital System

A general block diagram of this form is shown in Fig. 2-8 for $m = n$. If all the a_j and b_j terms are not zero and one, the number of storage registers for canonical programming is

Data	n
Coefficients	$m + n + 1$
Multiplications	$m + n + 1$
Additions	$m + n$
Transfers	n

2.5.3 Cascade Programming

The difference which describes the cascade programming form can be obtained by factoring Eq. (8) into the following form for $m = n$:

$$D(z) = \frac{a_0}{1 + d_1 z^{-1}} \frac{1 + e_2 z^{-1}}{1 + d_2 z^{-1}} \cdots \frac{1 + e_n z^{-1}}{1 + d_n z^{-1}} \quad (14)$$

$$= D_1(z) D_2(z) \cdots D_n(z) \quad (15)$$

$$= \frac{C_1(z)}{E_1(z)} \frac{C_2(z)}{C_1(z)} \cdots \frac{E_n(z)}{C_{n-1}(z)} \quad (16)$$

The difference equations for Eqs. (14) and (16) are:

$$\begin{aligned} C_1(k) &= a_0 e_1(k) - d_1 C_1(k-1) \\ C_2(k) &= C_1(k) + e_2 C_1(k-1) - d_2 C_2(k-1) \\ &\vdots \\ e(k) &= C_{n-1}(k) + e_n C_{n-1}(k-1) - d_n C_n(k-1) \end{aligned} \quad (17)$$

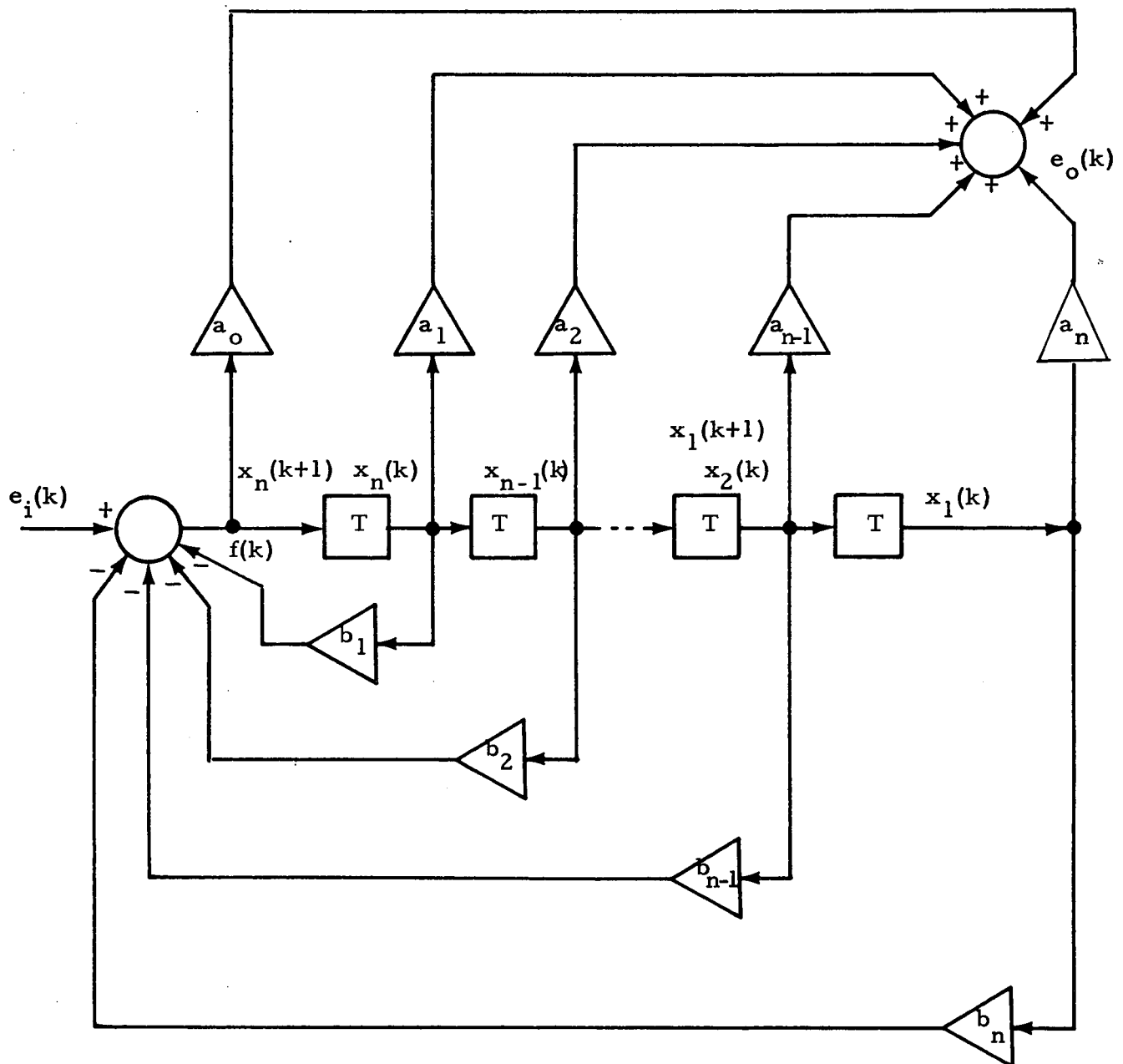


Fig. 2-8 - General Block Diagram of the Canonical Programming Form for a Digital System

A block diagram of this form is shown in Fig. 2-9. If each separate transfer function is programmed in the direct form and the output of one block is regarded as the input to the next one. Then the number of storage registers for this form is

Data	n
Coefficients	m + n + 1
Multiplications	m + n + 1
Additions	m + n
Transfers	n

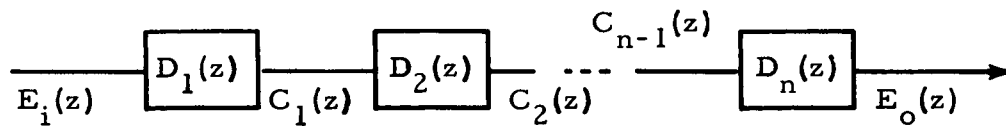


Fig. 2-9 - General Block Diagram of the Cascade Programming Form

2.5.4 Normal Programming

Normal programming is based on the partial-fraction expansion of Eq. (8):

$$D(z) = \frac{P_1}{1 + d_1 z^{-1}} + \frac{P_2}{1 + d_2 z^{-1}} + \dots + \frac{P_n}{1 + d_n z^{-1}} \quad (18)$$

where the d_i are the poles of $D(z)$ and the p_i are the residues of $D(z)$ at those poles. The difference equations for this form can be obtained by defining

$$D(z) = \frac{C_1(z)}{E_1(z)} + \frac{C_2(z)}{E_2(z)} + \dots + \frac{C_n(z)}{E_n(z)} \quad (19)$$

This leads to

$$\begin{aligned} c_1(k) &= p_1 e_i(k) - d_1 c_1(k-1) \\ c_2(k) &= p_2 e_i(k) - d_2 c_2(k-1) \\ &\vdots \\ c_n(k) &= p_n e_i(k) - d_n c_n(k-1) \end{aligned}$$

$$e_o(k) = \sum_{j=1}^n c_j(k) \quad (20)$$

A block diagram of the normal form is shown in Fig. 2-10. The corresponding storage registers for this form are:

Data	n
Coefficients	2n
Multiplications	2n
Additions	2n - 1
Transfers	n

The equipment and operation requirements for implementing an m^{th} order polynomial in z^{-1} in numerator and n^{th} order polynomial in z^{-1} in denominator of the function $D(z)$ are listed in Table 2-2 for the various forms. The total number of storage registers is the sum of those required for data, coefficients, multiplications, additions and data transfer storage. The total number of computer operations is the sum of multiplication, addition and data transfer operations. Assuming each operation

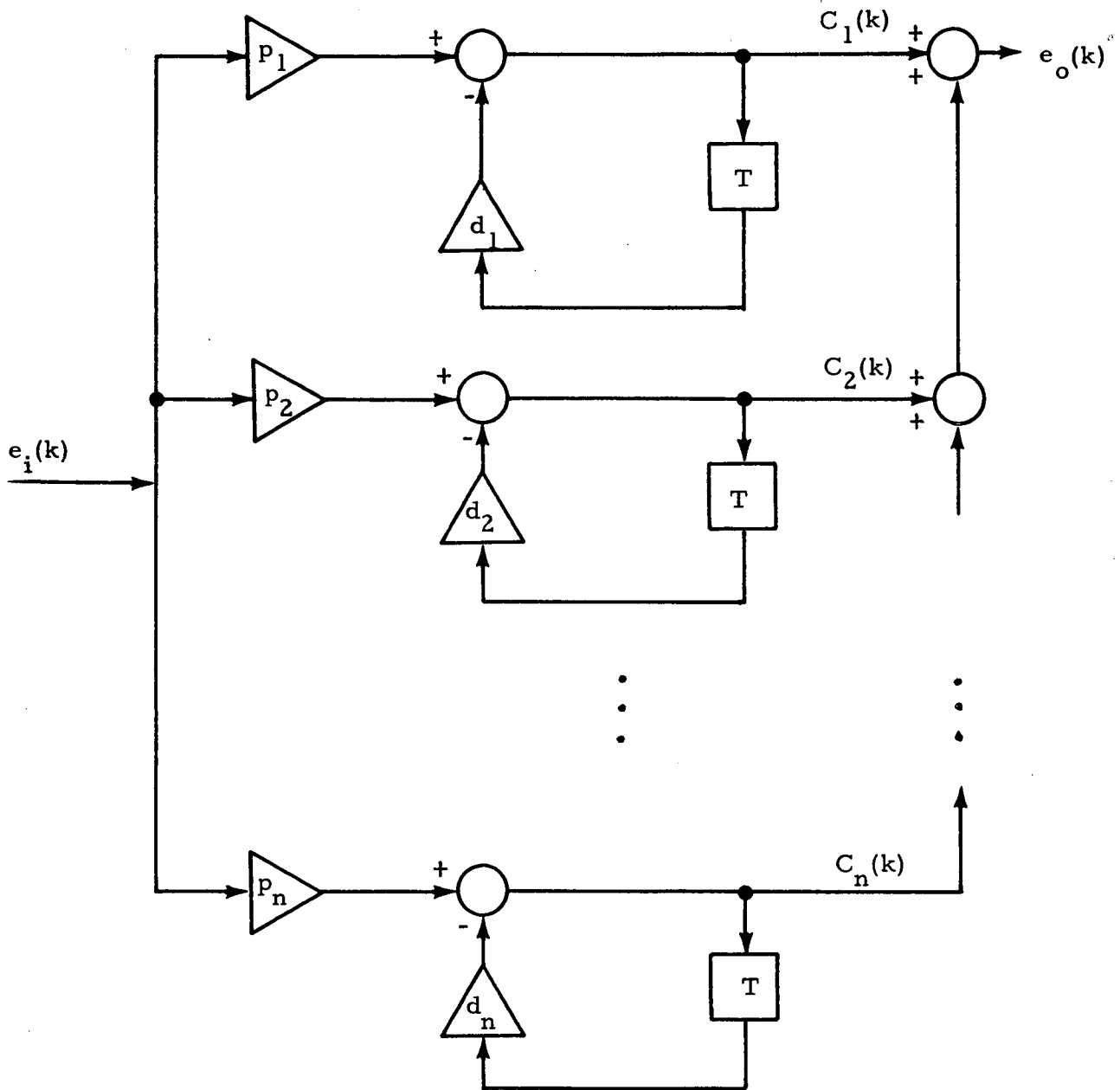


Fig. 2-10 - General Block Diagram of the Normal Programming Form for a Digital System

Table 2-2
EQUIPMENT AND OPERATION REQUIREMENTS
FOR D(z) REALIZATION

Storage Registers	Forms			
	Direct	Canonical	Cascade	Normal
Data	$m + n$	n	n	n
Coefficients	$m + n + 1$	$m + n + 1$	$m + n + 1$	$2n$
Multiplications	$m + n + 1$	$m + n + 1$	$m + n + 1$	$2n$
Additions	$m + n$	$m + n$	$m + n$	$2n - 1$
Transfers	$m + n$	n	n	n
Total Storage Registers	$5m + 5n + 2$	$3m + 5n + 2$	$3m + 5n + 2$	$8n - 1$
Total Computer Operations	$3m + 3n + 1$	$2m + 3n + 1$	$2m + 3n + 1$	$5n - 1$

requires the same execution time, the computing time is proportional to the total number of computer operations. In general, each of these computer operations requires a different execution time. This table plus the fact that complex poles and zeros must be realized indicate that the canonical form of programming is desired for implementing the linear networks of the high frequency cutoff filter.

2.6 QUANTIZATION ERROR

2.6.1 Introduction

Most numbers cannot be represented exactly in a digital system because of the finite word length of the system. The difference between the exact number and its representation in the digital system is referred to as the quantization error. This quantization error depends upon the type of mechanism used to represent the exact number. Generally, there are two types of quantization mechanisms used in digital devices — the truncation quantizer, and the roundoff quantizer. An input-output characteristic of a truncation quantizer is shown in Fig. 2-11. It represents only the first ℓ bits of an exact number, x . Therefore, the quantization error will not exceed

$$h = \pm 2^{-\ell} \quad (21)$$

where h is called the quantization granularity.

The input-output characteristics of a roundoff quantizer are shown in Fig. 2-12. For this quantizer, the maximum error due to quantization is

$$h/2 = \pm 2^{1-\ell} \quad (22)$$

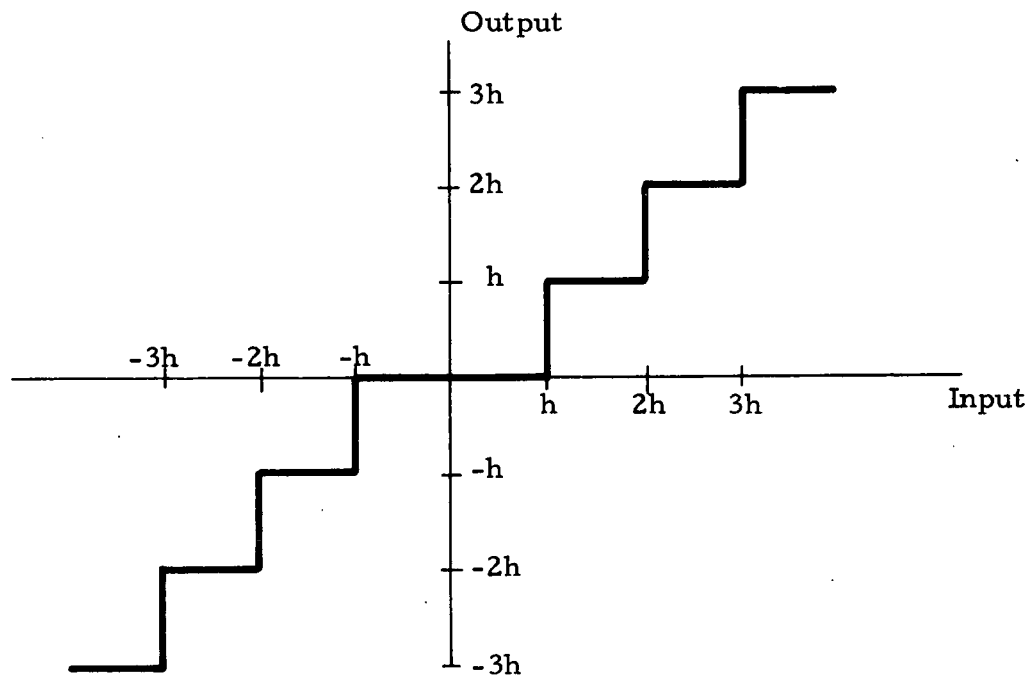


Fig. 2-11 - Input-Output Characteristics of a Truncation Quantizer

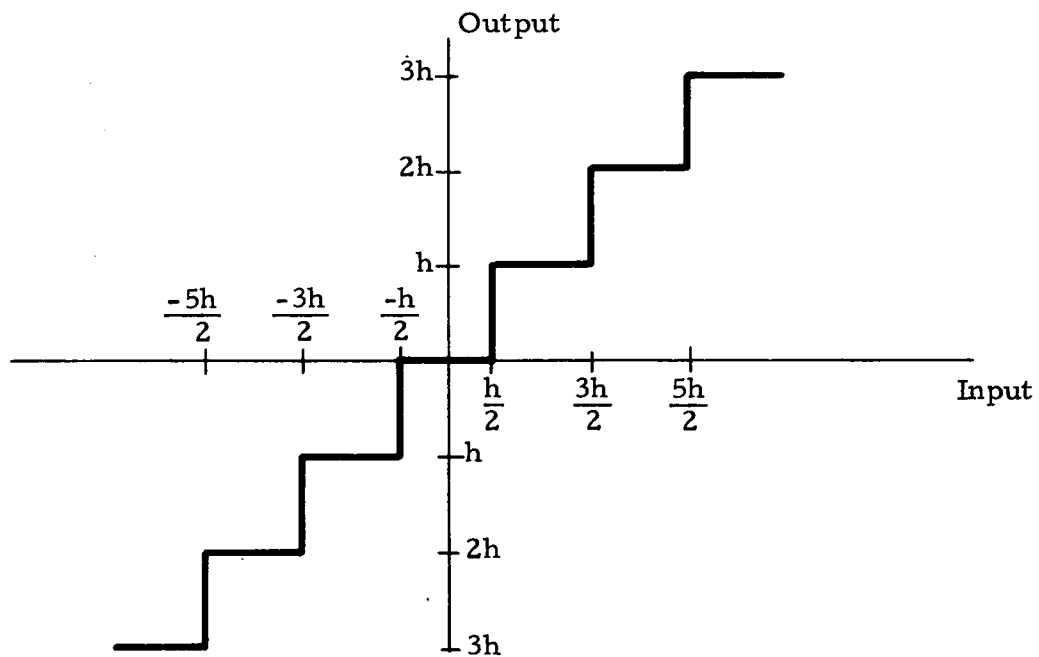


Fig. 2-12 - Input-Output Characteristics of a Roundoff Quantizer

In order to compare quantization errors in digital systems programmed in canonical form and in direct form, expressions for the error are required. These are derived in the following section under the following assumptions:

1. The digital filter is realized with fixed-point arithmetic
2. Input signal to the filter is normalized such that the maximum input signal never exceeds unity
3. All filter variables are scaled such that no overflows occur on addition.

Since quantization is a nonlinear phenomenon, the present study on quantization is primarily concerned with obtaining an upper bound on the system output error.

2.6.2 Quantization Error for Canonical Form

Consider the digital control system as shown in Fig. 2-13 where $D(z)$ is the pulse transfer function of a digital system (digital filter or digital controller), $G_{ho}(s)$ is the transfer function of a zero-order hold and $G(s)$ is the transfer function of a plant. Assume that the digital filter has the following n^{th} order pulse transfer function

$$D(z) = \frac{a_0 + a_1 z^{-1} + a_2 z^{-2} + \dots + a_m z^{-m}}{1 + b_1 z^{-1} + b_2 z^{-2} + \dots + b_n z^{-n}} \quad (21)$$

where $m \leq n$. If the digital system is programmed in the canonical form as shown in Fig. 2-8, and if each output of a time delay block is denoted as a state variable then the state equation can be represented as shown in Eq. (22).

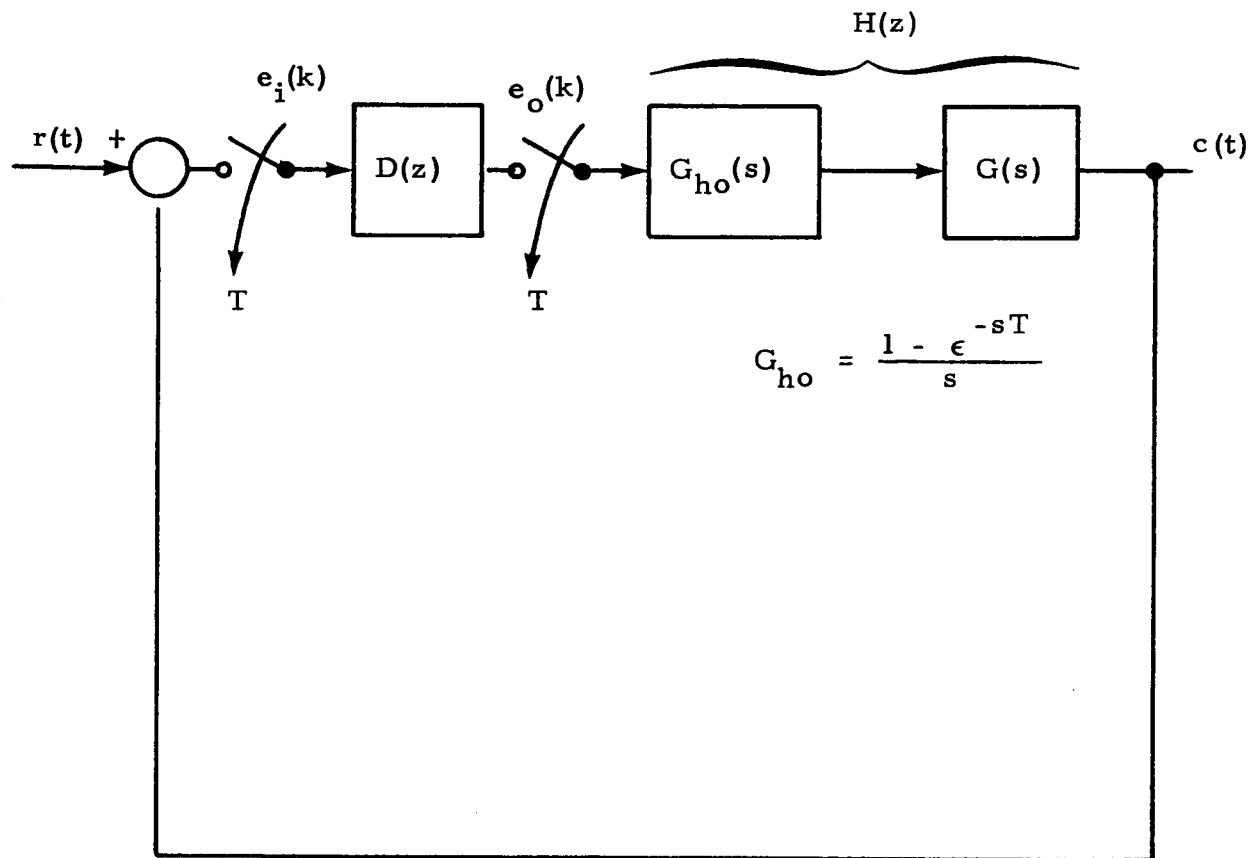


Fig. 2-13 - Block Diagram of Digital Control System

$$\begin{aligned}
x_1(k+1) &= x_2(k) \\
x_2(k+1) &= x_3(k) \\
&\vdots \\
x_{n-1}(k+1) &= x_n(k) \\
x_n(k+1) &= e_i(k) - \sum_{j=1}^n b_{n+1-j} x_j(k)
\end{aligned} \tag{22}$$

where $x_i(k)$ is the state variable x_i evaluated at time kT , and $e(k)$ is the input evaluated at time kT . An additional equation specifying the output $e_o(k)$ as a linear combination of the state variables is

$$e_o(k) = a_o e_i(k) + \sum_{j=1}^n (a_{n+1-j} - a_o b_{n+1-j}) x_j(k) \tag{23}$$

Since

$$e_i(k) = r(k) - c(k) \tag{24}$$

therefore Eqs. (22) and (23) can be rewritten as

$$\begin{aligned}
x_1(k+1) &= x_2(k) \\
x_2(k+1) &= x_3(k) \\
&\vdots \\
x_{n-1}(k+1) &= x_n(k) \\
x_n(k+1) &= r(k) - c(k) - \sum_{j=1}^n b_{n+1-j} x_j(k) \\
e_o(k) &= a_o [r(k) - c(k)] + \sum_{j=1}^n (a_{n+1-j} - a_o b_{n+1-j}) x_j(k)
\end{aligned} \tag{25}$$

Furthermore, assume that the z -transform of the plant-hold combination has the following ℓ^{th} order transfer function

$$H(z) = \frac{a'_0 + a'_1 z^{-1} + a'_2 z^{-2} + \dots + a'_\ell z^{-\ell}}{1 + b'_1 z^{-1} + b'_2 z^{-2} + \dots + b'_\ell z^{-\ell}} \quad (26)$$

The state equations for Eq. (26) in the canonical form becomes

$$\begin{aligned} y_1(k+1) &= y_2(k) \\ y_2(k+1) &= y_3(k) \\ &\vdots \\ y_{\ell-1}(k+1) &= e_o(k) - \sum_{j=1}^{\ell} b'_{\ell+1-j} y_j(k) \\ c(k) &= a'_0 e_o(k) + \sum_{j=1}^{\ell} (a'_{\ell+1-j} - a'_0 b'_{\ell+1-j}) y_j(k) \end{aligned} \quad (27)$$

Now the effect of input, output and multiplication quantization on system performance will be considered. Input quantization is caused by the conversion of input signal, $e_i(k)$, into a set of discrete levels. Output quantization is caused by the fact that not all the available bits of digital signal (e.g., $e_o(k)$) are converted to their analog equivalents. Multiplication quantization results when the product of two ℓ bit numbers is reduced to ℓ bits.

The same control system with quantizers is shown in Fig. 2-14, where the blocks labeled Q , Q_{10} , Q_{11} , \dots , are quantizers with quantization granularity h_1 , h_{10} , h_{11} , \dots , respectively. The state equations for the digital system with quantizers become:

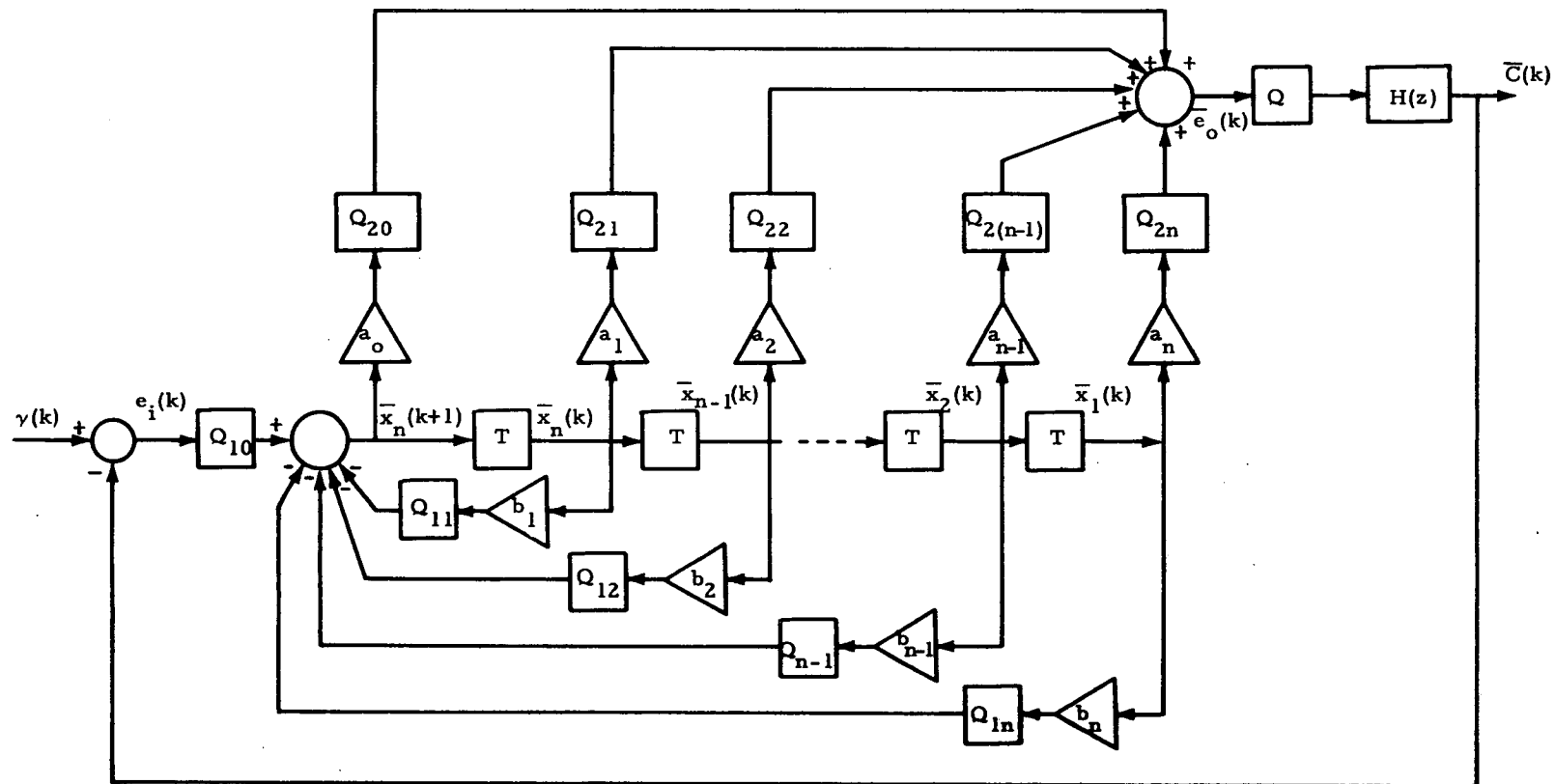


Fig. 2-14 - Canonical Programming Form with Quantizers

$$\begin{aligned}
 \bar{x}_1(k+1) &= \bar{x}_2(k) \\
 \bar{x}_2(k+1) &= \bar{x}_3(k) \\
 &\vdots \\
 \bar{x}_{n-1}(k+1) &= \bar{x}_n(k) \\
 \bar{x}_n(k+1) &= -Q_{1n} \left[b_n \bar{x}_1(k) \right] - Q_{1(n-1)} \left[b_{n-1} \bar{x}_2(k) \right] \dots \\
 &\quad - Q_{12} \left[b_2 \bar{x}_{n-1}(k) \right] - Q_{11} \left[b_1 \bar{x}_n(k) \right] + Q_{10} \left[r(k) - \bar{c}(k) \right] \\
 \bar{e}_o(k) &= Q_{2n} \left[a_n \bar{x}_1(k) \right] + Q_{2(n-1)} \left[a_{n-1} \bar{x}_2(k) \right] + \dots + Q_{21} \left[a_1 \bar{x}_n(k) \right] \\
 &\quad + Q_{20} \left\{ a_o \left[-Q_{1n} \left[b_n \bar{x}_1(k) \right] - Q_{1(n-1)} \left[b_{n-1} \bar{x}_2(k) \right] \right. \right. \\
 &\quad \left. \left. \dots - Q_{11} \left[b_1 \bar{x}_n(k) \right] + Q_{10} \left[r(k) - \bar{c}(k) \right] \right] \right\} \quad (28)
 \end{aligned}$$

The bar over the state variables indicates that quantization effects have been included in the system. $Q_i \left[b_i \bar{x}_j(k) \right]$ indicates the quantized value of $b_i \bar{x}_j(k)$. Now, $Q_i \left[b_i \bar{x}_j(k) \right]$ may be defined as

$$Q_i \left[b_i \bar{x}_j(k) \right] = b_i \bar{x}_j(k) + q_i(k)$$

where $q_i(k)$ is the error caused by the quantizer Q_i operating on $b_i \bar{x}_j(k)$ at the sampling instant $t = kT$. Similarly

$$Q_i \left\{ a_o \left[Q_j \left[b_\ell \bar{x}_m(k) \right] \right] \right\} = a_o b_\ell \bar{x}_m(k) + a_o q_j(k) + q_i(k).$$

Expanding Eq. (28) yields

$$\begin{aligned}
\bar{x}_1(k+1) &= \bar{x}_2(k) \\
\bar{x}_2(k+1) &= \bar{x}_3(k) \\
&\vdots \\
\bar{x}_{n-1}(k+1) &= \bar{x}_n(k) \\
\bar{x}_n(k+1) &= r(k) - \bar{c}(k) - \sum_{j=1}^n b_{n+1-j} \bar{x}_j(k) \\
&\quad + q_{10}(k) - \sum_{j=1}^n q_{1j} \\
\bar{e}_o(k) &= a_o \left[r(k) - \bar{c}(k) \right] + \sum_{j=1}^n (a_{n+1-j} - a_o b_{n+1-j}) \bar{x}_j(k) \\
&\quad + \sum_{j=1}^n q_{2j}(k) + q_{20}(k) - a_o \sum_{j=1}^n q_{1j}(k) + a_o q_{10}(k)
\end{aligned} \tag{29}$$

The quantized state equations for $H(z)$ is

$$\begin{aligned}
\bar{y}_1(k+1) &= \bar{y}_2(k) \\
\bar{y}_2(k+1) &= \bar{y}_3(k) \\
&\vdots \\
\bar{y}_1(k+1) &= Q \left[\bar{e}_o(k) \right] - \sum_{j=1}^{\ell} b'_{\ell+1-j} \bar{y}_j(k) \\
&= \bar{e}_o(k) - \sum_{j=1}^{\ell} b'_{\ell+1-j} \bar{y}_j(k) + q(k)
\end{aligned}$$

$$\begin{aligned}
\bar{c}(k) &= a'_o Q \left[\bar{e}_o(k) \right] + \sum_{j=1}^{\ell} (a'_{\ell+1-j} - a'_o b_{\ell+1-j}) \bar{y}_j(k) \\
&= a'_o \bar{e}_o(k) + \sum_{j=1}^{\ell} (a'_{\ell+1-j} - a'_o b_{\ell+1-j}) \bar{y}_j(k) + a'_o q(k)
\end{aligned} \tag{30}$$

Since the effect of quantization on the system response is of interest, we may define error variables as

$$\begin{aligned}
\gamma_i(k) &= \bar{x}_i(k) - x_i(k) \\
u(k) &= \bar{e}_o(k) - e_o(k) \\
\beta_i(k) &= \bar{y}_i(k) - y_i(k) \\
v(k) &= \bar{c}(k) - c(k)
\end{aligned} \tag{31}$$

Subtracting Eq. (25) from Eq. (29) and Eq. (27) from Eq. (30) yields

$$\begin{aligned}
\gamma_1(k+1) &= \gamma_2(k) \\
\gamma_2(k+1) &= \gamma_3(k) \\
&\vdots \\
\gamma_{n-1}(k+1) &= \gamma_n(k) \\
\gamma_n(k+1) &= -v(k) - \sum_{j=1}^n b_{n+1-j} \gamma_j(k) + q_{10}(k) - \sum_{j=1}^n q_{1j} \\
u(k) &= -a_o v(k) + \sum_{j=1}^n (a_{n+1-j} - a_o b_{n+1-j}) \gamma_j(k) \\
&\quad + \sum_{j=1}^n q_{2j}(k) + q_{20}(k) - a_o \sum_{j=1}^n q_{1j}(k) + a_o q_{10}(k)
\end{aligned}$$

$$\begin{aligned}
 \beta_1(k+1) &= \beta_2(k) \\
 \beta_2(k+1) &= \beta_3(k) \\
 &\vdots \\
 \beta_{\ell-1}(k+1) &= \beta_{\ell}(k) \\
 \beta_{\ell}(k+1) &= u(k) - \sum_{j=1}^{\ell} b'_{\ell+1-j} \beta_j(k) + q(k) \\
 v(k) &= a'_o u(k) + \sum_{j=1}^{\ell} (a'_{\ell+1-j} - a'_o b_{\ell+1-j}) \beta_j(k) + a'_o q(k)
 \end{aligned} \tag{32}$$

Taking the z-transformation and assuming zero initial conditions, Eq. (32) may be expressed as

$$\begin{aligned}
 z \Gamma_1(z) &= \Gamma_2(z) \\
 z \Gamma_2(z) &= \Gamma_3(z) \\
 &\vdots \\
 z \Gamma_{n-1}(z) &= \Gamma_n(z) \\
 z \Gamma_n(z) &= -V(z) - \sum_{j=1}^n b_{n+1-j} \Gamma_j(z) + Q_{10}(z) - \sum_{j=1}^n Q_{1j}(z) \\
 U(z) &= -a_o V(z) + \sum_{j=1}^n (a_{n+1-j} - a_o b_{n+1-j}) \Gamma_j(z) \\
 &\quad + \sum_{j=1}^n Q_{2j}(z) + Q_{20}(z) - a_o \sum_{j=1}^n Q_{1j}(z) + a_o Q_{10}(z)
 \end{aligned}$$

$$\begin{aligned}
z B_1(z) &= B_2(z) \\
z B_2(z) &= B_3(z) \\
&\vdots \\
z B_{\ell-1}(z) &= B_{\ell}(z) \\
z B_{\ell}(z) &= U(z) - \sum_{j=1}^{\ell} b'_{\ell+1-j} B_j(z) + Q(z) \\
V(z) &= a'_0 U(z) + \sum_{j=1}^{\ell} (a'_{\ell+1-j} - a'_0 b'_{\ell+1-j}) B_j(z) + a'_0 Q(z)
\end{aligned} \tag{33}$$

The steady state output error due to quantization can be obtained by simultaneously solving Eq. (33) for $V(z)$ and then by applying the final value theorem (i.e. $\lim_{k \rightarrow \infty} v(k) = \lim_{z \rightarrow 1} (1-z^{-1}) V(z)$)

For $a_0 = a'_0 = 0$

$$\begin{aligned}
\lim_{k \rightarrow \infty} v(k) &= \left(\sum_{i=1}^{\ell} a'_i \right) \left\{ \left(\sum_{i=1}^n a_i \right) \left(\lim_{k \rightarrow \infty} \sum_{i=0}^n q_{1i}(k) \right) + \right. \\
&\quad \left. \frac{\left(1 + \sum_{i=1}^n b_i \right) \lim_{k \rightarrow \infty} \left[\sum_{i=0}^n q_{2i}(k) + q(k) \right]}{\left(1 + \sum_{i=1}^n b_i \right) \left(1 + \sum_{i=1}^{\ell} b'_i \right) + \left(\sum_{i=1}^n a_i \right) \left(\sum_{i=1}^{\ell} a'_i \right)} \right\}
\end{aligned} \tag{34}$$

Note that the maximum value of any of the $q_i(k)$ cannot exceed one quantization granularity k_i . Therefore, the maximum steady state quantization error in the system output is:

$$\lim_{k \rightarrow \infty} v(k) = \frac{\left(\sum_{i=1}^{\ell} a'_i \right) \left\{ \left(\sum_{i=1}^n a_i \right) \left(\sum_{i=0}^n h_{1i} \right) + \left(1 + \sum_{i=1}^n b_i \right) \left(\sum_{i=0}^n h_{2i} + h \right) \right\}}{\left(1 + \sum_{i=1}^n b_i \right) \left(1 + \sum_{i=1}^{\ell} b'_i \right) + \left(\sum_{i=1}^n a_i \right) \left(\sum_{i=1}^{\ell} a'_i \right)} \quad (35)$$

2.6.3 Quantization Error for Direct Form

An upper bound on the steady state quantization error for the digital system programmed in the direct form can be obtained using a similar technique. A general block diagram of the direct programming form of a digital system whose transfer function is characterized by Eq. (21) was presented in Fig. 2-7. From Fig. 2-7, the state equations can be written as

$$\begin{bmatrix} x_1(k+1) \\ x_2(k+1) \\ \vdots \\ x_{n-1}(k+1) \\ x_n(k+1) \\ \\ x_{n+1}(k+1) \\ x_{n+2}(k+1) \\ \vdots \\ x_{2n-1}(k+1) \\ x_{2n}(k+1) \end{bmatrix} = \begin{bmatrix} 0 & 1 & 0 & \dots & 0 & 0 \\ 0 & 0 & 1 & \dots & 0 & 0 \\ \vdots & & & & & \\ \vdots & & & & & \\ 0 & 0 & 0 & \dots & 0 & 1 \\ 0 & 0 & 0 & \dots & 0 & 0 \\ \\ 0 & 1 & 0 & \dots & 0 & 0 \\ 0 & 0 & 1 & \dots & 0 & 0 \\ \vdots & & & & & \\ \vdots & & & & & \\ 0 & 0 & 0 & \dots & 0 & 1 \\ 0 & 0 & 0 & \dots & 0 & 0 \end{bmatrix} \begin{bmatrix} x_1(k) \\ x_2(k) \\ \vdots \\ x_{n-1}(k) \\ x_n(k) \\ \\ x_{n+1}(k) \\ x_{n+2}(k) \\ \vdots \\ x_{2n-1}(k) \\ x_{2n}(k) \end{bmatrix} + \begin{bmatrix} 0 \\ 0 \\ \vdots \\ \vdots \\ 1 \\ \\ 0 \\ 0 \\ \vdots \\ \vdots \\ 0 \\ 0 \end{bmatrix} e_i(k) + \begin{bmatrix} 0 \\ 0 \\ \vdots \\ \vdots \\ 0 \\ 0 \\ 0 \\ 0 \\ \vdots \\ \vdots \\ 0 \\ 1 \end{bmatrix} e_0(k) \quad (36)$$

or

$$\underline{x}(k+1) = \underline{E} \underline{x}(k) + \underline{F} e_i(k) + \underline{G} e_o(k) \quad (37)$$

where \underline{E} , \underline{F} and \underline{G} are defined by the equivalence of Eqs. (24) and (25). The output $e_o(k)$ of the direct programming form is

$$e_o(k) = \sum_{i=1}^n a_i x_{(n+1)-i}(k) - \sum_{i=1}^n b_i x_{(2n+1)-i}(k) + a_o e_i(k) \quad (38)$$

Now the effect of signal and coefficient quantization on system performance will be considered. The digital system with quantizers is shown in Fig. 2-15. Let $\bar{x}(k)$ represent the state of the digital system with quantization included. Then the state equations of the system are

$$\bar{x}(k+1) = \underline{E} \bar{x}(k) + \underline{F} Q_{10} [e_i(k)] + \underline{G} \bar{e}_o(k) \quad (39)$$

$$\begin{aligned} \bar{e}_o(k) = & \sum_{i=1}^n Q_{2i} [a_i \bar{x}_{(n+1)-i}(k)] - \sum_{i=1}^n Q_{1i} [b_i \bar{x}_{(2n+1)-i}(k)] \\ & + Q_{20} [a_o Q_{10} [e_i(k)]] \end{aligned}$$

Expanding Eq. (39)

$$\begin{aligned} \bar{x}(k+1) = & \underline{E} \bar{x}(k) + \underline{F} e_i(k) + \underline{G} \bar{e}_o(k) + \underline{F} q_{10}(k) \\ \bar{e}_o(k) = & \sum_{i=1}^n a_i \bar{x}_{(n+1)-i}(k) - \sum_{i=1}^n b_i \bar{x}_{(2n+1)-i}(k) + a_o e_i(k) \\ & + \sum_{i=0}^n q_{2i}(k) - \sum_{i=1}^n q_{1i}(k) + a_o q_{10}(k) \end{aligned} \quad (40)$$

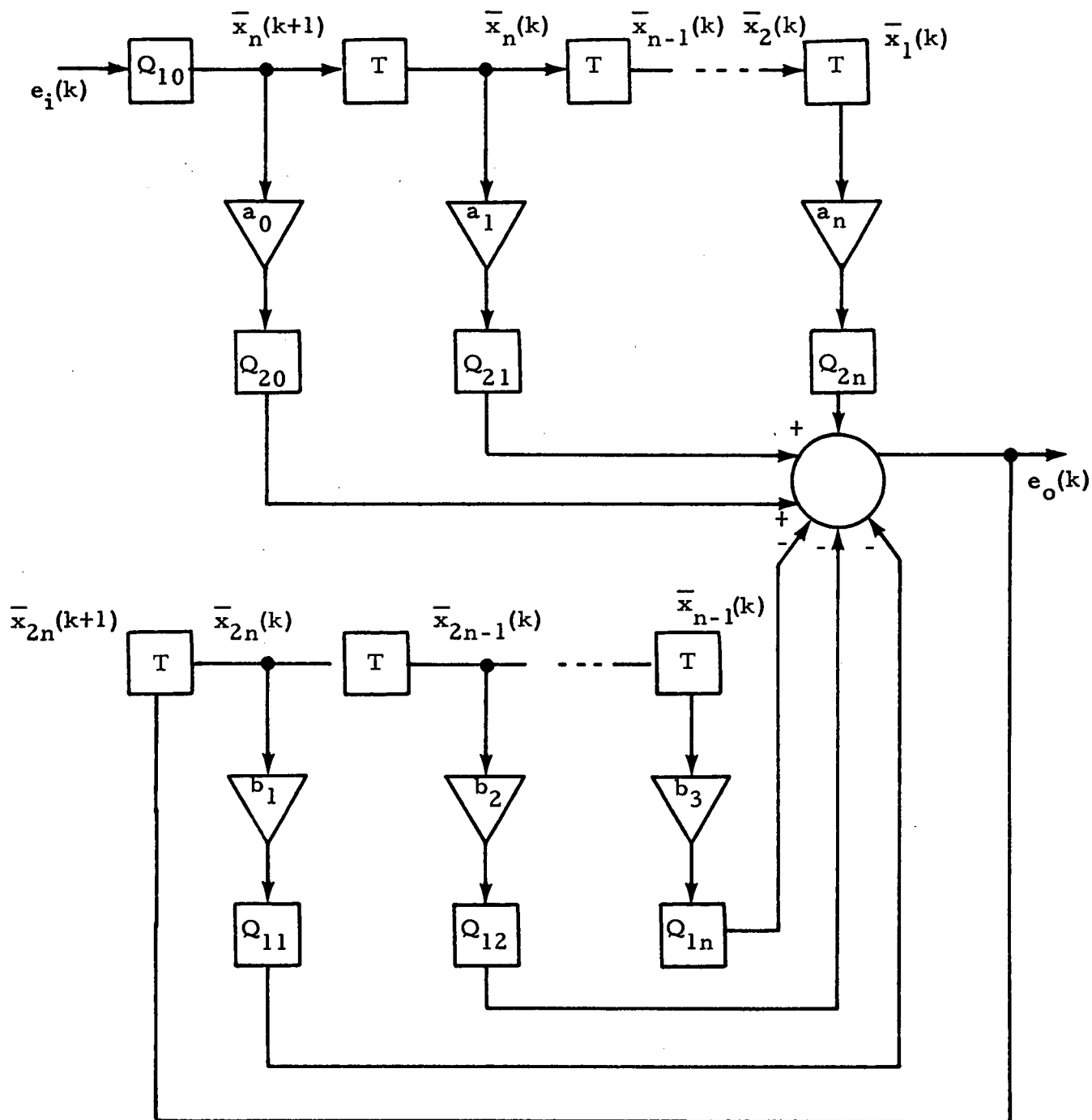


Fig. 2-15 - Direct Programming Form with Quantizers

Let

$$\underline{\gamma}(k) = \underline{\bar{x}}(k) - \underline{x}(k) \quad . \quad (41)$$

and

$$u(k) = \bar{e}_o(k) - e_o(k) \quad .$$

From Eqs. (37), (38), (40) and (24), the following system error equations are obtained

$$\underline{\gamma}(k+1) = \underline{E} \underline{\gamma}(k) + \underline{G} u(k) + \underline{F} q_{10}(k) - \underline{F} v(k) \quad (42)$$

$$\begin{aligned} u(k) &= \sum_{i=1}^n a_i \gamma_{(n+1)-i}(k) - \sum_{i=1}^n b_i \gamma_{(2n+1)-i}(k) - a_o v(k) \\ &+ \sum_{i=0}^n q_{2i}(k) - \sum_{i=1}^n q_{1i}(k) + a_o q_{10}(k) \end{aligned}$$

The quantization error in the system output can be obtained by taking the z-transformation of Eq. (42)

$$z \underline{\Gamma}(z) = \underline{E} \underline{\Gamma}(z) + \underline{G} U(z) + \underline{F} Q_{10}(z) - \underline{F} V(z) \quad (43)$$

$$\begin{aligned} U(z) &= \sum_{i=1}^n a_i \Gamma_{(n+1)-i}(z) - \sum_{i=1}^n b_i \Gamma_{(2n+1)-i}(z) - a_o V(z) \\ &+ \sum_{i=0}^n Q_{2i}(z) - \sum_{i=1}^n Q_{1i}(z) + a_o Q_{10}(z) \end{aligned}$$

Together with the corresponding error equations for $H(z)$ (from Eq. (33)), the steady state output error due to quantization for the direct programming form can be obtained. For $a_0 = a'_0 = 0$, the maximum steady state quantization error in the system output for the direct programming form is

$$\lim_{k \rightarrow \infty} v(k) = \frac{\left(\sum_{i=1}^{\ell} a'_i \right) \left[\sum_{i=1}^n a_i h_{10} + \sum_{i=0}^n h_{2i} + \sum_{i=1}^n h_{1i} + \left(1 + \sum_{i=1}^n b_i \right) h \right]}{\left(1 + \sum_{i=1}^n b_i \right) \left(1 + \sum_{i=1}^{\ell} b'_i \right) + \left(\sum_{i=1}^n a_i \right) \left(\sum_{i=1}^{\ell} a'_i \right)} \quad (44)$$

Comparing Eq. (44) with Eq. (35) shows that the canonical programming form gives less quantization error than the direct form for those cases shown in Table 2-1 on page 10 if all the quantizers have the same quantization granularity. Note that h is a function of digital word length and the coefficients a , b , a' and b' are functions of sampling rate and system time constants; therefore, Eqs. (35) and (44) may be used to estimate the digital word length and sampling rate required to achieve a given system specification.

2.7 ANALYTICAL DESCRIPTION OF DIODE BRIDGE CIRCUIT*

The nonlinear circuit consists of a diode bridge and an integrating amplifier with an input capacitance C equal to the feedback capacitance as shown in Fig. 2-16.

2.7.1 Amplifier Transfer Function

Let z be the input voltage to the capacitance C of the amplifier with grid voltage e_g and gain factor K , then

* Acknowledgement is made to Dr. W. Trautwein of Lockheed-Huntsville for the analytical description of the diode bridge.

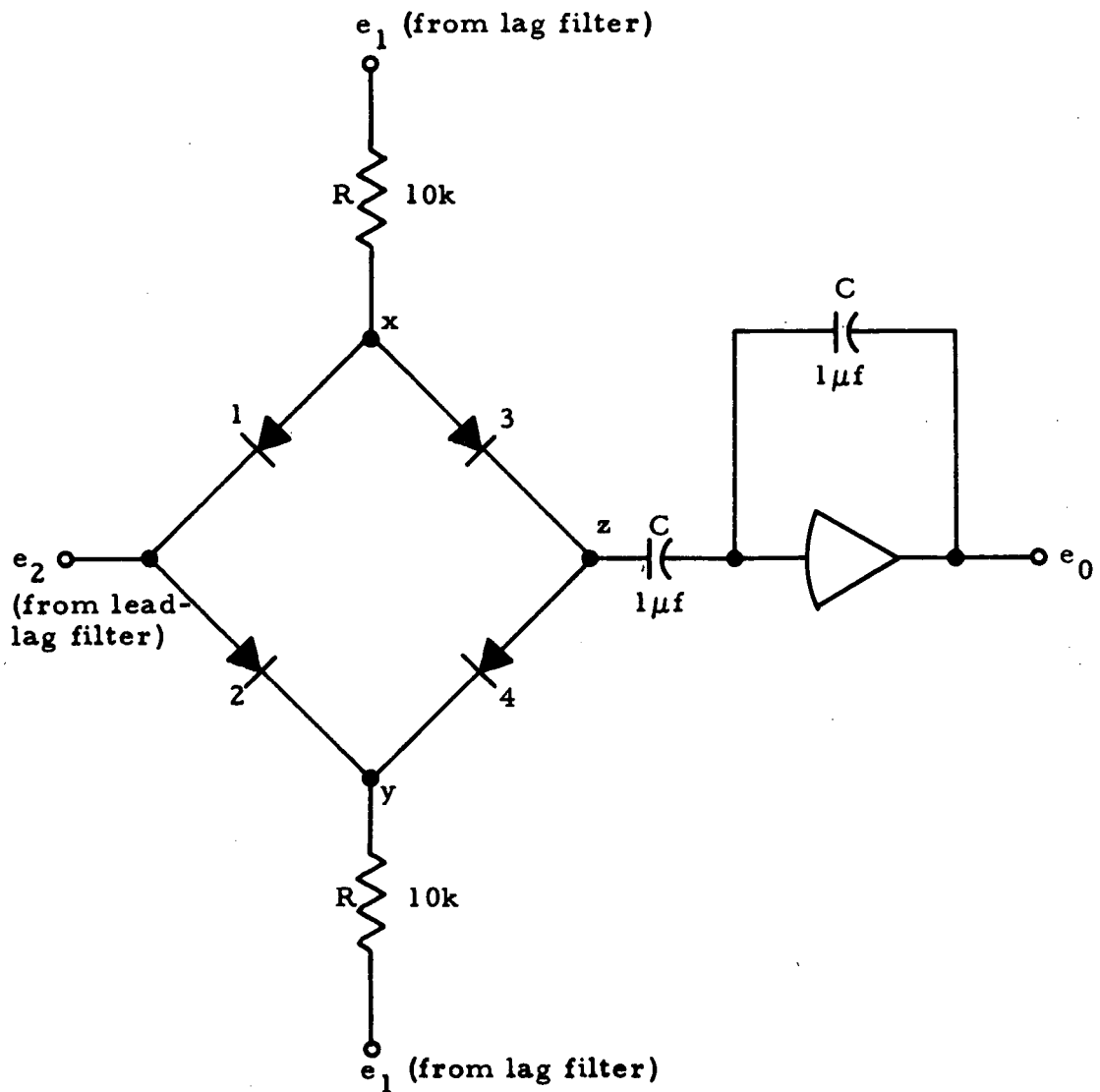


Fig.2-16 - Nonlinear Part of Cutoff Filter

$$C \frac{d}{dt} (z - e_g) = -C \frac{d}{dt} (e_0 - e_g)$$

and

$$e_0 = -K e_g$$

Substituting yields

$$\frac{d}{dt} \left(z + \frac{e_0}{K} \right) = - \frac{d}{dt} \left(e_0 + \frac{e_0}{K} \right)$$

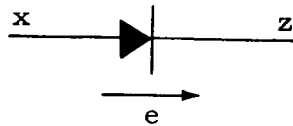
For K large, we obtain

$$e_0 \approx -z$$

i.e., the amplifier acts like an inverter.

2.7.2 Diode Operation

It is assumed that the bridge diodes have ideal switching characteristics that can be described by



$$R = \begin{cases} \infty & \text{if } e < 0 \\ 0 & \text{if } e \geq 0 \end{cases}$$

where e is the voltage across the diode.

2.7.3 Diode Bridge Switching Logic

The switching logic is governed by the respective values of the input voltages (e_1, e_2) and the bridge output z .

There exist six different conditions for the diodes which result in three different bridge outputs z as listed in Table 2-3.

Table 2-3
BRIDGE OUTPUT AS A FUNCTION OF RESPECTIVE
INPUT AND OUTPUT VOLTAGES

Case No.	Input-Output Voltage Relation	Resulting Diode States				Resulting Bridge Voltages		Resulting Bridge Output
		Diode No.				x	y	
		1	2	3	4			
1a	$e_2 > e_1 \geq z$	N	C	C	N	e_1	e_2	$z = e_1$
1b	$z \geq e_1 > e_2$	C	N	N	C	e_2	e_1	$z = e_1$
2a	$e_1 > e_2 \geq z$	C	N	C	N	e_2	e_1	$z = e_2$
2b	$z \geq e_2 > e_1$	N	C	N	C	e_1	e_2	$z = e_2$
3a	$e_1 \geq z > e_2$	C	N	N	N	e_2	e_1	$z = z(0)$
3b	$e_2 > z \geq e_1$	N	C	N	N	e_1	e_2	$z = z(0)$

C = conducting; N = nonconducting

Note that both Diodes 3 and 4 are blocked in Case 3 which makes it impossible for the capacitor to discharge. This results in a "hold"-type bridge output in Case 3. The value $z(0)$ in Table 2-3 is to be taken at the most recent switching time of the diodes.

The complete bridge plus capacitor plus amplifier signal transfer can now be described by the relationship:

$$e_0 = -z = \begin{cases} -e_1 & \text{if } e_2 > e_1 \geq z(0) \\ & \text{or } z(0) \geq e_1 > e_2 \\ -e_2 & \text{if } e_1 > e_2 \geq z(0) \\ & \text{or } z(0) \geq e_2 > e_1 \\ -z(0) & \text{if } e_1 \geq z(0) > e_2 \\ & \text{or } e_2 > z(0) \geq e_1 \end{cases} \quad (45)$$

Equation (45) can be readily programmed for a digital computer by a number of logical decisions; e.g.,

$AMX = AMAX1(e1, e2)$

$AMN = AMIN1(e1, e2)$

If $(Z \cdot GT \cdot AMX)$ $e0 = -AMX$

If $(Z \cdot LT \cdot AMN)$ $e0 = -AMN$

Section 3

HIGH FREQUENCY CUTOFF FILTER PERFORMANCE

3.1 ANALOG FILTER PERFORMANCE

The analog realization of the cutoff filter is analyzed to determine its input-output characteristics. This analysis included the dc input plus high frequency signal.

3.1.1 DC Signal Only

An analog simulation of this filter is shown in Fig. 3-1. The primary reason for conducting this experiment was to test the dc characteristics of a circuit with an amplifier using capacitive input and feedback elements. As one may see from the test results, the filter performs at dc quite satisfactorily. The various results are shown in Figs. 3-2 and 3-3.

TEST PROCEDURE

The analog circuit of Fig. 3-1 was simulated using the parameter values shown in Table 3-1. The dc input-output characteristics were found by two methods, slope input and step input.

Table 3-1

PARAMETER VALUES USED IN THE SIMULATION OF FIG. 3-1

$\frac{1}{2\pi} \omega_c = 0.50 \text{ Hz}$	$\zeta_1 = 0.45$
$\frac{1}{2\pi} \omega_1 = 0.75 \text{ Hz}$	$\zeta_2 = 0.55$
$\frac{1}{2\pi} \omega_2 = 1.00 \text{ Hz}$	



- LMSC-HREC D225642-II

Fig. 3-1 - Analog Simulation Diagram for HFCF Filter

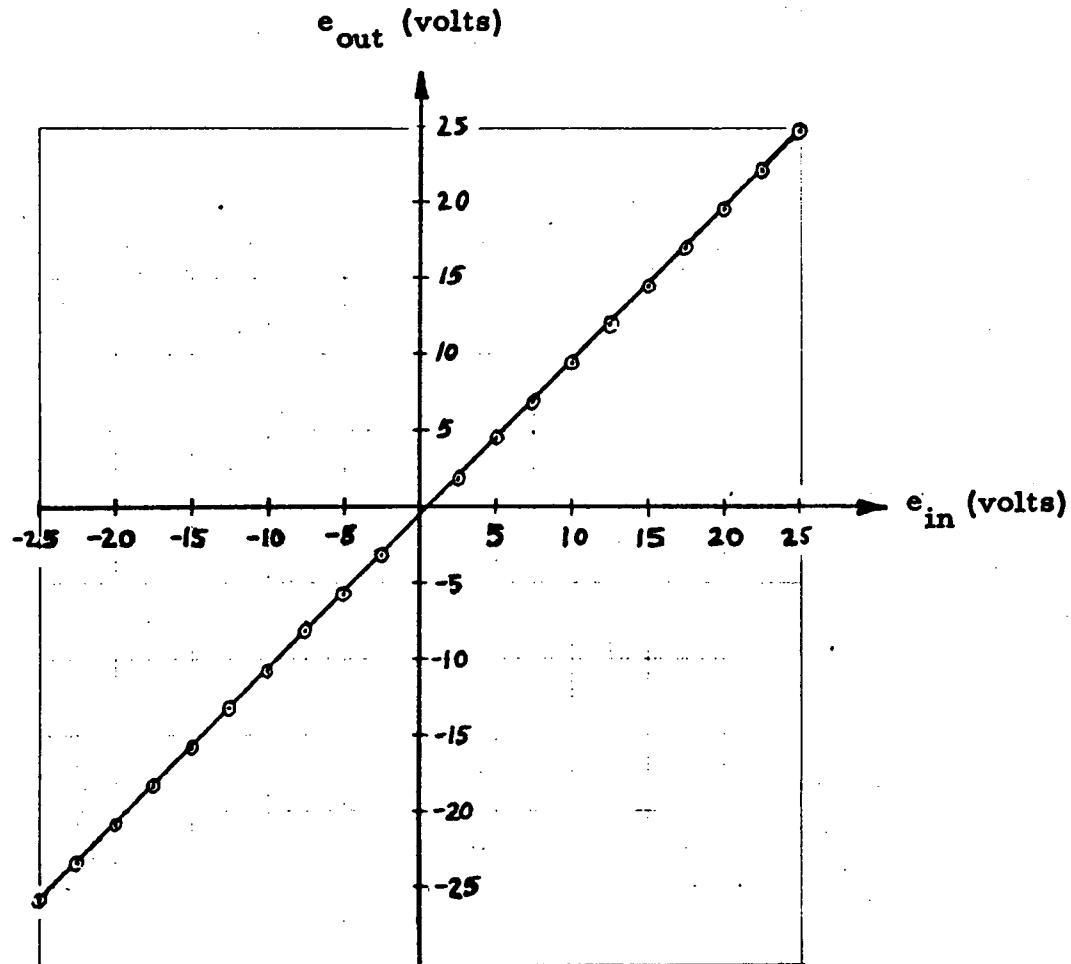


Fig. 3-2 - Input-Output Characteristics of the Cutoff Filter

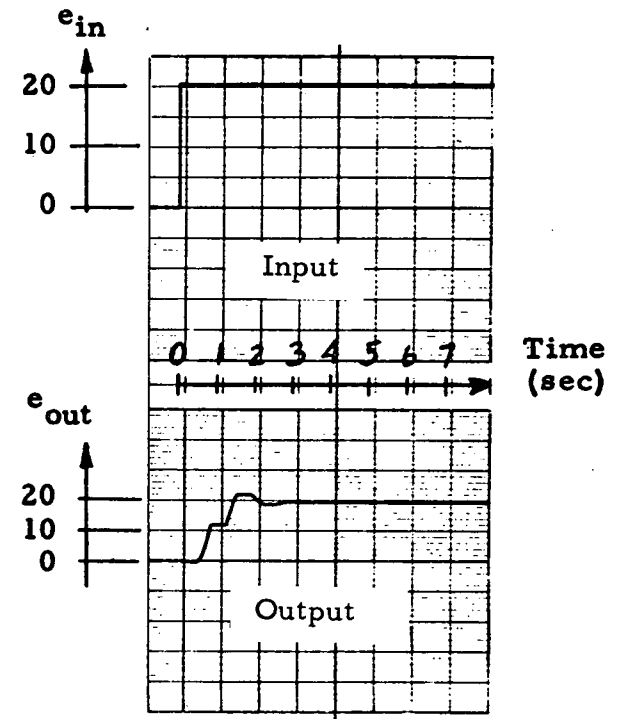


Fig. 3-3 - Step Function Response of the Cutoff Filter for Filter Parameters Shown in Table 3-1

Slope Input Test

The input to the circuit was made to follow a ramp function from -25 volts to +25 volts in approximately 520 seconds. The output, after an initial transient, was also a ramp function, slightly delayed, and of almost equal magnitude. It was thus ascertained that the dc operation of the filter was approximately linear.

Step Input Test

To construct an input-output curve of the filter (shown in Fig. 3-2), a series of step function inputs was made to the filter. These inputs were varied from -25 volts to +25 volts in 2.5 volt intervals. The outputs were obtained and the steady-state output values were recorded by a digital voltmeter print-out. These input-output voltages are the points shown in Fig. 3-2. As may be seen, a constant dc offset of -0.05 volts was encountered. The step function response is shown in Fig. 3-3 for an input of 20 volts. The transient response shows that the filter clips oscillations in the same way as in previous high-frequency tests (Ref. 1). The particular rise time, settling time, etc., of the step response in Fig. 3-3 is of course a function of the parameters chosen and given in Table 3-1. The step response could obviously be altered by varying these parameters within the bounds given in Fig. 2-1.

3.1.2 DC Plus High Frequency Signal

In the previous section, the results of dc input-output characteristics of a high-frequency cut-off filter were presented. These characteristics indicated a linear relationship between input and output dc levels. The question arises, will this relationship remain linear if the filter is subjected to an input consisting of dc plus a high frequency sinusoid whose amplitude is greater than the dc level. The answer was determined to be negative. In order to maintain the desired linear relationship, it is necessary that the dc level be greater in amplitude than the negative peak value of the time varying input. This is easily accomplished, however, as indicated by the block diagram of Fig. 3-4, which illustrates a modification of the cut-off filter which allows the

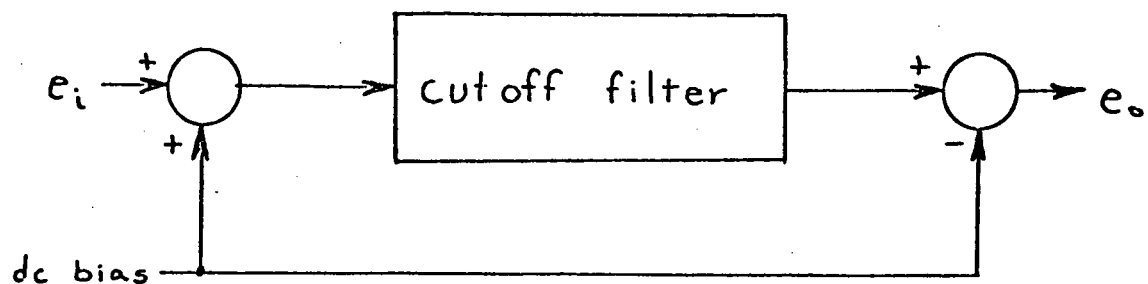


Fig. 3-4 - Modified Cut-off Filter Representation.

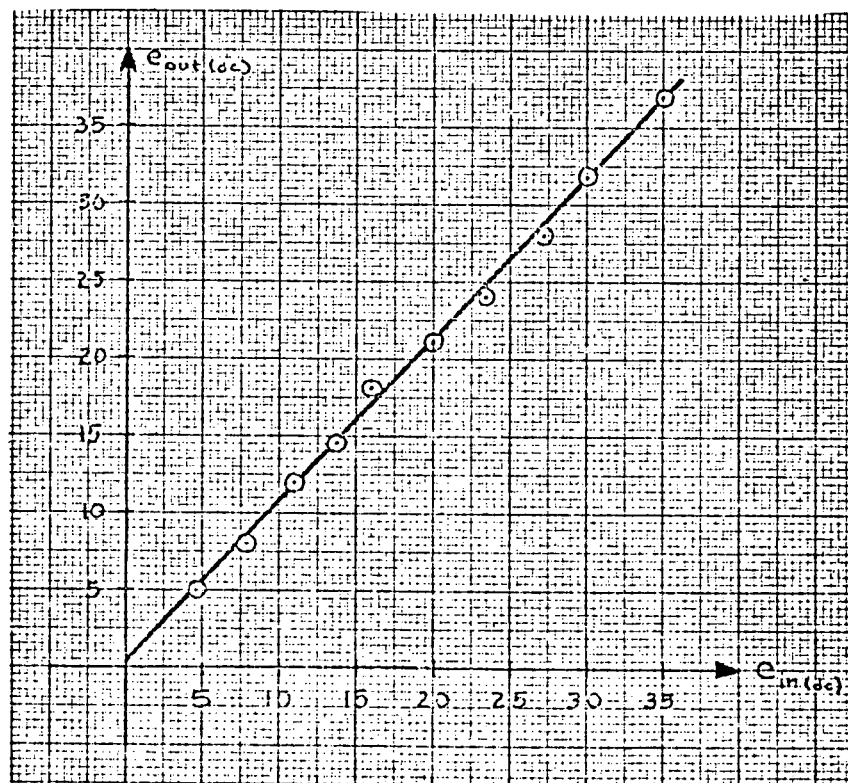


Fig. 3-5 - DC Input-Output Characteristic of Modified Cut-off Filter with $e_i = e_{in}(dc) + 10\sin\omega t$ volts, dc bias = 25 volts.

dc transfer function to be held essentially constant (as shown in Fig. 3-5). Some error was introduced to the data plotted in Fig. 3-5 by the necessity to read values from strip chart recordings, which are reproduced in Fig. 3-6. The requirement that the dc bias signal be chosen to maintain a positive waveform into the original filter is not restrictive and very much simplifies a describing function approach to analysis since the number of possible input cases is then reduced by one half.

3.2 DIGITAL FILTER PERFORMANCE

A flow chart of the digital program for the high frequency cutoff filter is shown in Fig. 3-7. The linear filter networks are programmed in the canonical form.

The program has the capability to read in sampling period, cutoff frequency, filter frequencies and damping ratios. It then calculates the corresponding HFCF coefficients, frequency characteristics of both continuous filter and digitized filter, and time responses for different inputs. Both the frequency response and time response subroutines of the program contain plot routines.

3.2.1 Transient Response

Figures 3-8 through 3-17 show the transient response of the digital high frequency cutoff filter for various combinations of ζ_1 and ζ_2 . The purpose of this is to study the effect of damping ratio upon the transient response of the filter. The figures show that the amount of overshoot depends on the damping ratios ζ_1 and ζ_2 . If one of the ζ is critically damped, i.e., damping ratio equal to one, there is no or little overshoot. If both ζ_1 and ζ_2 are underdamped, i.e., damping ratios less than one, overshoot occurs. The peak overshoot is the first overshoot. The output also oscillates around the final value. The overdamped system is slow-acting but does not oscillate about the final value. The underdamped system reaches the final value faster than the overdamped case, but the response oscillates about the final value. The amount of permissible

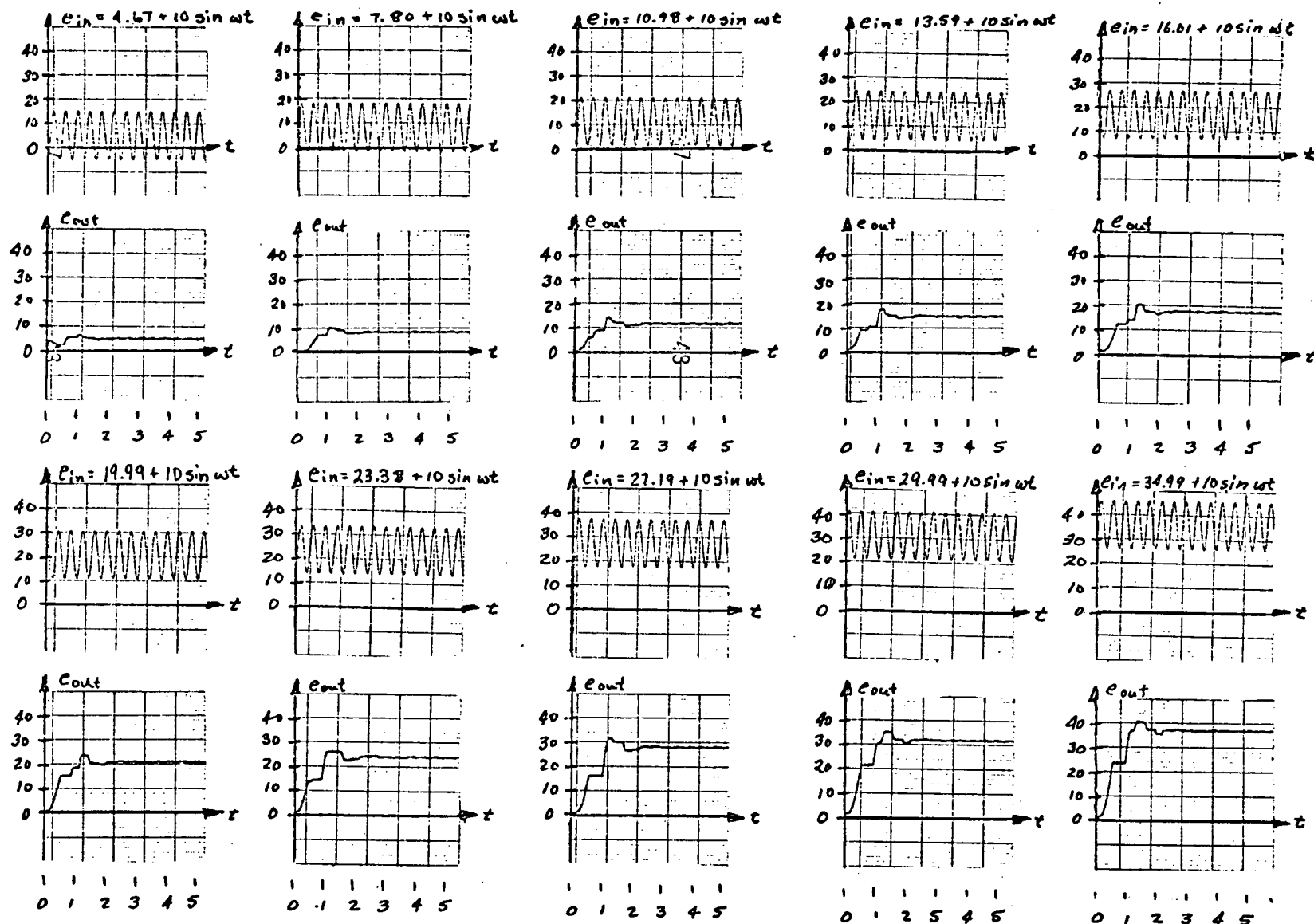


Fig. 3-6 - Responses to step input plus sinusoid, for $\omega = 5\pi$ and $\omega_c = \pi$, with $e_{bias} = 25$ volts

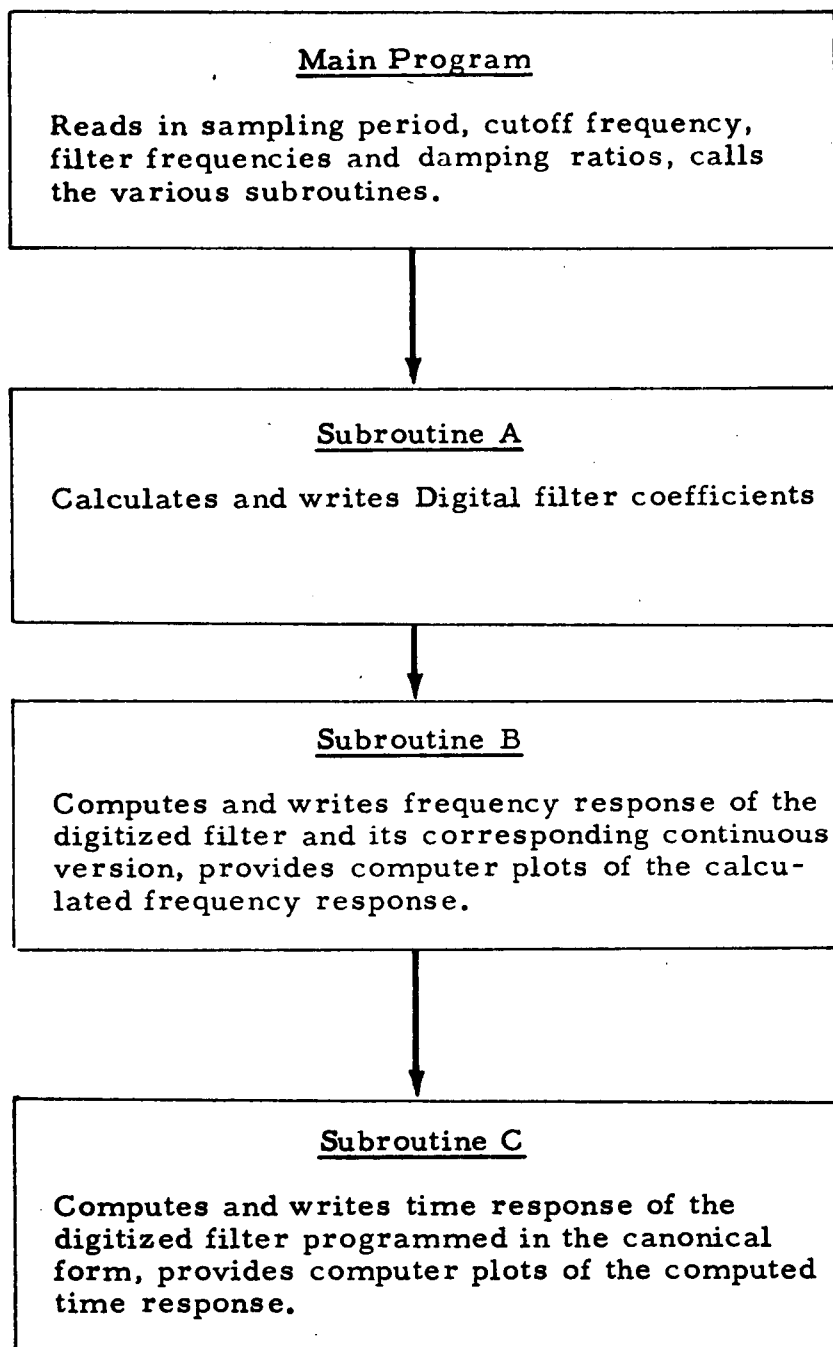


Fig. 3-7 - Flow Chart of Digital Program to Calculate HFCE Coefficients, Frequency Characteristics and Time Responses

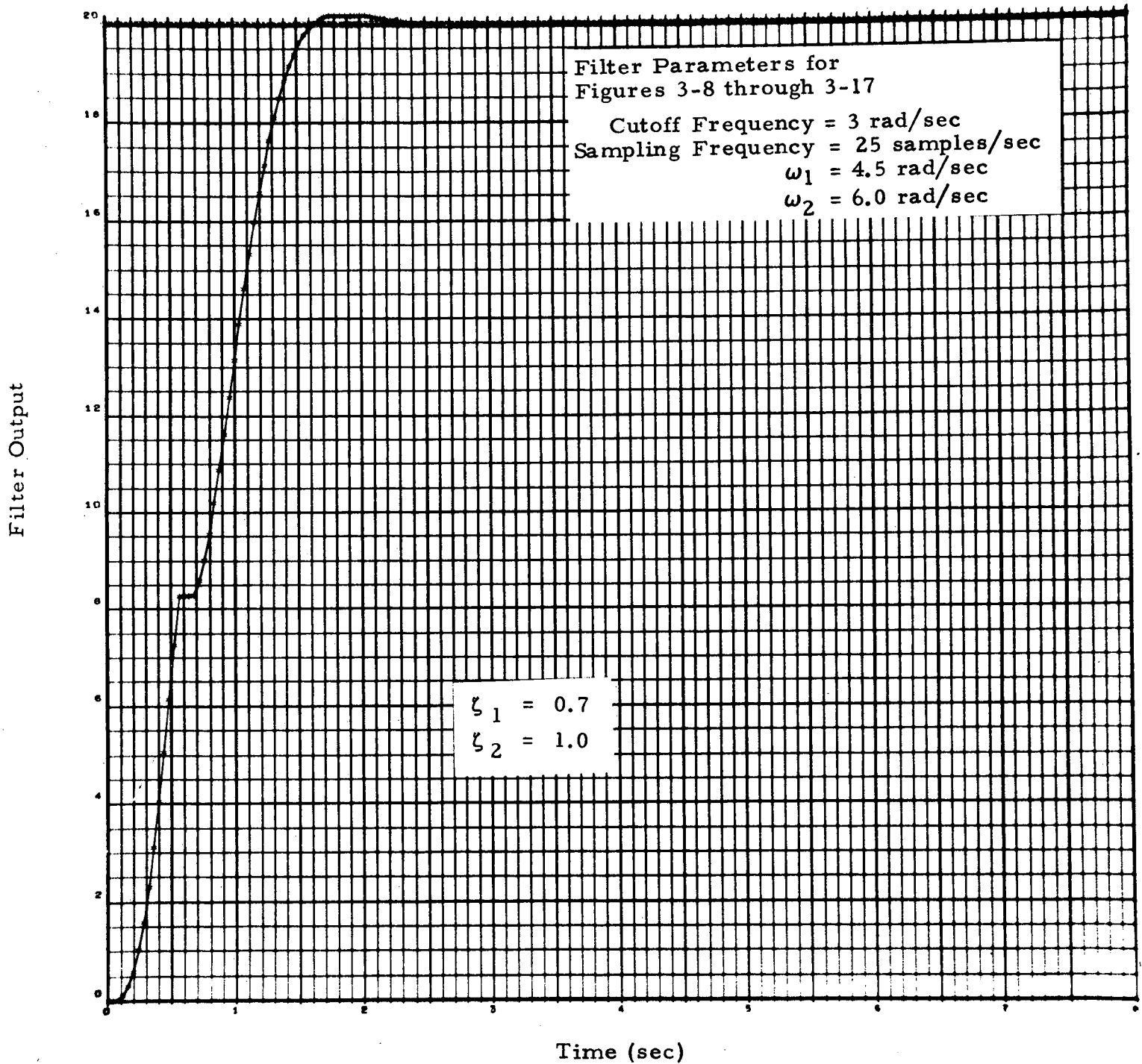


Fig. 3-8 - Time Response of Digital Filter
(Step Input = 20 at $t \geq 0$)

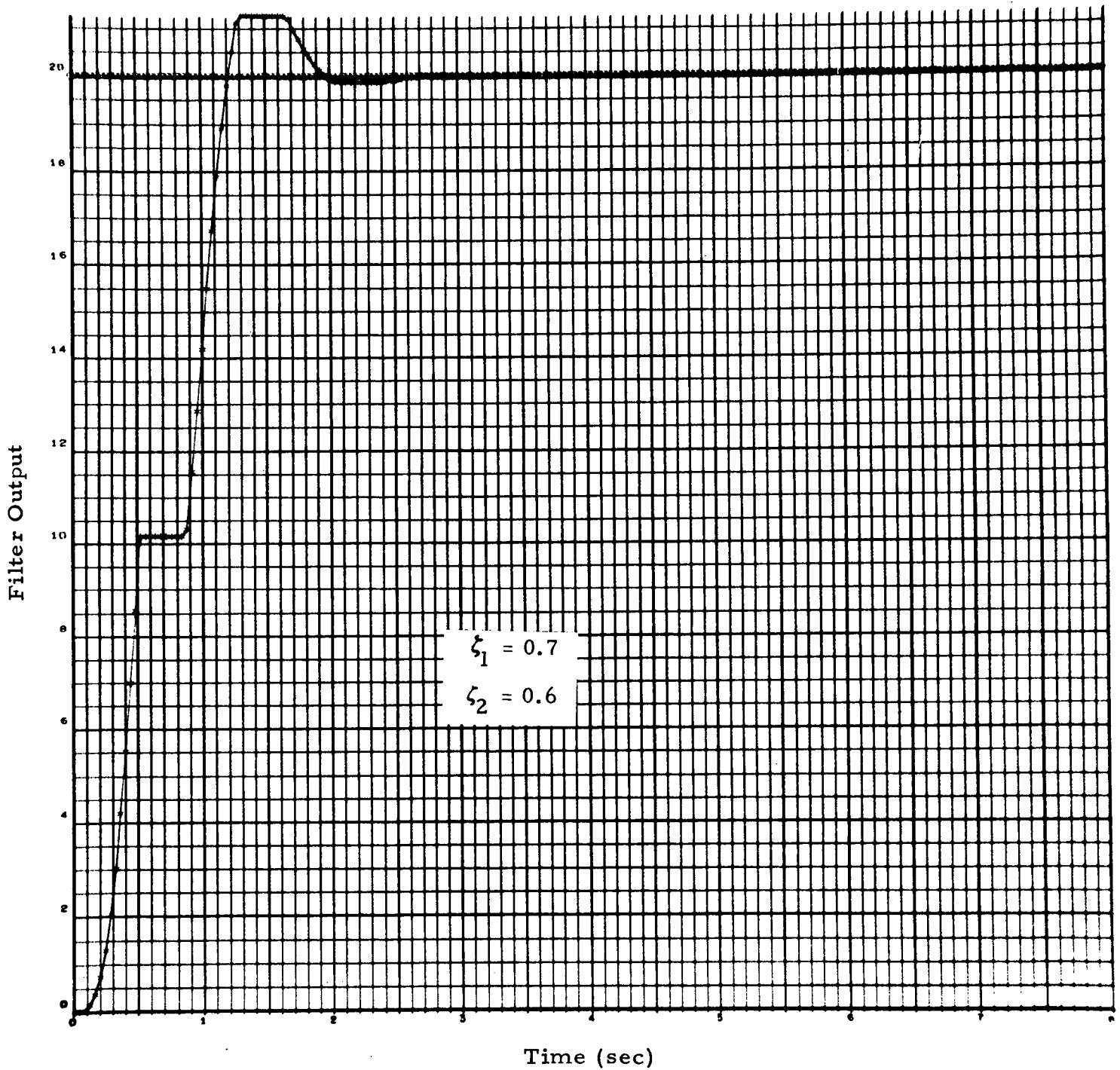


Fig. 3-9 - Time Response of Digital Filter (Step input = 20
at $t \geq 0$)

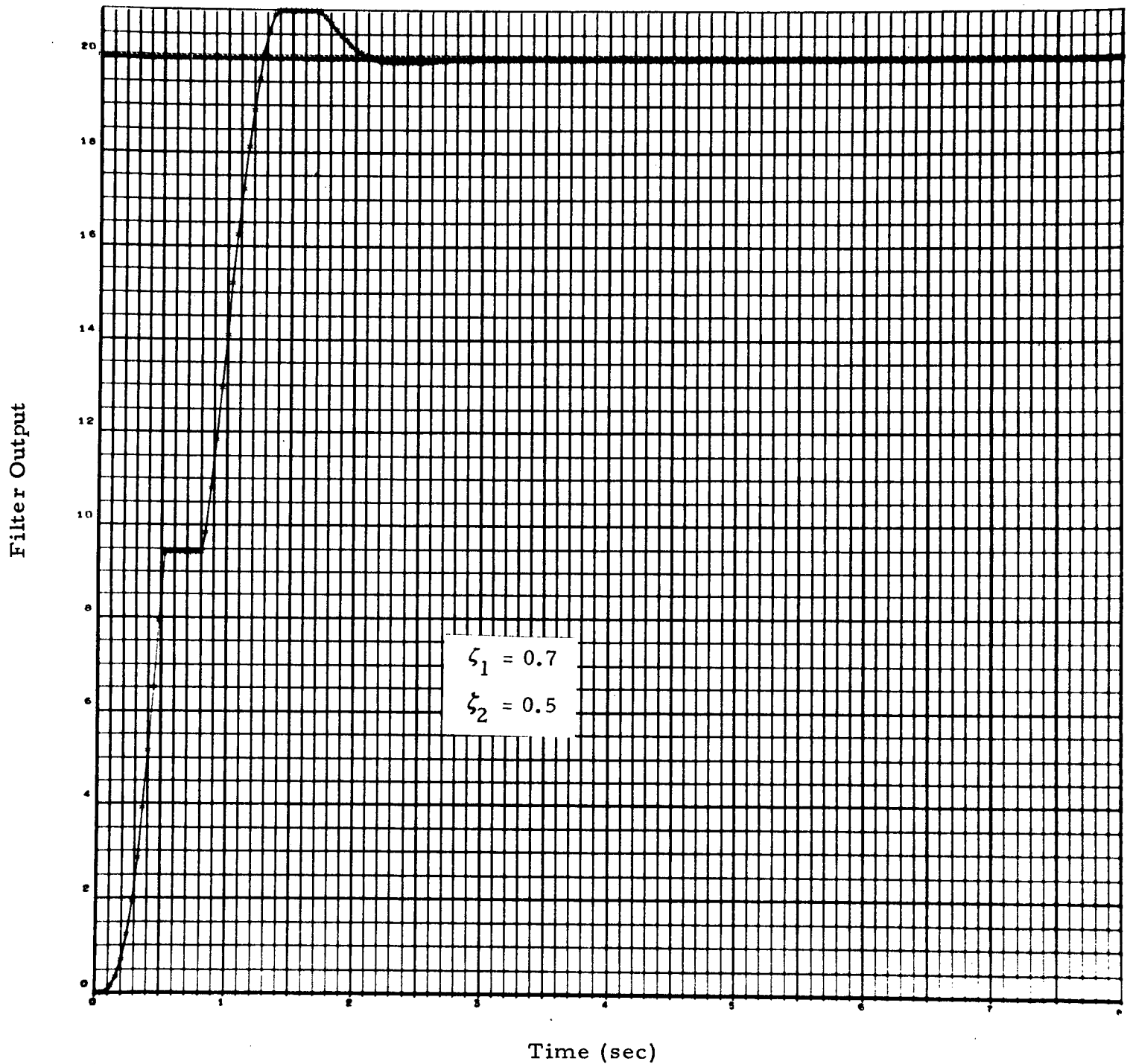


Fig. 3-10 - Time Response of Digital Filter (Step input = 20 at $t \geq 0$)

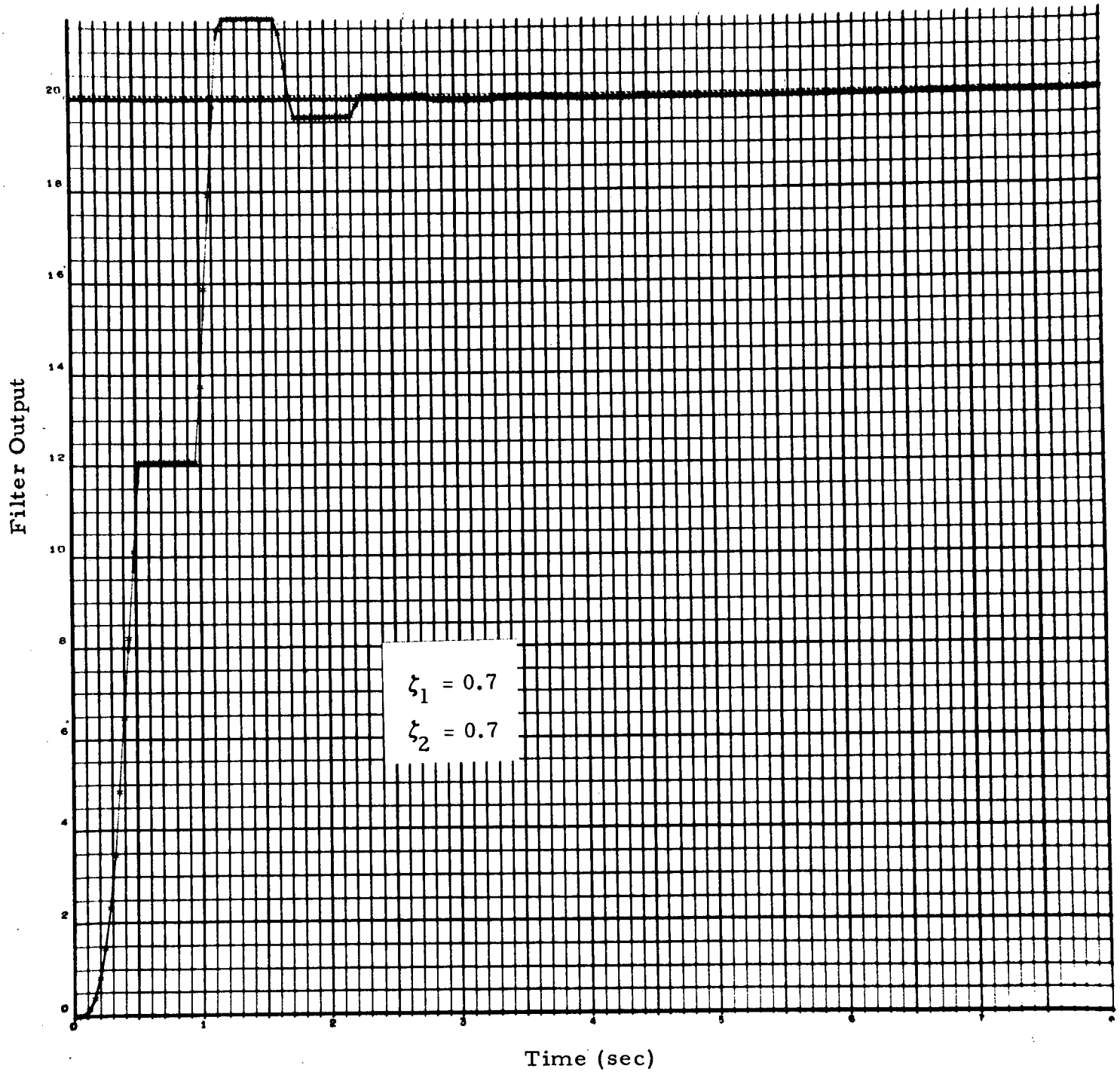


Fig. 3-11 - Time Response of Digital Filter (Step input = 20 at $t \geq 0$)

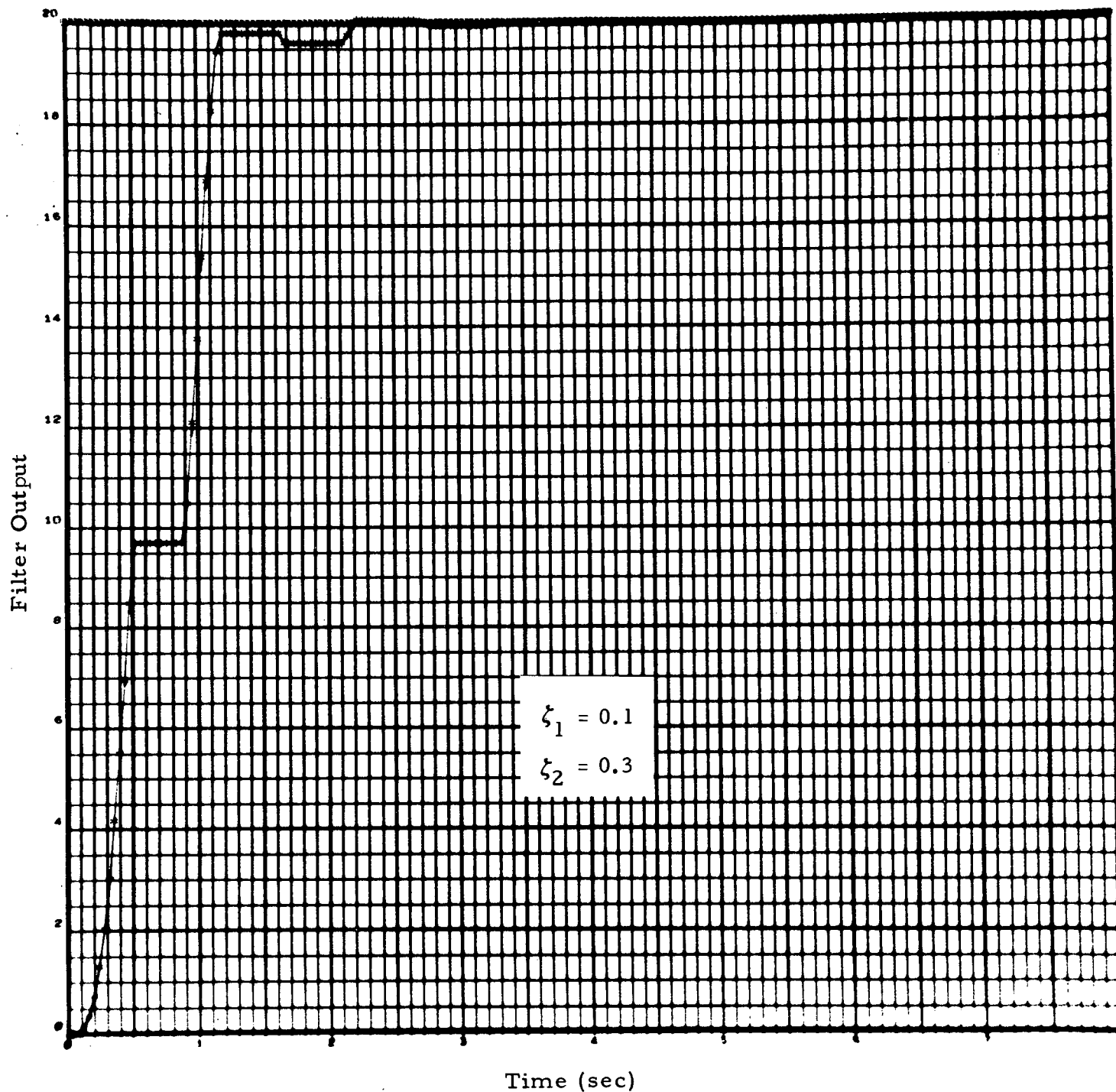


Fig. 3-12 - Time Response of Digital Filter (Step input = 20 at $t \geq 0$)

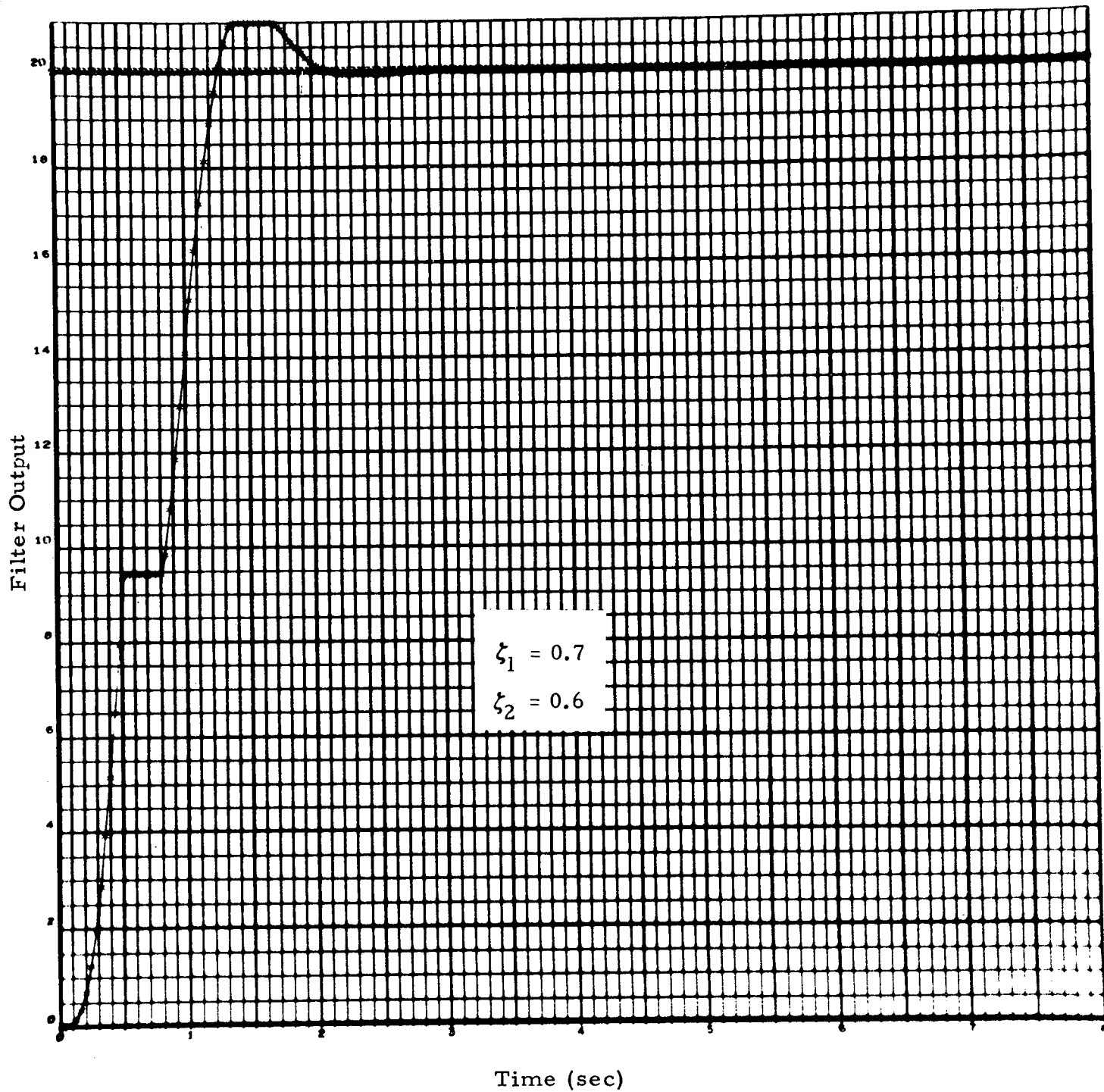


Fig. 3-13 - Time Response of Digital Filter (Step input = 20
at $t \geq 0$)

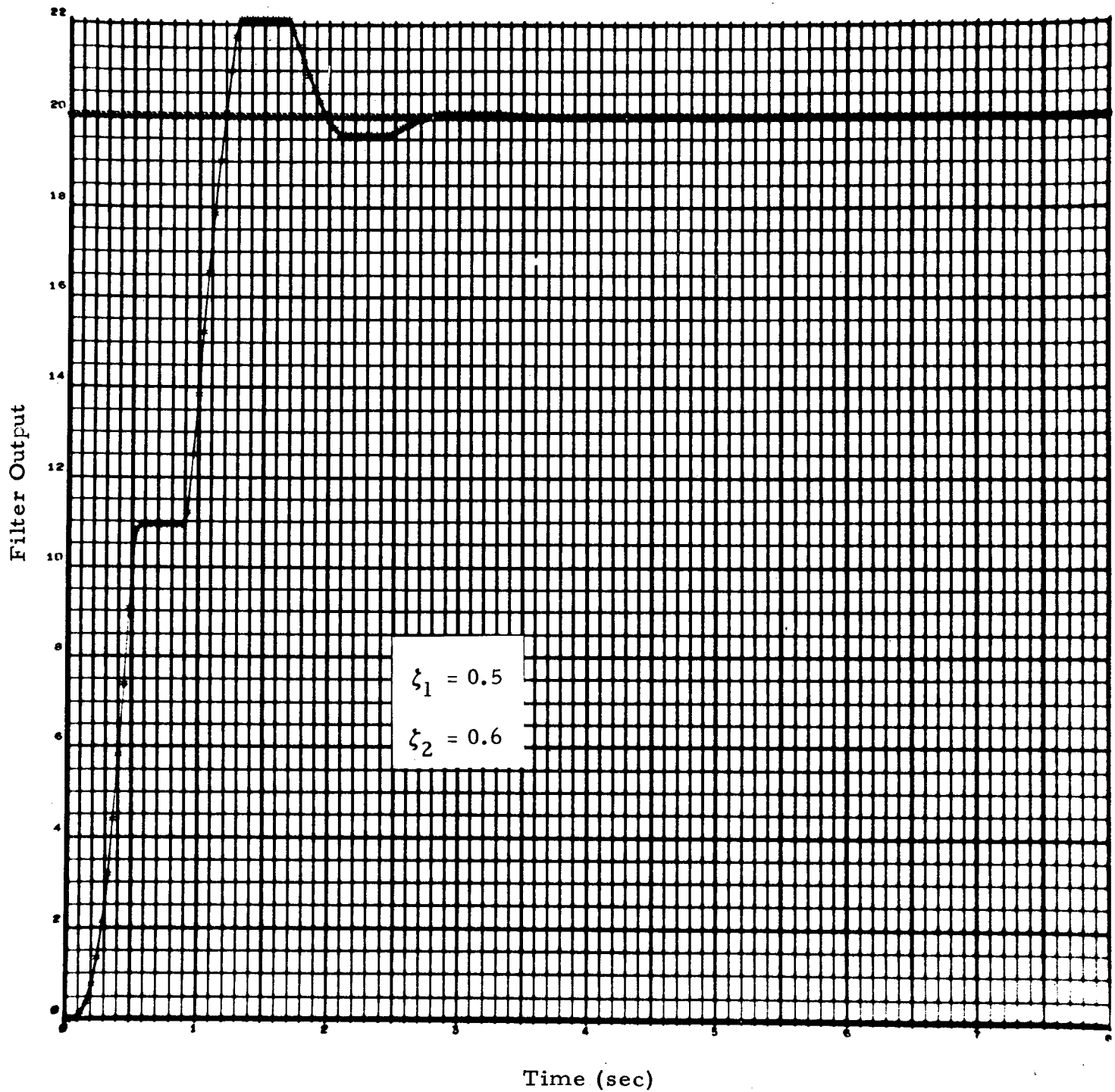


Fig. 3-14 - Time Response of Digital Filter
 (Step Input = 20 at $t \geq 0$)

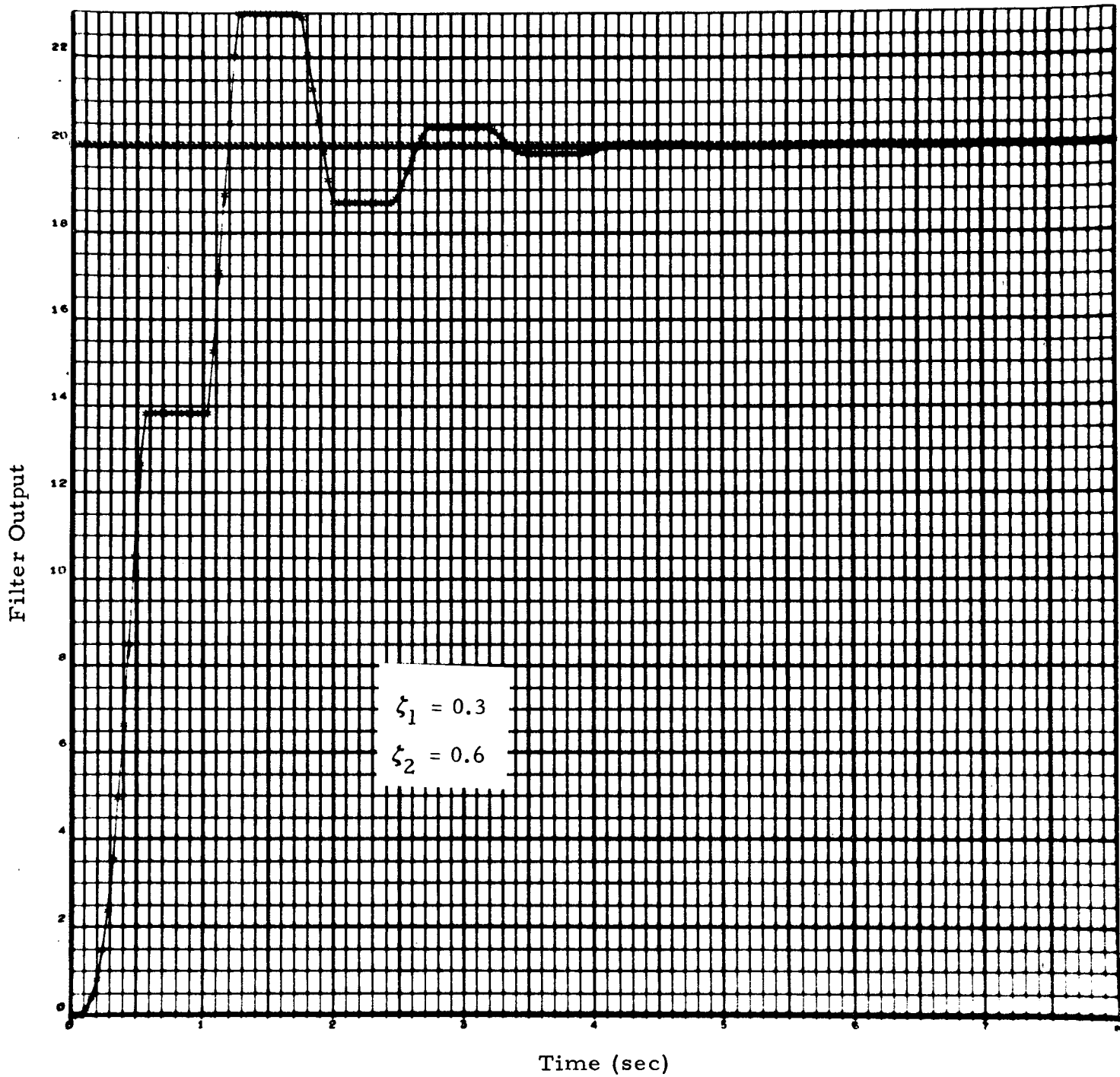


Fig.3-15 - Time Response of Digital Filter
(Step Input = 20 at $t \geq 0$)

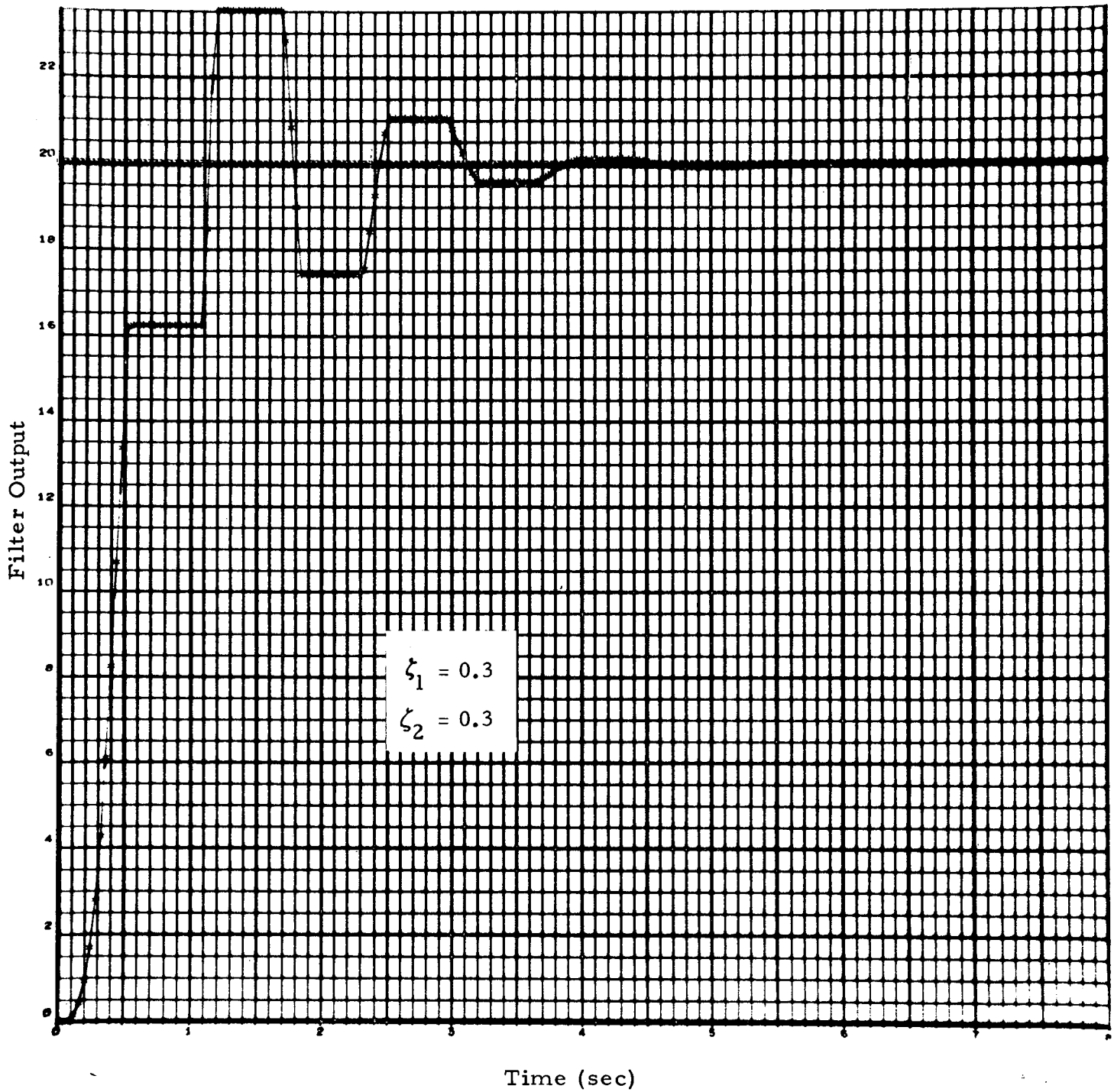


Fig.3-16 - Time Response of Digital Filter
(Step Input = 20 at $t \geq 0$)

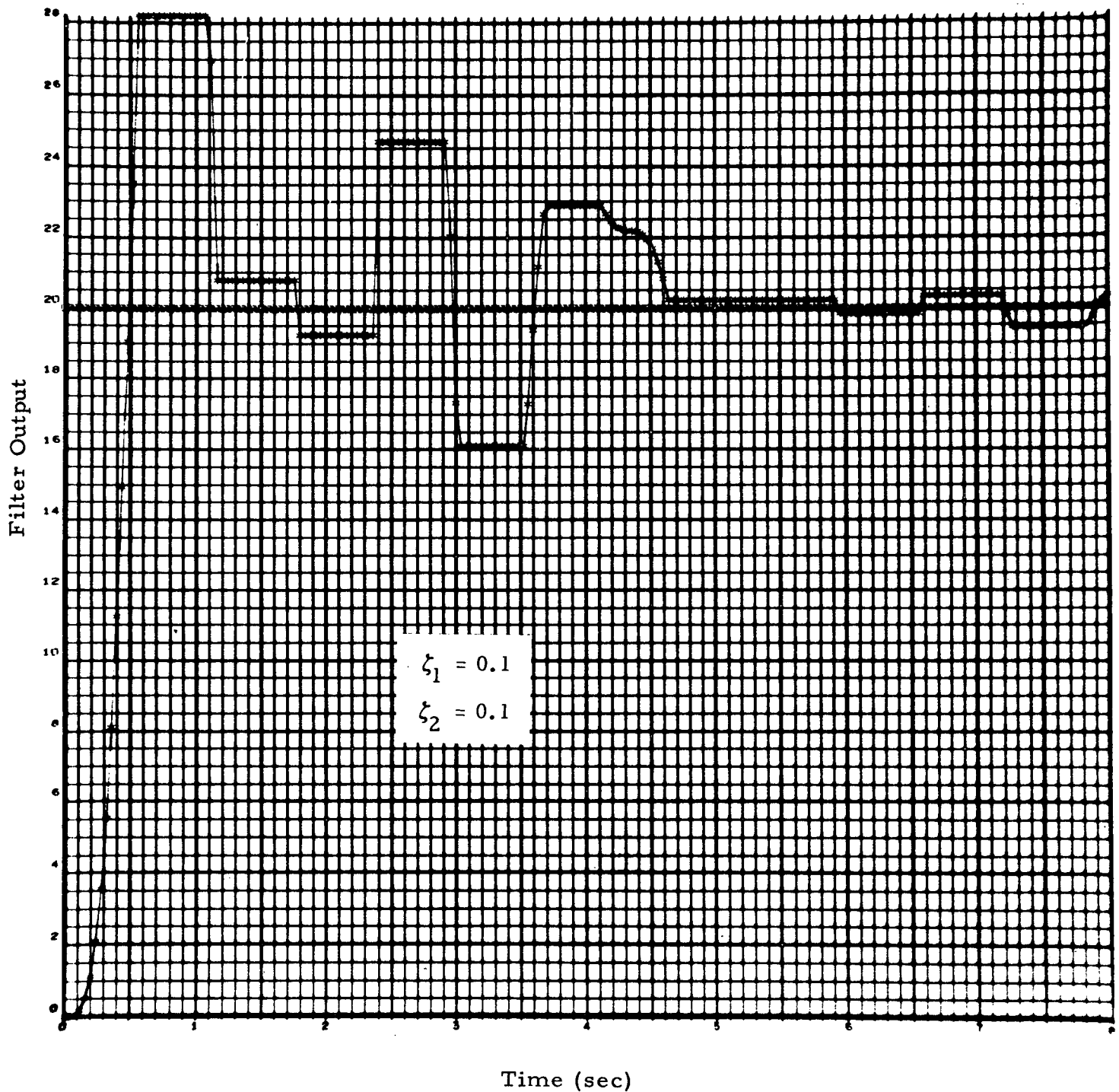


Fig. 3-17 - Time Response of Digital Filter (Step Input = 20 at $t \geq 0$)

overshoot determines the desirable values of damping ratios. Figure 3-18 shows the responses of the HFCF for a constant ζ_2 of 0.7 and three different values of ζ_1 . A family of log magnitude curves and phase curves for these combinations of damping ratios are also plotted in Figs. 3-19 and 3-20. These curves show the effects of damping ratio upon the frequency response of the linear portions of the digital filter for input frequencies equal to or less than one half the sampling frequency.

3.2.2 DC Plus High Frequency Signals

A number of simulations were run for various inputs to investigate the time response and input-output relations of the digital high frequency cutoff filter. Some time responses of the filter are shown in Figs. 3-21 through 3-24. The following filter parameters were used.

HFCF Parameters

Cutoff Frequency, ω_c	3 rad/sec
Sampling Frequency, f_s	25 samples/sec
ω_1	4.5 rad/sec
ζ_1	0.5
ω_2	6.0 rad/sec
ζ_2	0.6

Figures 3-22 and 3-23 show that for dc plus a single high frequency signal, the dc signal is transmitted and the high frequency signal is blocked by the digital filter.

A comparison of filter response to a step input (Fig. 3-21) with the response of the filter to a step input plus high frequency signal (Figs. 3-22 and 3-23) shows that the high frequency signal has caused a decrease in rise time and an increase in overshoot. The step response of the filter in the presence of one, two, three and five tones of high frequency signals is shown in Fig. 3-24. Figure 3-25

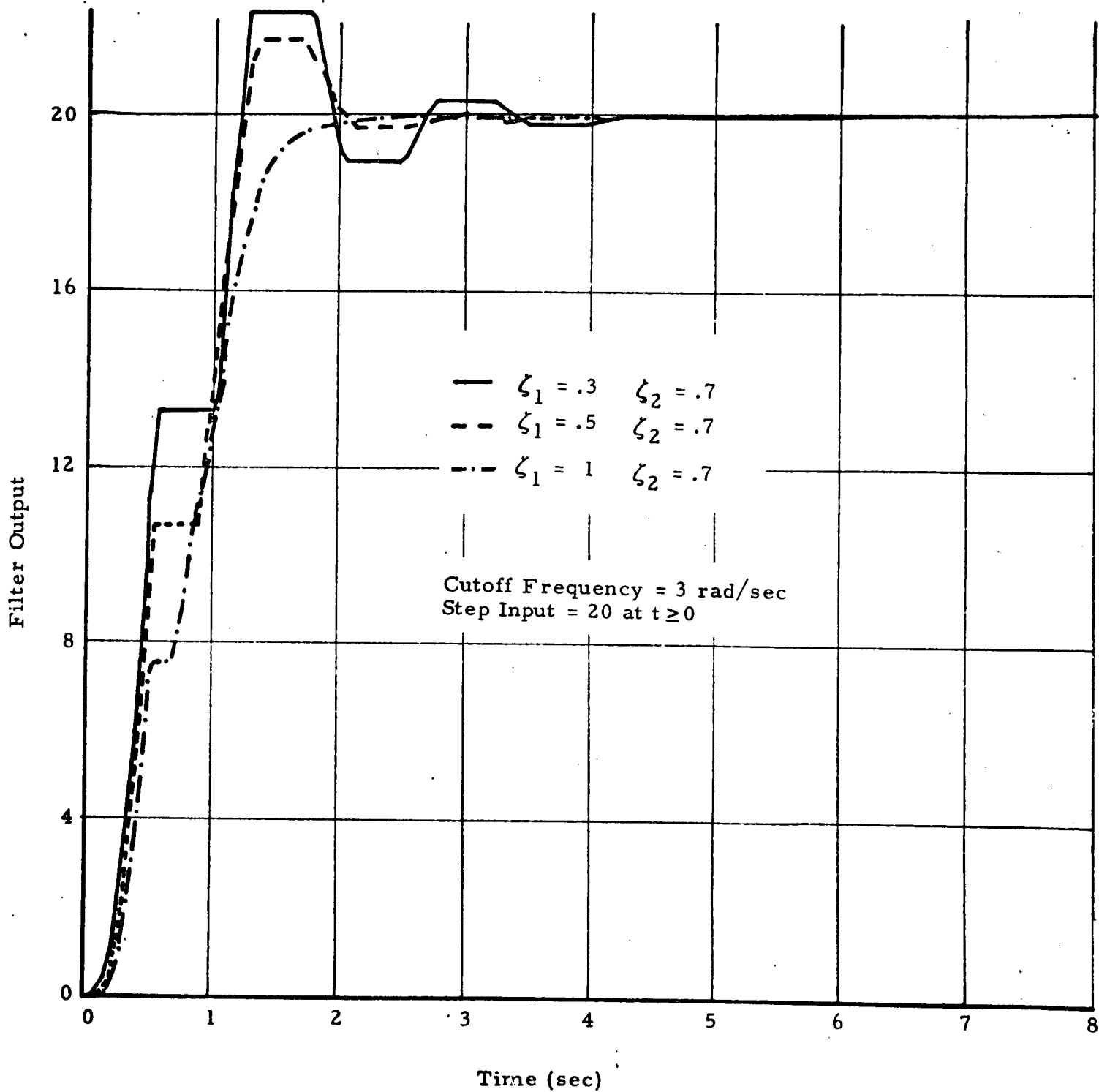


Fig. 3-18 - Time Response of High Frequency Cutoff Filter
for Three Different Values of ζ_1

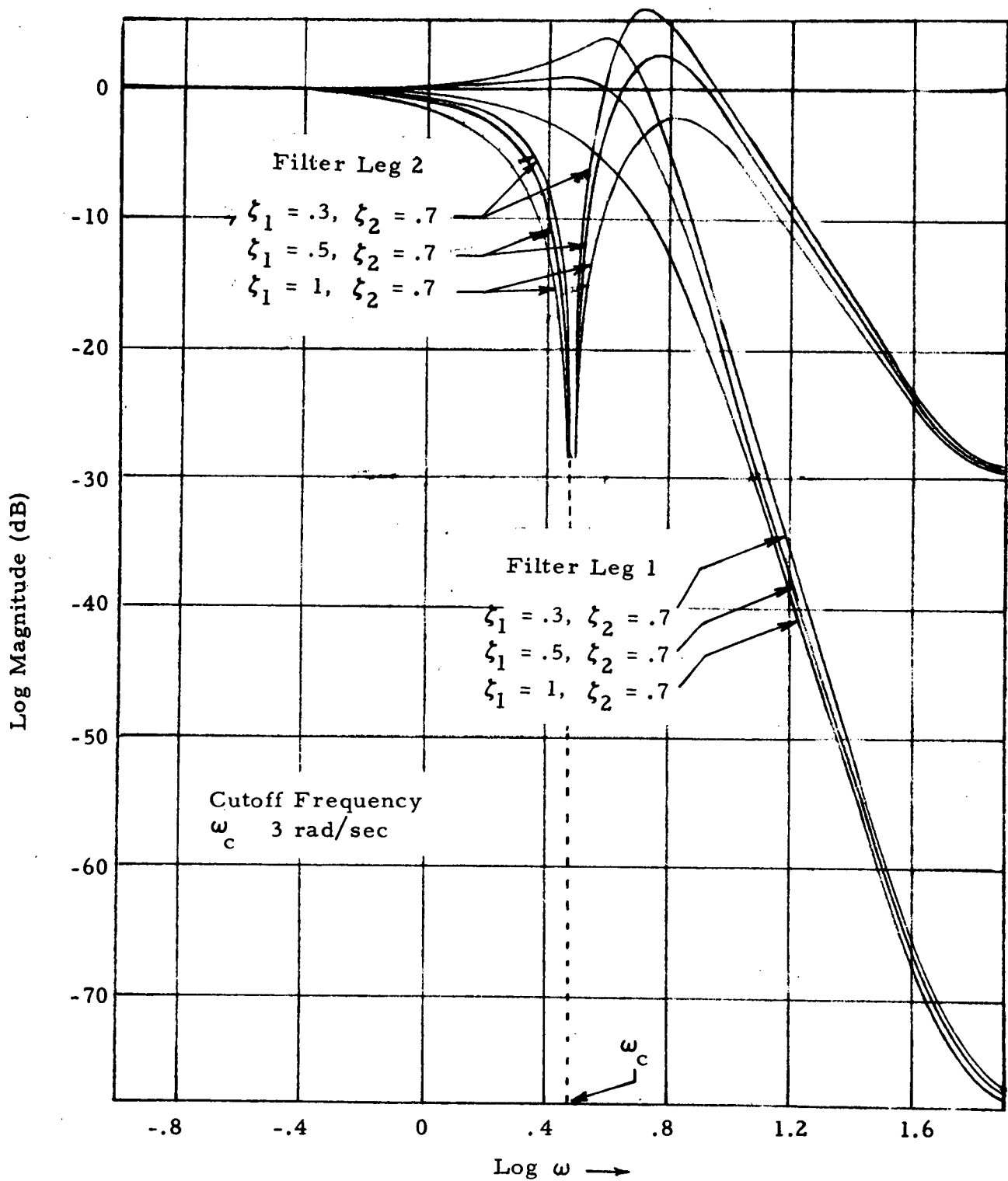


Fig. 3-19 - Log Magnitude Diagram for the HFCF for Several Combinations of ζ_1 and ζ_2

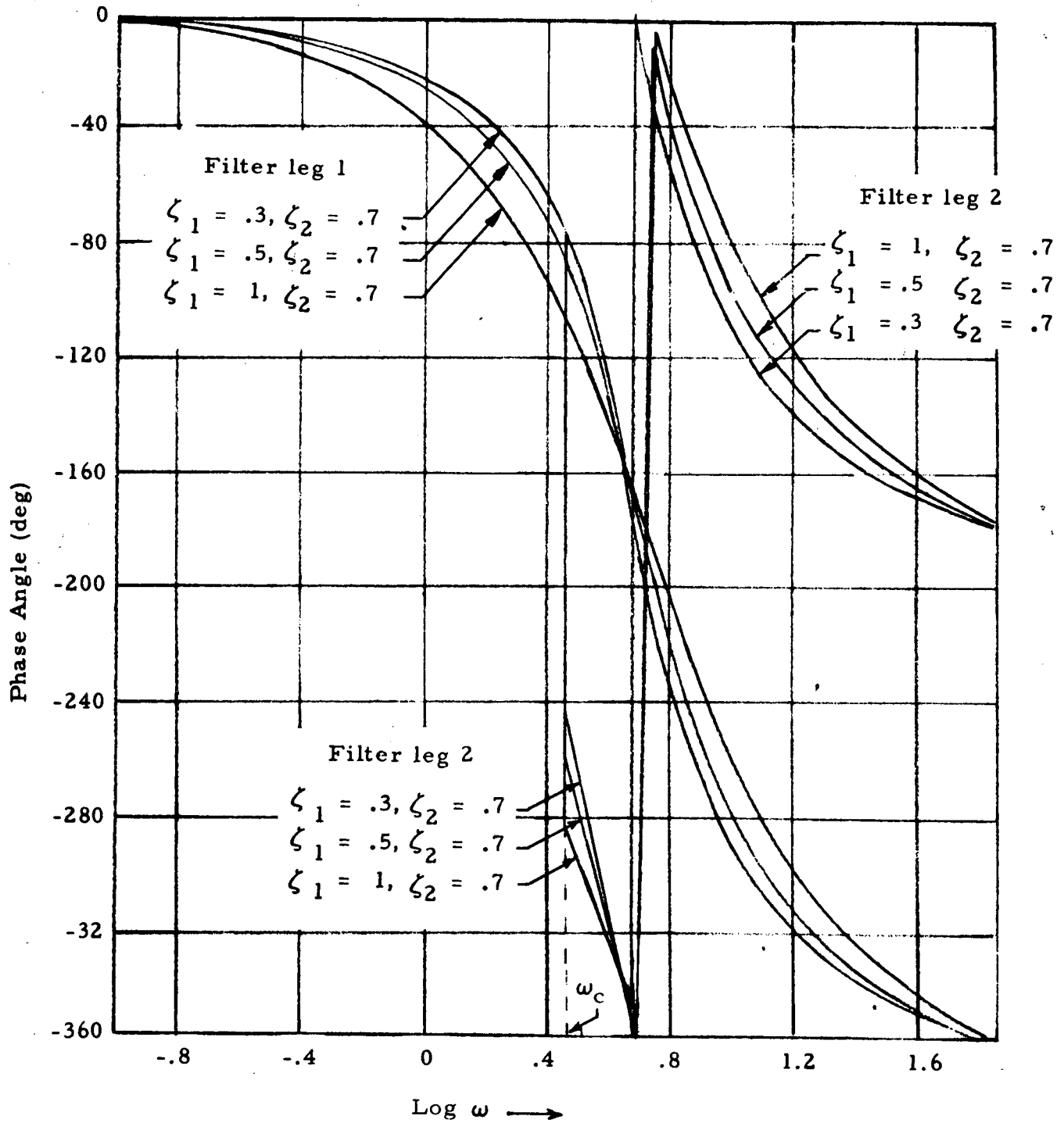


Fig. 3-20 - Phase Diagram for the HFCF for Several Combinations of ζ_1 and ζ_2

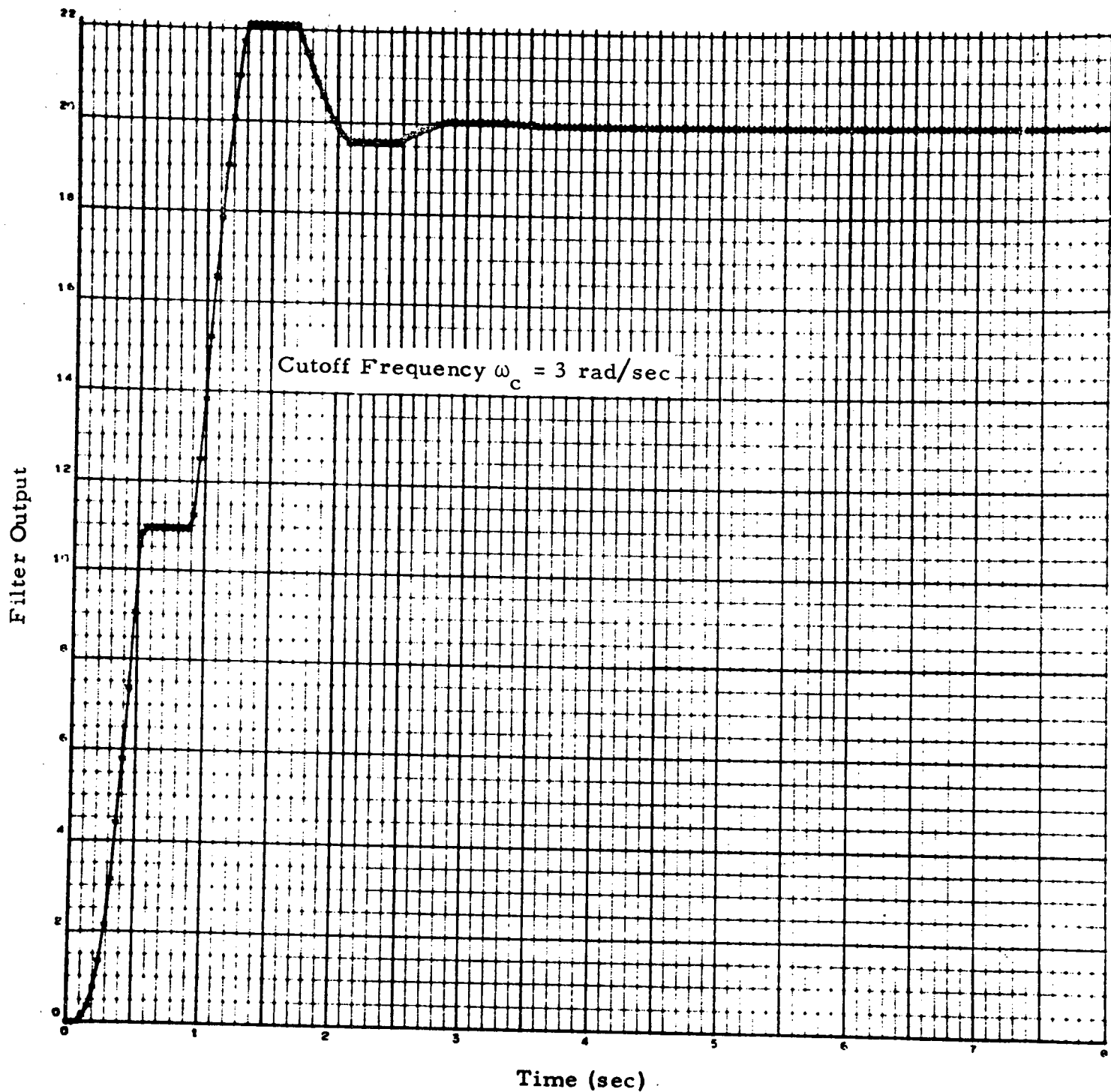


Fig. 3-21 - Time Response of High Frequency Cutoff Filter
(Step Input = 20 at $t \leq 0$)

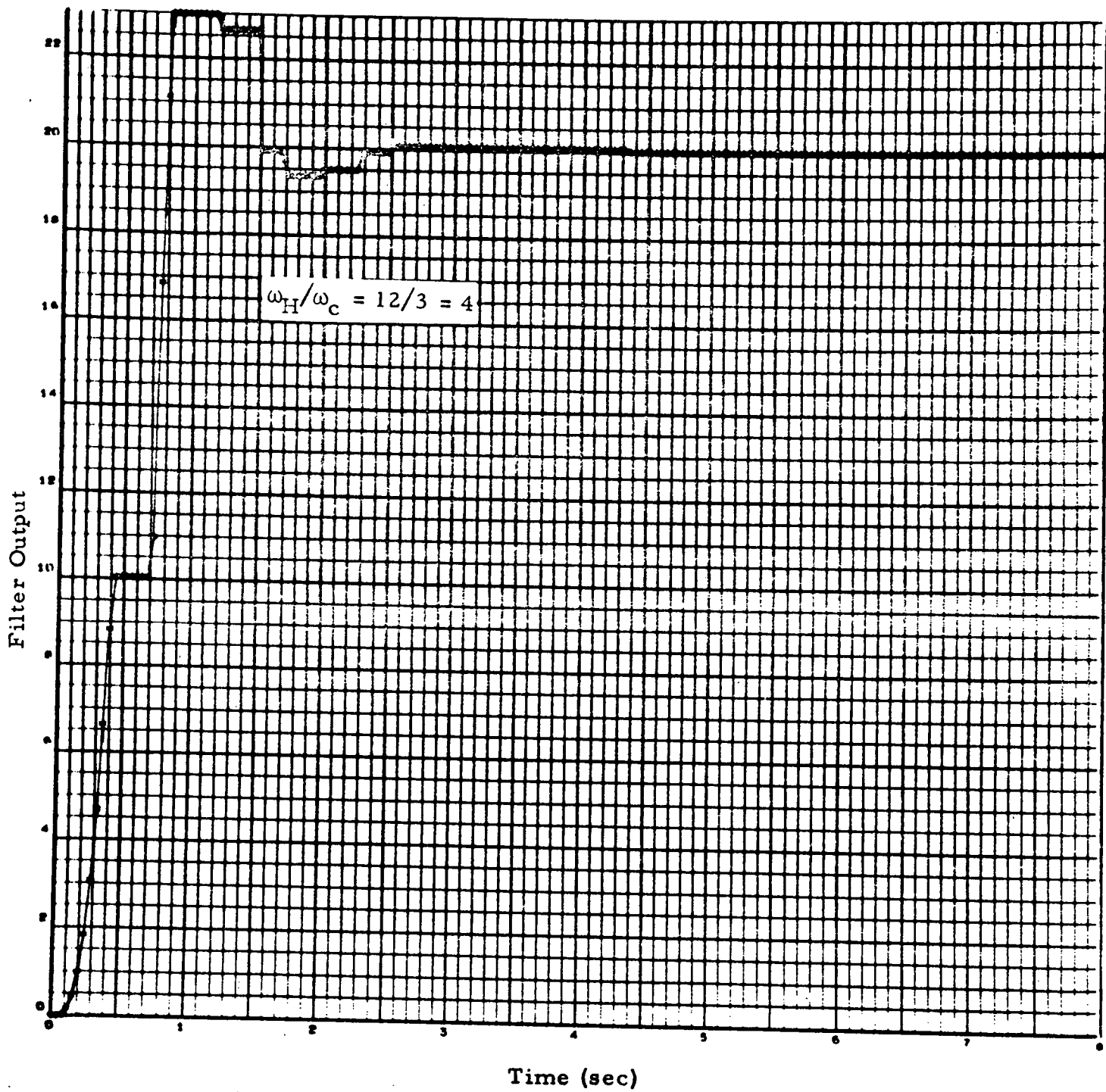


Fig. 3-22 - Time Response of High Frequency Cutoff Filter (Input = $20 + 20 \sin 12t$)

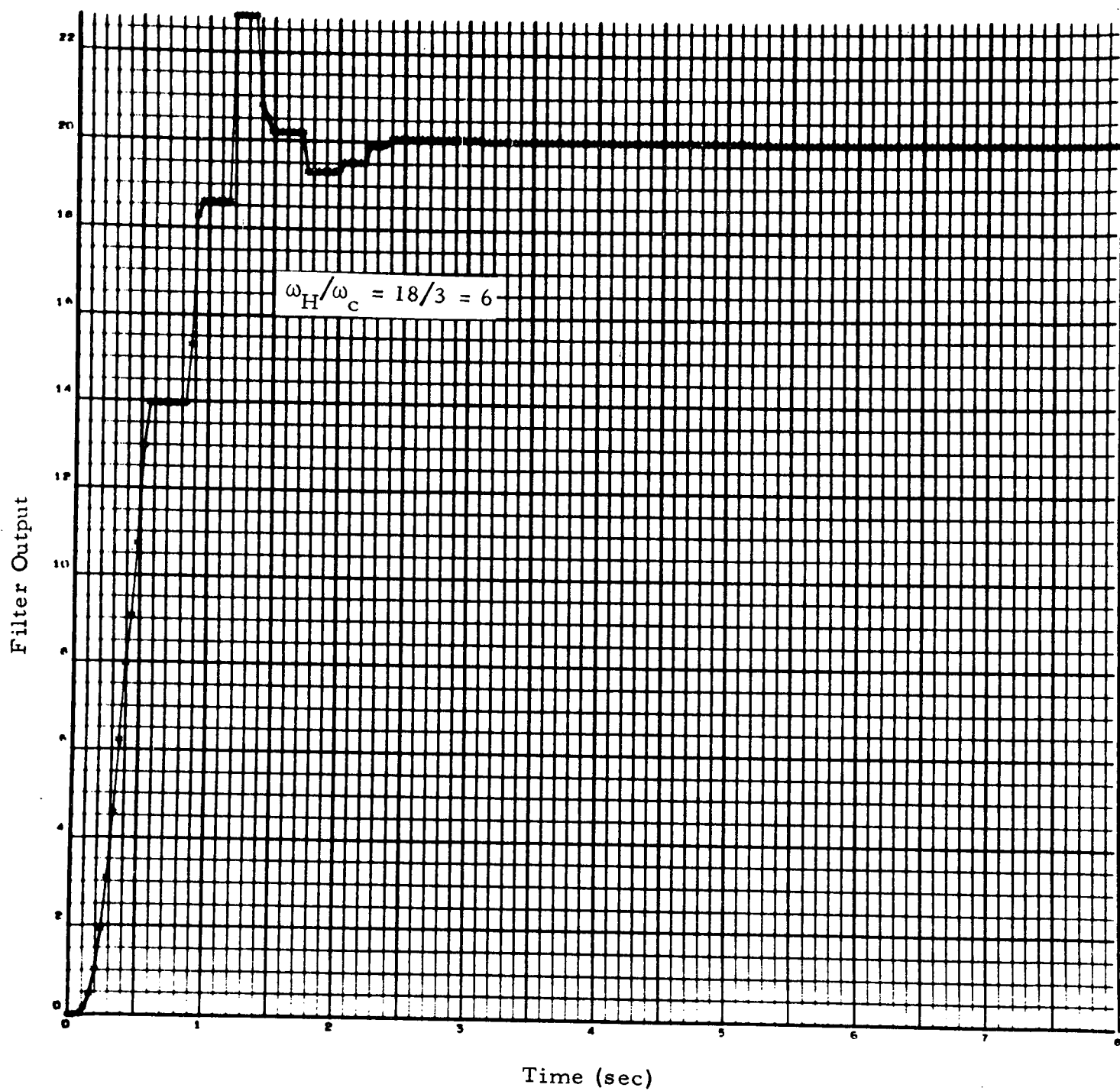


Fig. 3-23- Time Response of High Frequency Cutoff Filter (Input = $20 + 20 \sin 18t$)

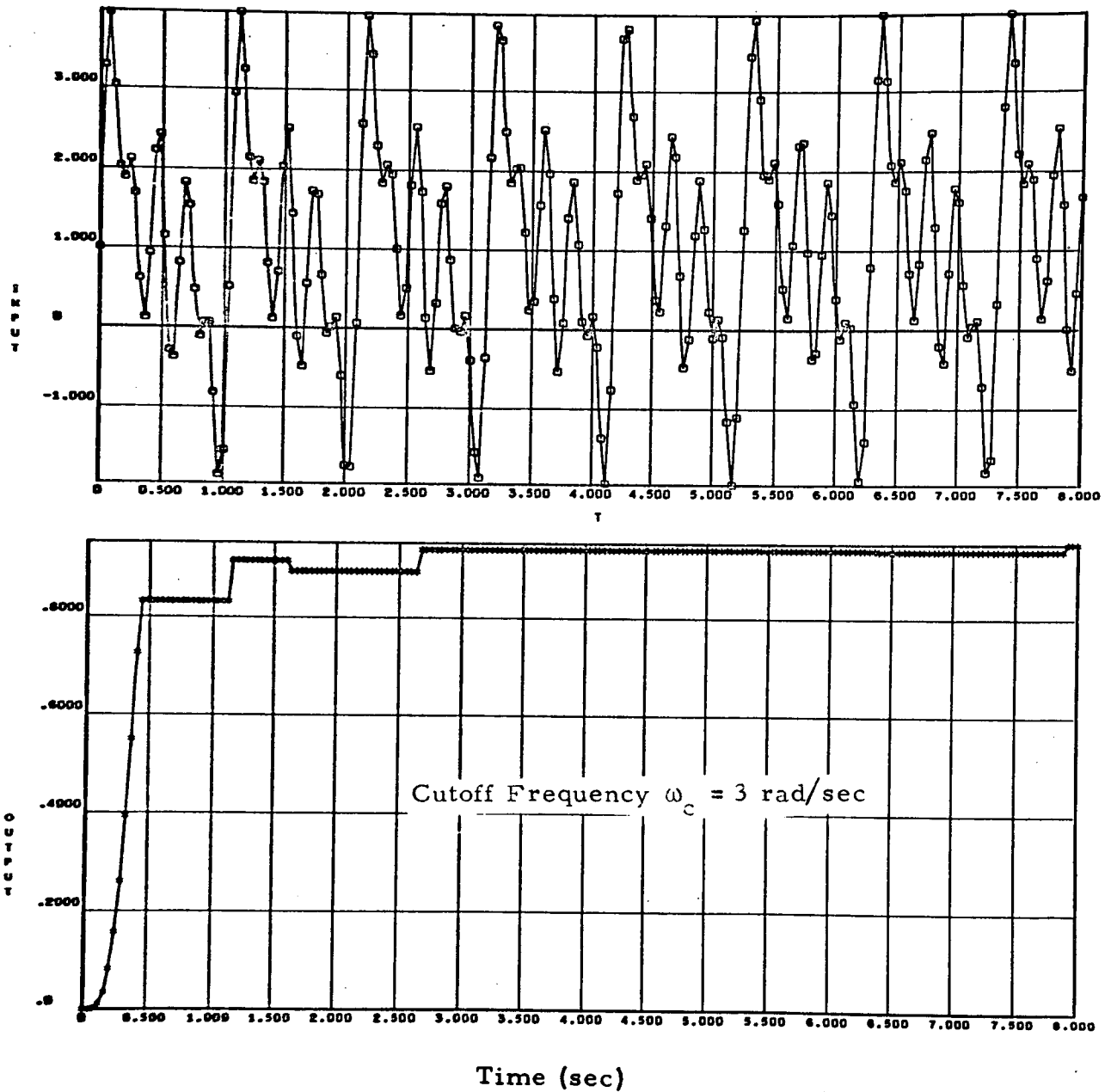


Fig. 3-24 - Time Response of High Frequency Cutoff Filter (Input = $1 + \sin 6t + \sin 12t + \sin 18t + \sin 30t$)

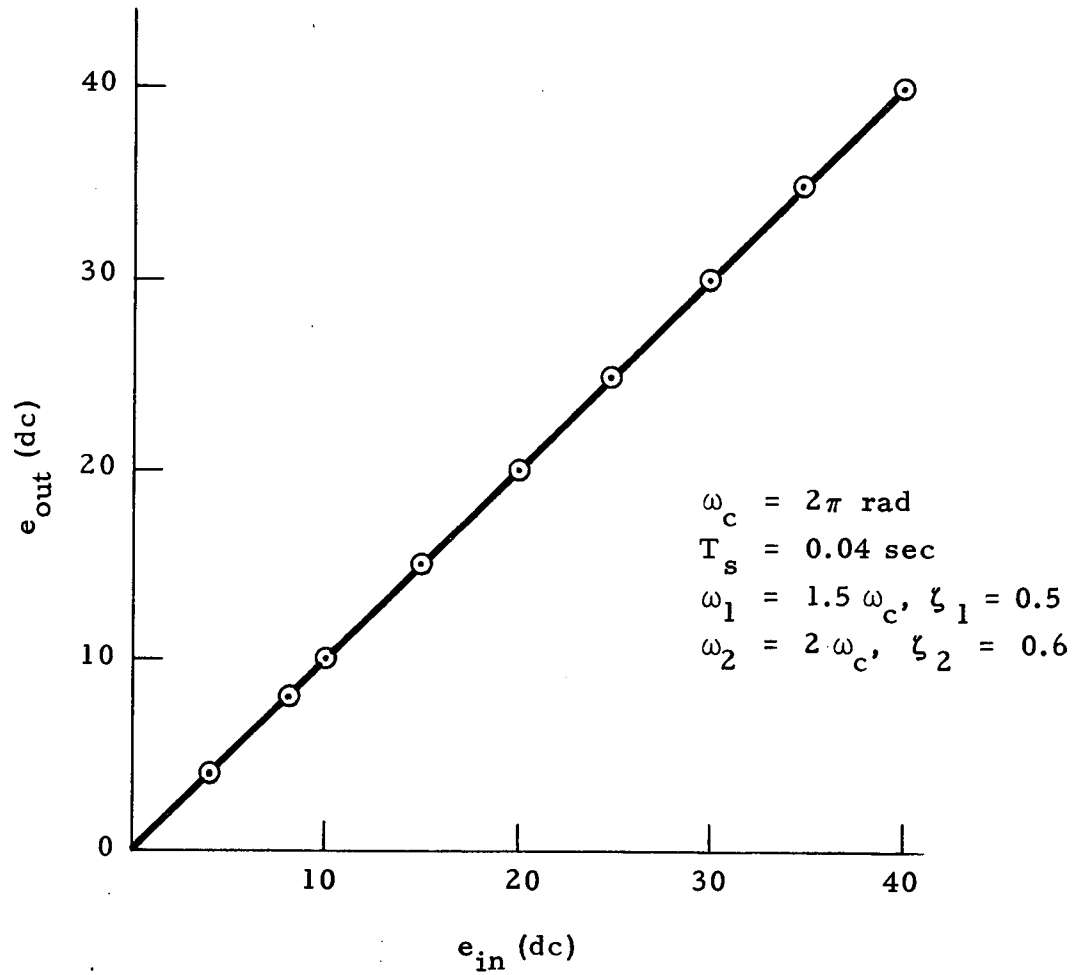


Fig. 3-25 - DC Input-Output Characteristics of the Digital Cutoff Filter with $e_i = e_{in(dc)} + \sin 5\omega_c t$

shows the dc input-output characteristic of the digital high frequency cutoff filter. Note the linear relationship between dc input and output level.

3.2.3 DC Plus Low Frequency Signal

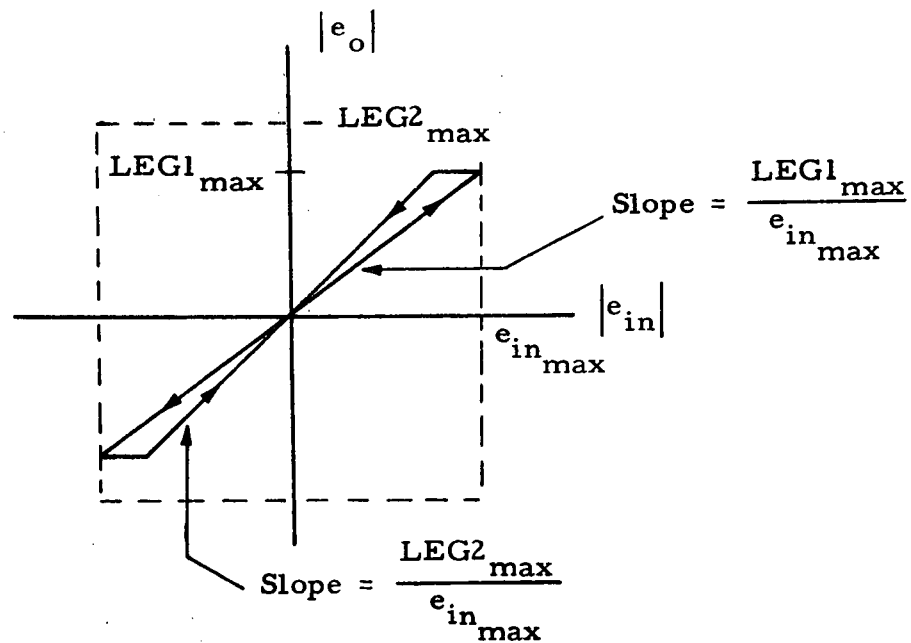
Figure 3-26 shows the response of the digital filter to a dc plus a low frequency signal for the following filter parameters

Cutoff Frequency, ω_c	3 rad/sec
Sampling Frequency, f_s	25 samples/sec
ω_1	4.5 rad/sec
ζ_1	1.0
ω_2	6.0 rad/sec
ζ_2	0.7

As may be observed, both the dc and the low frequency signals are transmitted by the digital filter. Hysteresis effect occurred because of the high frequency cutoff characteristics of the filter logic.

3.2.4 Low Frequency Signal

Figures 3-27, 3-28 and 3-29 show the time responses of the digital filter to sinusoidal signals of frequencies $0.4 \omega_c$, $0.6 \omega_c$ and $0.8 \omega_c$, respectively. The filter output is characterized by hysteresis. This effect is greater as the signal frequency approaches the cutoff frequency. The hysteresis is due to the high frequency cutoff characteristic of the digital logic. Note that the steady state low frequency magnitude characteristic of the HFCE can be described by the hysteresis loop as shown in the sketch on the following page.



HFCE Hysteresis Characteristic

3.2.5 Low Frequency and Multiple High Frequency Inputs

Figure 3-30 shows the time history of the filter output in response to an input containing multiple high frequency components in addition to a low frequency component. Figure 3-31 is a plot of the filter output and the low frequency component of the input. The filter parameters are the same as those used in Section 3.2.3. We see from these plots that the low frequency component is passed in a "quasi-sampled" manner.

It has been shown (Ref. 1) that due to the high frequency attenuation pattern, the filter output has an appearance similar to that resulting from the superposition of a single high frequency signal on that of a low frequency. This single high frequency is the lowest expected frequency above ω_c . Hence, regardless of the high frequency content of the input, analytical studies to describe the nonlinear low frequency effects due to quasi-sampling can be based on a filter input consisting of a single high frequency signal superimposed on a signal of low frequency.

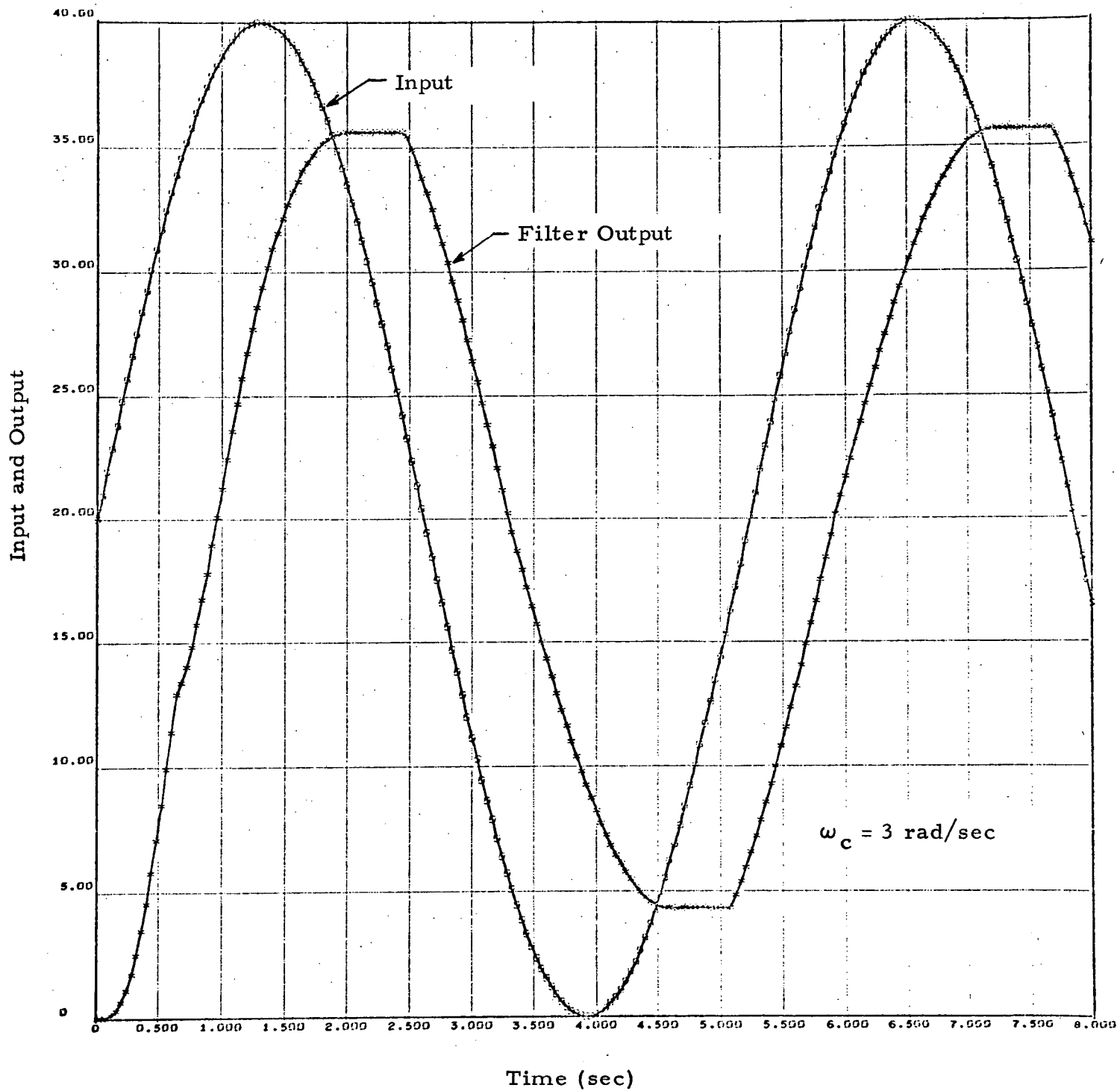


Fig. 3-26 - Time Response of High Frequency Cutoff Filter
(Input = $20 + 20 \sin 1.2t$)

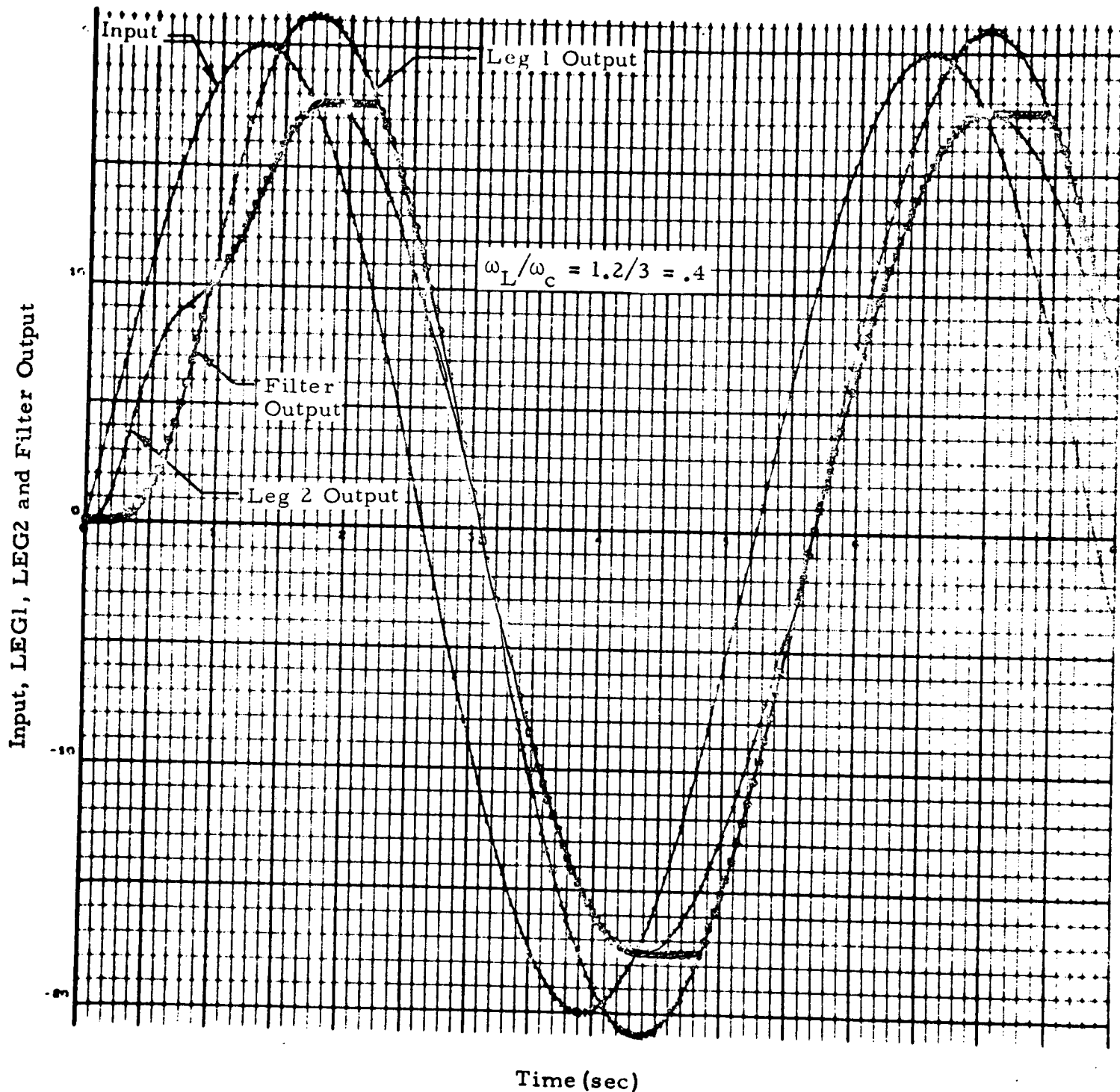


Fig. 3-27 - Time Response of High Frequency Cutoff Filter
(Input = $20 \sin 1.2t$)

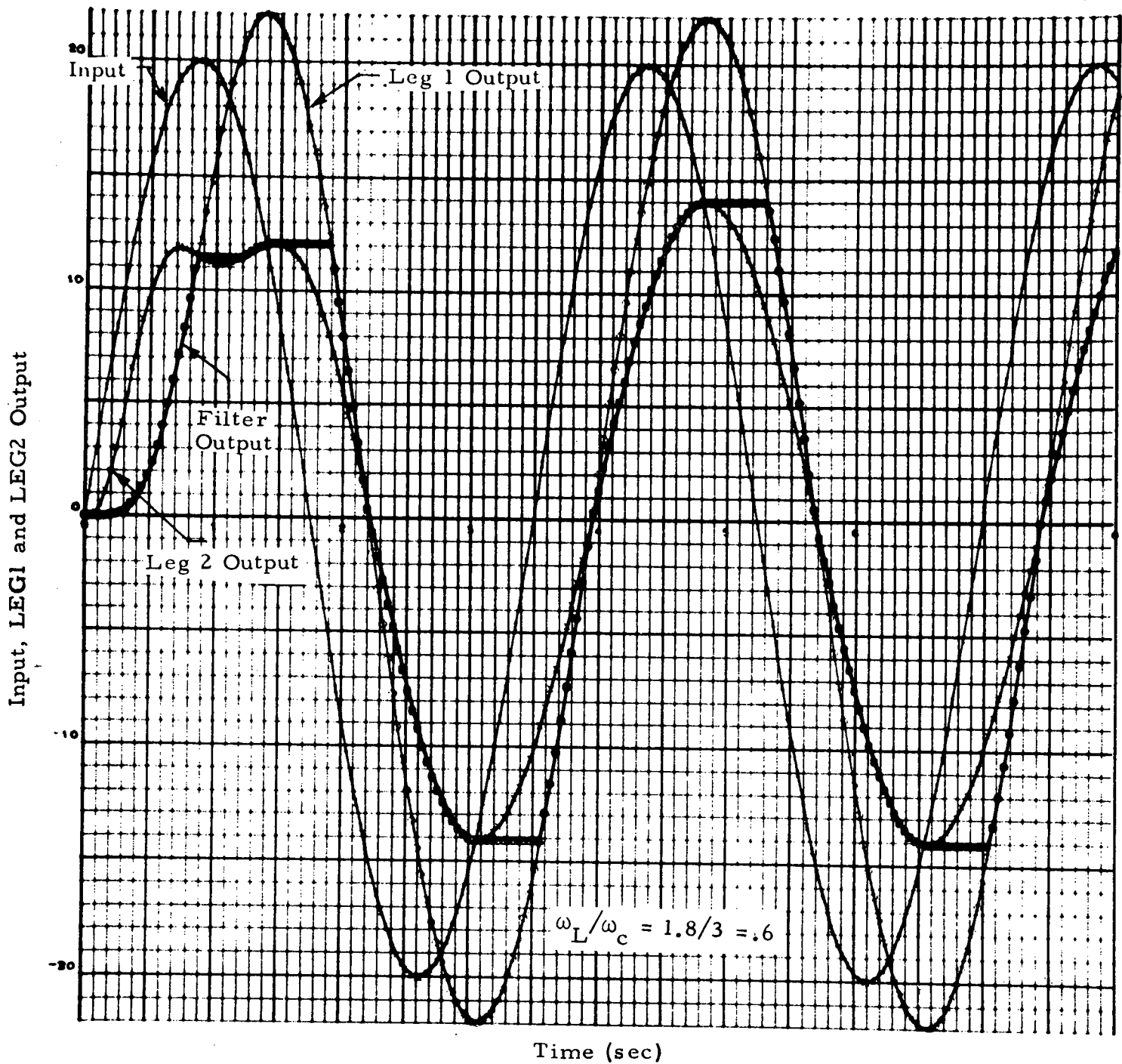


Fig. 3-28 - Time Response of High Frequency Cutoff Filter
(Input = $20 \sin 1.8t$)

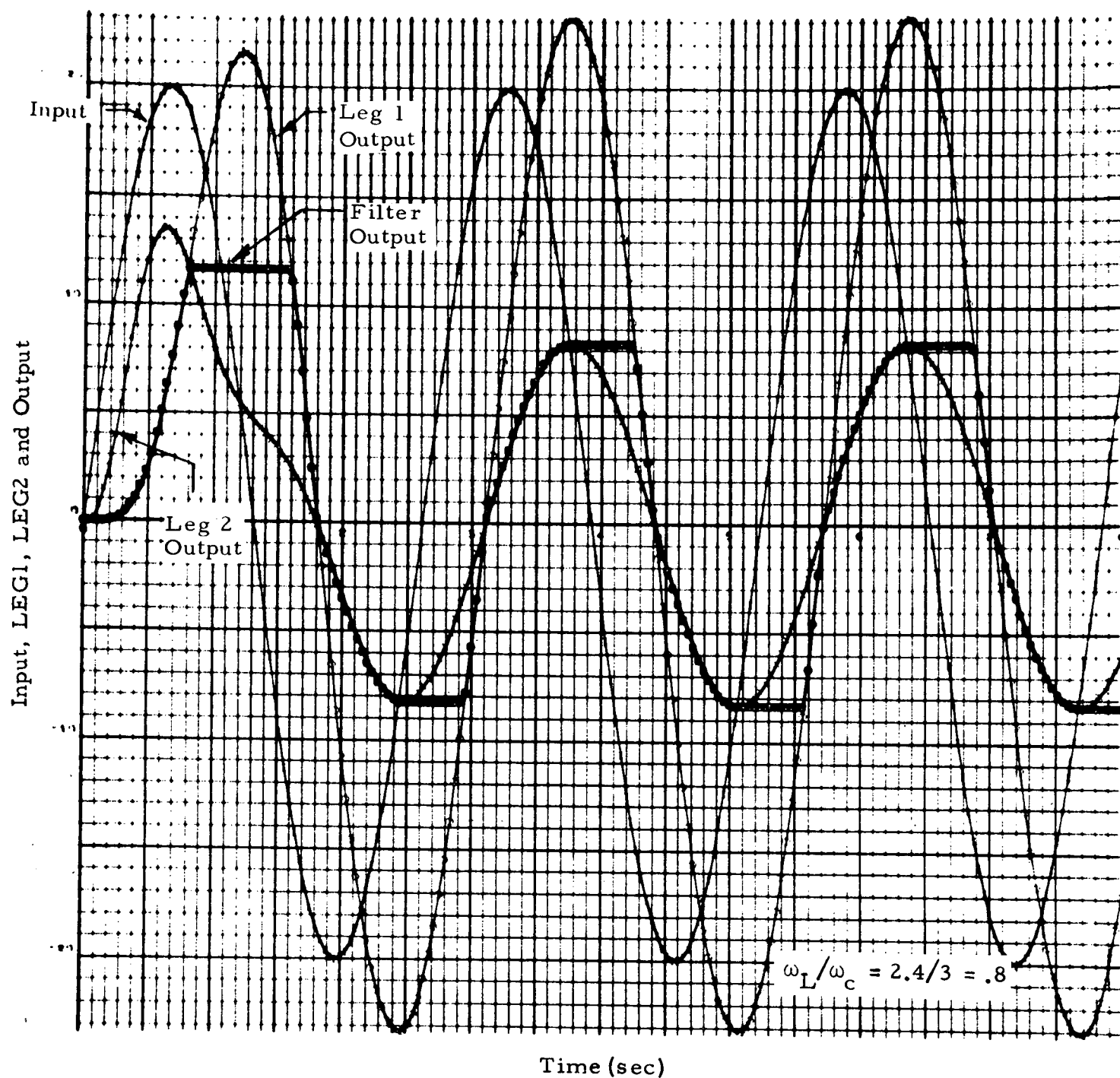


Fig. 3-29 - Time Response of High Frequency Cutoff Filter (Input = $20 \sin 2.4t$)

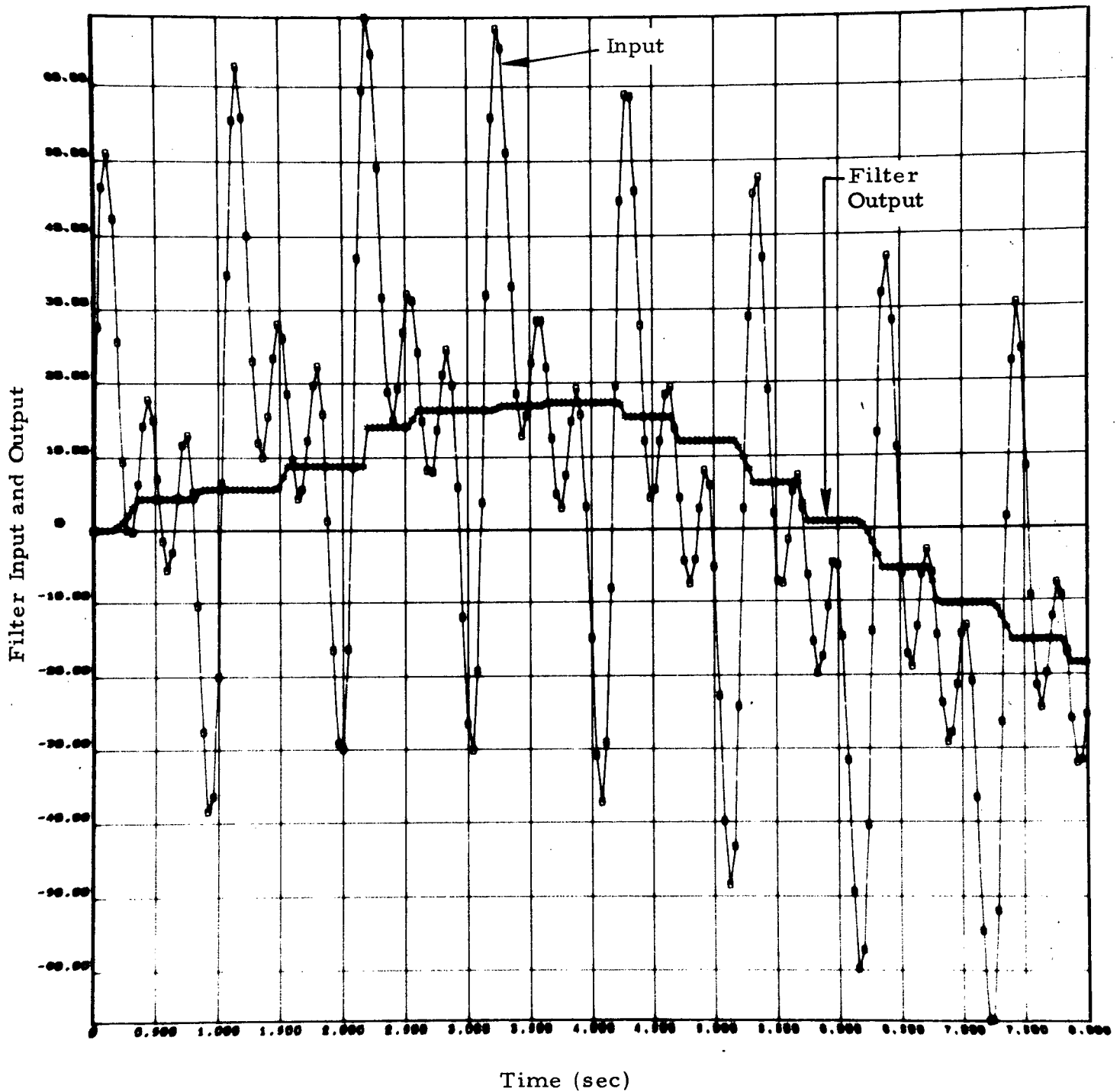


Fig. 3-30 - Time Response of High Frequency Cutoff Filter
(Input = $20 (\sin 0.6t + \sin 6t + \sin 12t + \sin 18t)$)

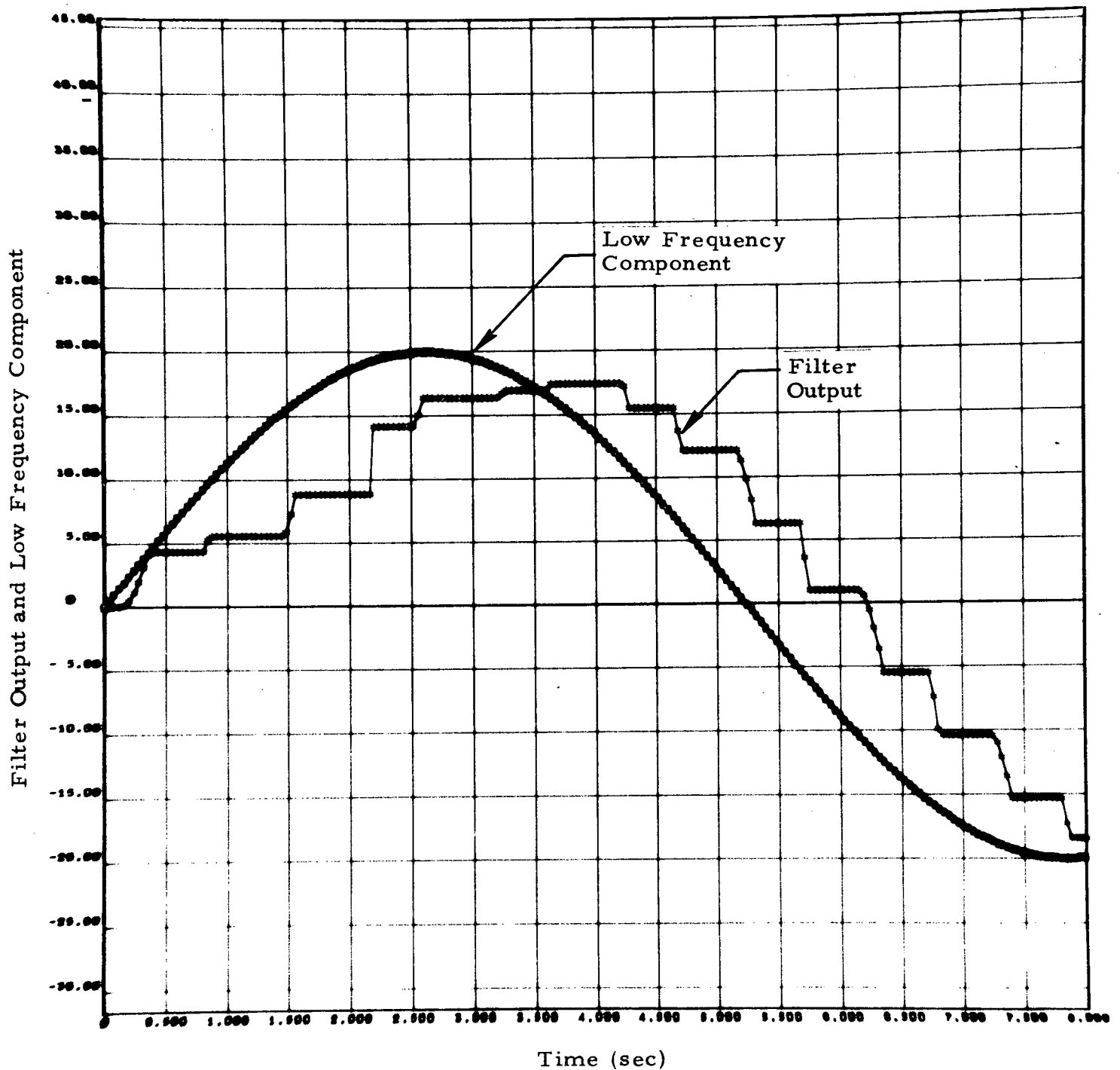


Fig. 3-31 - Time Response of High Frequency Cutoff Filter
(Input = $20 (\sin 0.6t + \sin 6t + \sin 12t + \sin 18t)$)

3.2.6 High Frequency Signal

Figures 3-32, 3-33 and 3-34 show the time responses of the digital filter to sinusoidal signals of frequencies ω_c , $4\omega_c$ and $8\omega_c$, respectively. The following filter parameters were used:

ω_c	3 rad/sec
f_s	25 samples/sec
ω_1	4.5 rad/sec
ζ_1	0.5
ω_2	6.0 rad/sec
ζ_2	0.6

These figures show that when a high frequency signal alone appears at the filter input, sharp cutoff occurs and the input is subdued.

Figures 3-35 and 3-36 show that the time response of the digital filter output to two out-of-phase high frequency signals is periodic. The filter parameters used were

ω_c	2π rad/sec
ω_1	3π rad/sec
ζ_1	0.5
ω_2	4π rad/sec
ζ_2	0.6

For a sampling period of 0.04 second, the period of the output waveform is 5 seconds and for a sampling period of 0.08 second, the period of the output waveform is 10 seconds. These are equal to the least common multiple of the periods of the high frequency signals and the sampling period. Note also that the magnitude of the output is very small compared to the magnitude of the input.

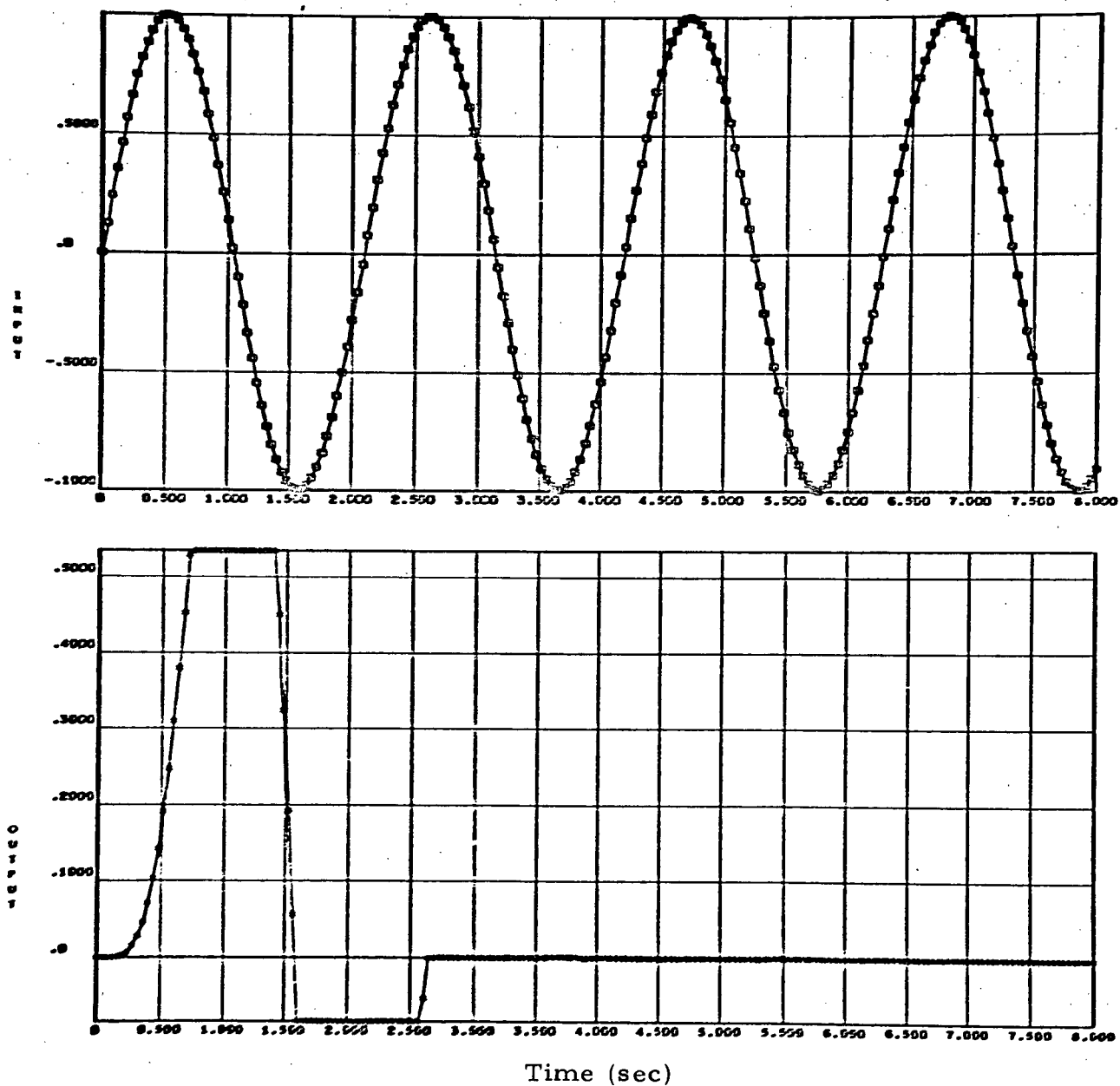


Fig. 3-32 - Filter Response to High Frequency Signal
(Input = $\sin 3t$, $\omega_H/\omega_c = 1$)

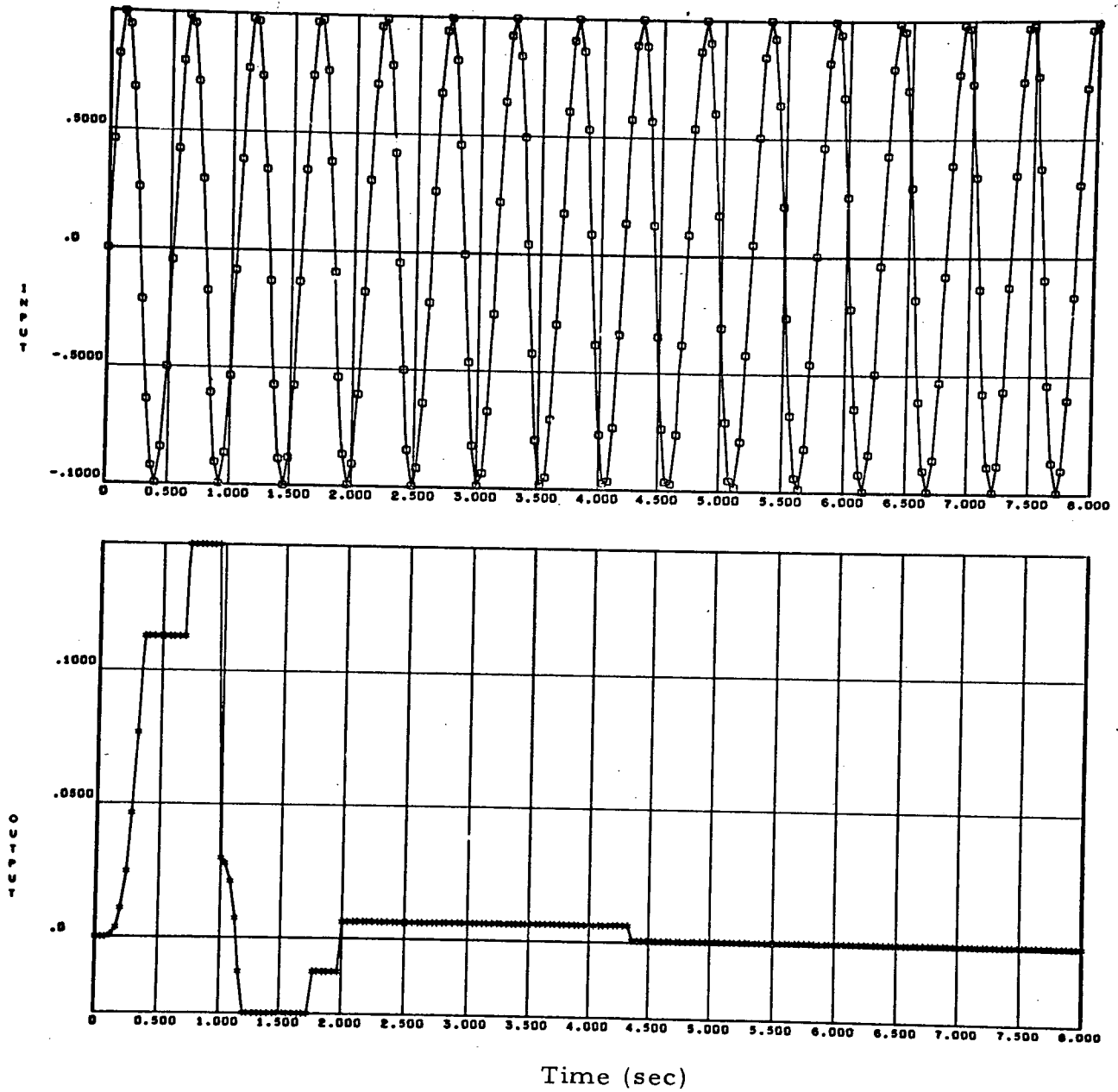


Fig. 3-33 - Filter Response to High Frequency Signal
(Input = $\sin 12t$, $\omega_H/\omega_c = 4$)

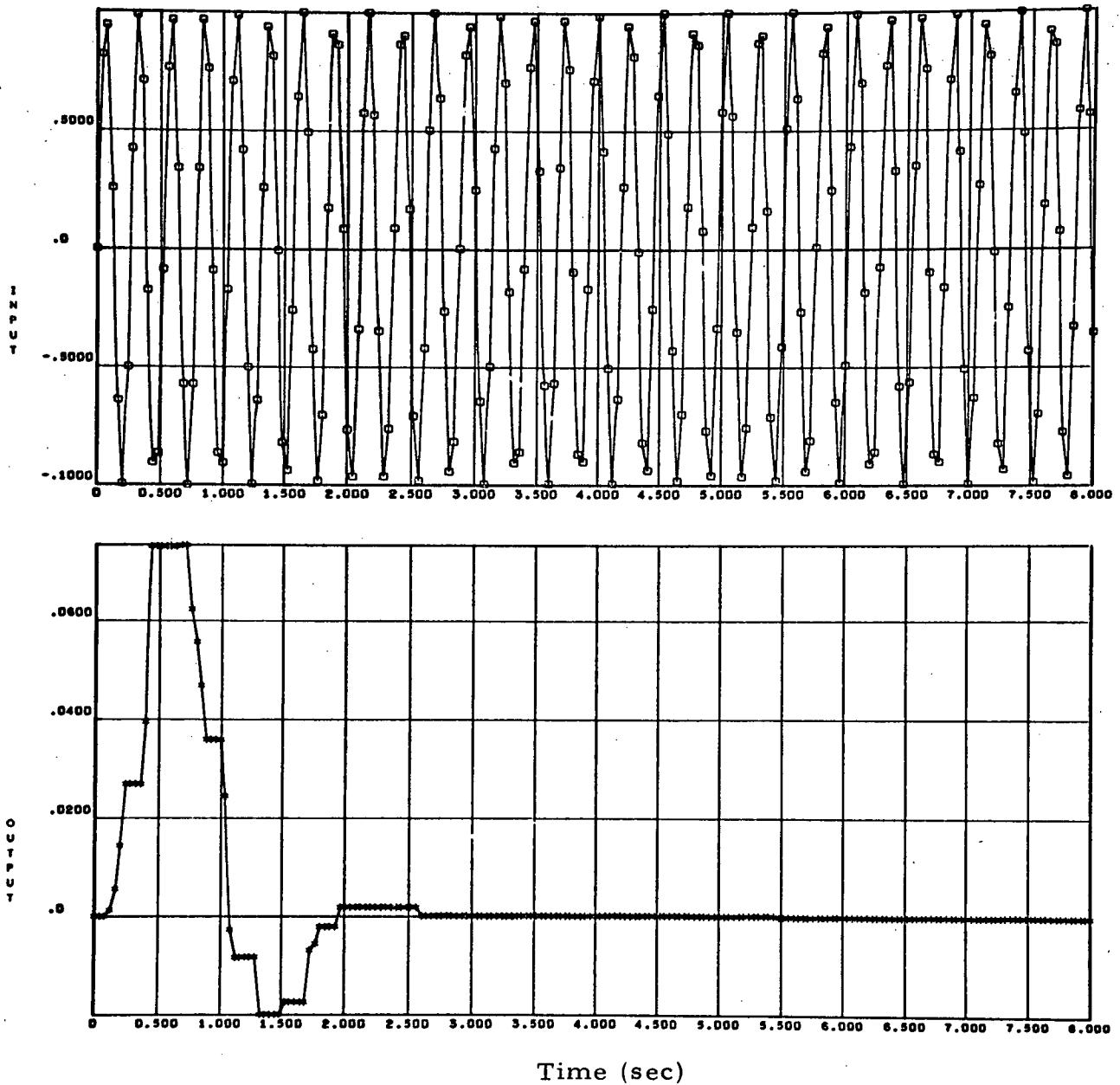


Fig. 3-34 - Filter Response to High Frequency Signal
(Input = $\sin 24t$, $\omega_H/\omega_C = 8$)

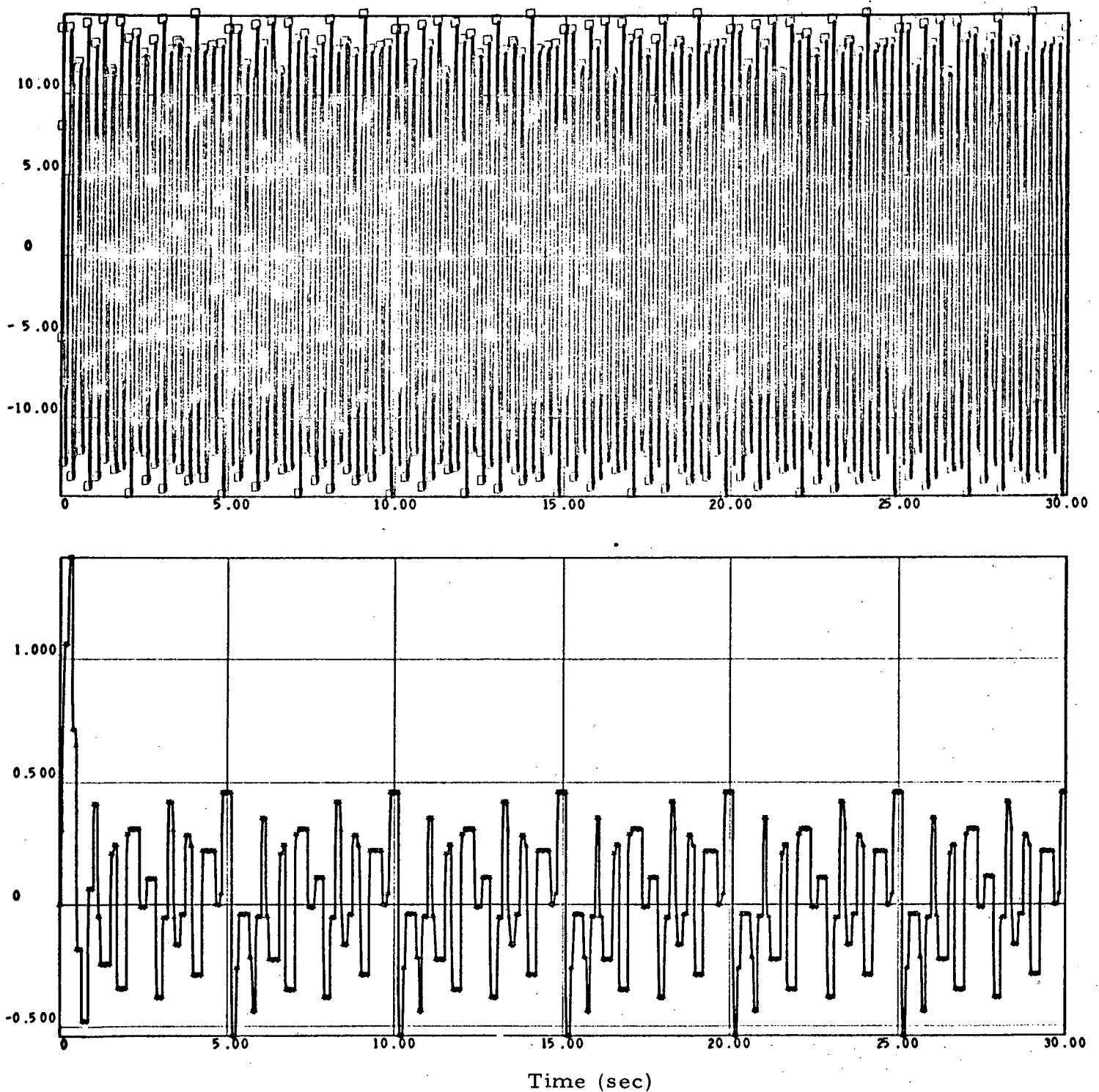


Fig. 3-35 - Filter Response to Out-of-Phase High Frequency Signals
(Input = $\sin 36\pi t + 14 \cos 8\pi t$, Sampling Period = 0.04 sec)

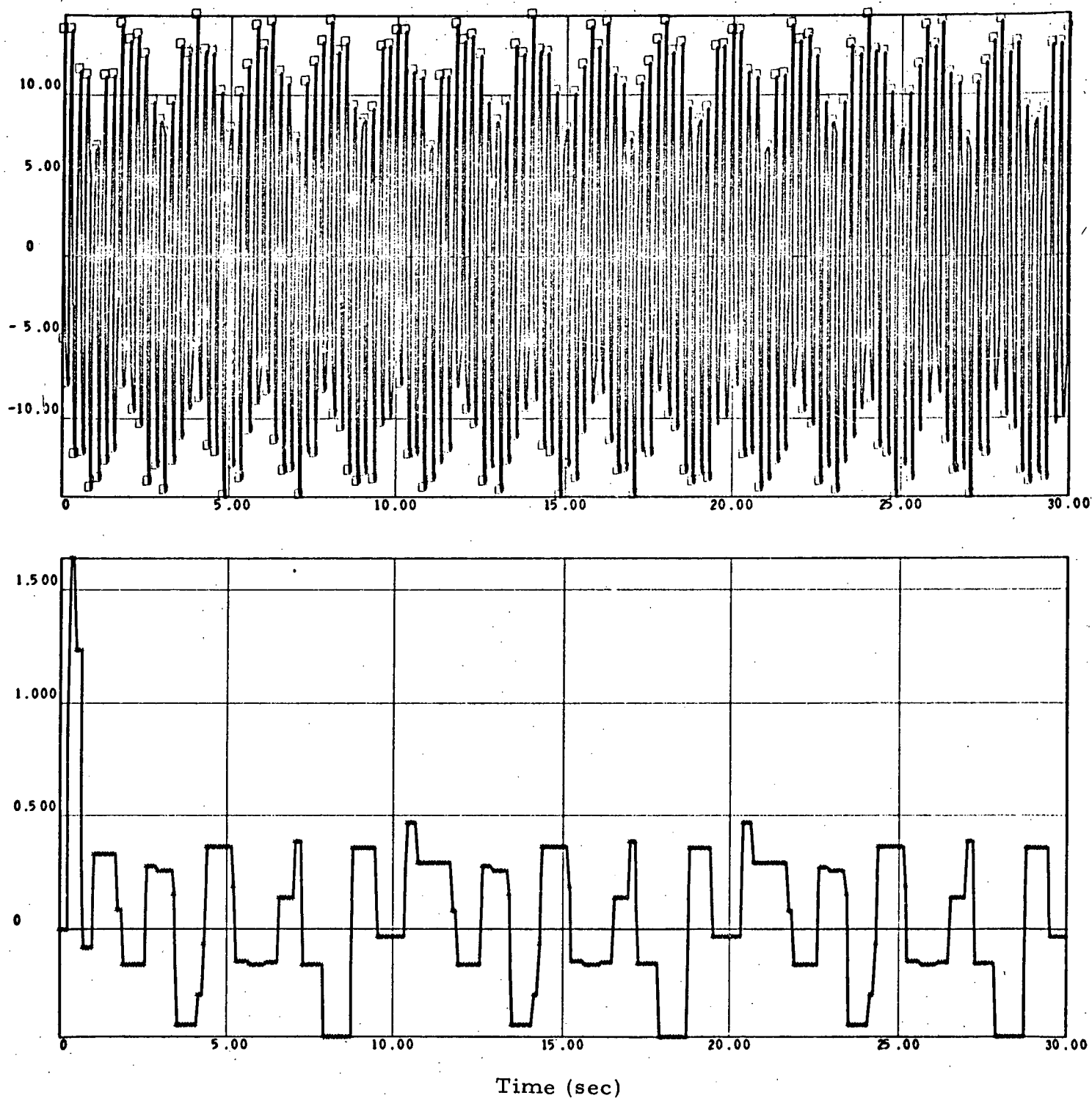


Fig. 3-36 - Filter Response to Out-of-Phase High Frequency Signals
 (Input = $\sin 3.6\pi t + 14 \cos 8\pi t$, Sampling Period = 0.08 sec)

Section 4

CONCLUSIONS AND RECOMMENDATIONS

The problem of digital implementation of a cutoff filter developed by Lockheed Missiles & Space Company's Huntsville Research & Engineering Center is approached with consideration to word length, sampling rate, accuracy requirements, computing time and hardware restrictions.

Upper bounds for the steady state system output error due to quantization for digital control systems containing a digital network programmed both in the direct form and in the canonical form were derived. This was accomplished by defining a set of error equations in the z domain then applying the final value theorem to the solution. Quantization error was found to depend upon the digital word length, sampling rate, and system time constants. The error bound developed may be used to estimate the digital word length and sampling rate required to achieve a given system specification.

Computing time and hardware requirements for four possible programming forms for the linear portions of the filter were determined. From the quantization error accumulation, computing time and hardware point of view, and the fact that complex poles and zeros must be realized, the canonical form of programming seems preferable.

Finally, the basic input-output characteristics of the digitized high frequency cutoff filter were investigated. The filter demonstrated its ability to pass signals with minimum distortion in a given frequency band while minimizing signals whose frequencies lie outside the band.

Since the most important performance criterion of all is overall system stability, it is recommended that this study be continued so that the following stability problems can be investigated:

1. Development of a general method (e.g., Lyapunov's 2nd method) to analyze the stability of a given control system containing the high frequency cutoff filter.
2. Extension of the above developed method to analyze the stability of sampled-data control systems containing the digitized high frequency cutoff filter.
3. Investigation of sampling frequency effects on the stability of a sampled-data system containing the digitized filter.

It is also recommended that the analytical results on quantization error be verified by simulating the high frequency cutoff filter using fixed point arithmetic.

Section 5
REFERENCES

1. Earl, J. E., "A Nonlinear Filter for High Frequency Cutoff," LMSC-HREC A782442, Lockheed Missiles & Space Company, Huntsville, Ala., 13 April 1966.
2. Earl, J. E., "The Nonlinear Filter in the Saturn V Vehicle with Time Varying Coefficients," LMSC-HREC A783123, Lockheed Missiles & Space Company, Huntsville, Ala., August 1966.
3. Hewitt, G. R., and J. G. Tuck, "Digitized Nonlinear Filter for Launch Vehicle Application," LMSC-HREC A784590-I, Lockheed Missiles & Space Company, Huntsville, Ala., 22 September 1967.
4. Shaw, H., "Discrete Analogs for Continuous Filters," J. Assoc. Comp. Mach., Vol. 13, No. 4, October 1966, pp. 600-604.
5. Salzer, John M., "Frequency Analysis of Digital Computers Operating in Real Time," Proc. I. R. E., Vol. 42, No. 2, 1954, pp. 457-466.
6. Jury, E. I., Sampled-Data Control Systems, John Wiley, New York, 1958.
7. Derusso, P. M., R. J. Roy, and C. M. Close, State Variables for Engineers, John Wiley, New York, 1965.
8. Hildebrand, F. B., Introduction to Numerical Analysis, McGraw-Hill, New York, 1956.

Appendix A
HYSTERESIS OF DIGITAL HIGH FREQUENCY
CUTOFF FILTER

A-1

Appendix A

In the case where no high frequency signals are present the passage of a low frequency signal is characterized by hysteresis. To describe the phase and gain characteristics due to hysteresis, the describing function of the non-linearity is derived. From Fig. 3-29 it is observed that the digital output e_o is neither an even nor odd function and therefore must be described by both the $\sin n \omega t$ and $\cos n \omega t$ terms of the Fourier series. Assuming e_o has a period of 2π and the sampling rate is n , then the Fourier series of the output is given by

$$e_o(k) = a_o/2 + \sum_{i=1}^{\infty} \left[a_i \cos \left(\frac{2\pi}{n+1} k \right) i + b_i \sin \left(\frac{2\pi}{n+1} k \right) i \right]$$

where $k = 0, 1, \dots, n$.

The coefficients of the first H harmonics are given by Ref. 8.

$$a_i = \frac{\partial}{\partial i} \sum_{k=0}^n e_o(k) \cos \frac{2\pi k}{n+1} i$$

$$b_i = \frac{\partial}{\partial i} \sum_{k=0}^n e_o(k) \sin \frac{2\pi k}{n+1} i$$

For input $= E_1 \sin t$, the describing function of the nonlinearity is then given by

$$G = \frac{Z_1}{E_1} \angle \phi_1$$

A-1-a

where

$$Z_1 = (a_1^2 + b_1^2)^{\frac{1}{2}}$$

and

$$\phi_1 = \tan^{-1} \frac{a_1}{b_1}$$

Using the above method, the describing function for several values of ω is determined and listed in Table A-1 for the following digital filter parameters.

Cutoff Frequency, ω_c	2π rad/sec
Sampling Frequency, f_s	25 samples/sec
ω_1	$1.5 \omega_c$
ζ_1	0.5
ω_2	$2.0 \omega_c$
ζ_2	0.6

Table A-1
VALUES FOR DESCRIBING FUNCTION

ω/ω_c	E_1	a_1	b_1	z_1	ϕ_1
.2	10	-.121	9.86	9.86	42'
.3	10	-.251	9.67	9.67	1° 30'
.4	10	-.425	9.16	9.18	2° 38'
.5	10	-.564	8.61	8.63	3° 45'
.6	10	-.718	7.80	7.85	5° 16'
.7	10	-.708	6.36	6.40	6° 21'
.8	10	-.738	4.75	4.80	8° 48'
.9	10	-.512	2.54	2.60	11° 32'